**The Henryk Niewodniczański**
**Institute of Nuclear Physics**
**Polish Academy of Sciences**

Radzikowskiego 152, 31−342 Kraków, Poland

www.ifj.edu.pl/publ/reports

---

RAPORT NR 2001/AP

# THE USE OF ATOMIC FORCE MICROSCOPY AS A TECHNIQUE FOR THE IDENTIFICATION OF CANCEROUS CELLS

**Małgorzata Lekka**

*(Habilitation thesis)*

**Kraków, November 2007**

# *Abstract*

The monograph presents the use of atomic force microscopy (AFM) as a tool for the identification of cancerous cells by studies of the expression of different types of molecules directly on the surface of living cells.

The full quantitative description (that is not accessible by other techniques) performed for a given type of molecular interactions has been obtained by using the following quantities: an unbinding force, probability, rupture length and the effective spring constant taking into account the stiffness of a single complex. All, these parameters were extracted from AFM measurements
The analysis of the interaction forces performed by AFM allows the quantitative determination of: i) the static properties of a single molecular complex where its strength of interaction and stiffness of the studied complex can be obtained, ii) dynamic properties, on the basis of which the kinetic properties of the unbinding process can be delivered, and iii) properties of adhesion clusters, where the interrelation between single complexes can be characterized, in particular the mechanism of the unbinding can be obtained.

The presented characterization of the interaction force between single molecules demonstrates that atomic force microscopy can be used as exceptional technique to study the expression of molecules on a cell surface. Such measurements are not limited to a typical interactions occurring between single molecules but also it is possible to study the interactions between parts of molecules. The results presented in this monograph point to a novel approach to identify cancer−related changes in a quantitative way what can be used for describing and confirming the pathological state of a single cell.

# Table of contents

**CHAPTER 1. Introduction** **6**
1.1. Adhesion between cells 7
1.2. Unbinding force measurements 10
1.3. Detection of malignant alterations in cancerous cells by AFM 14
1.4. Overview of the monograph 19

**CHAPTER 2. Molecules on a cell surface** **22**
2.1. Cell surface adhesion molecules 23
2.2. Glycans 26
2.3. Molecules on a cancer cell surface 26

**CHAPTER 3. Models for molecule unbinding** **29**
3.1. Force−induced single bond dissociation 32
*3.1.1. Hierarchic crossing through the energy barrier* *35*
*3.1.2. The height of the energy barrier* *39*
3.2. Multiple-bond disruption 40
*3.2.1. Sequential bond rupture − the "zipper-like" model* *40*
*3.2.2. Simultaneous bond rupture − the "parallel-like" model* *42*

**CHAPTER 4. Force spectroscopy** **44**
4.1. Atomic force microscope (AFM) 45
*4.1.1. Cantilevers* *45*
*4.1.2. Deflection measuring system* *46*
*4.1.3. Scanning and positioning system* *47*
4.2. Force spectroscopy mode 47
*4.2.1. Force curves* *47*
*4.2.2. Force versus sample−distance conversion* *50*
*4.2.3. Elements that should be calibrated* *52*
4.3. Tip and surface functionalization 59
*4.3.1. Tip functionalization* *60*
*4.3.2. Surface modification* *61*
4.4. Inhibition of binding sites 64

**CHAPTER 5. Data analysis** **66**
5.1 Force curve selection 66
5.2 Parameters derived from a single force curve 68
*5.2.1. The pull-off force and force histogram* *69*
*5.2.2. The rupture length and its histogram* *74*
*5.2.3. The bond stiffness* *76*
*5.2.4. The number of ruptured bonds* *78*
*5.2.5. The unbinding probability* *79*

**CHAPTER 6. Cancerous changes studied by AFM** **80**
6.1 Molecules on a cell surface 80
*6.1.1. N-cadherin* *80*
*6.1.2. Glycans* *81*
6.2 AFM studies of N-cadherin and of glycans interactions 83
*6.2.1. Force histogram and unbinding force determination* *84*
*6.2.2. Bell model parameters* *91*
*6.2.3. Energy landscape reconstruction* *96*
*6.2.4. Lifetime of the studied complexes* *99*
*6.2.5. Kinetic profiles* *101*
*6.2.6. Unbinding length and bond stiffness* *103*
*6.2.7. Number of ruptured bonds* *108*
*6.2.8. Unbinding probability* *110*
*6.2.9. Summary* *111*

**CHAPTER 7. Conclusions** **115**

**ACKNOWLEDGEMENTS** **118**

**PUBLICATIONS** **119**

**REFERENCES** **120**

**FIGURE CAPTIONS** **128**

**TABLES** **134**

**APPENDICES** **135**
Appendix 1. Protein structure organization 135
Appendix 2. Cantilever and piezoelectric scanner properties 138
Appendix 3. Equations of the analytical solution for the cantilever normal spring constant determination 139
Appendix 4. Distribution of the resonant frequencies 141
Appendix 5. The influence of the contact time on the unbinding force 142
Appendix 6. Young's modulus determination 143
Appendix 7. Hydrodynamic drag force 144
Appendix 8. Monosaccharide structure – glucose as an example 147

# ABBREVIATIONS

AFM – atomic force microscopy,
AMPA – amino-3-hydroxy-5-methylisoxazole-4-propionic acid,
a-BSA – monoclonal antibody against bovine serum albumin (BSA),
a-PSMA – monoclonal antibody against membrane form of prostate specific antigen (PSMA),
ATCC – American Type Culture Collection,
ATP − adenosine tri-phosphate
A375 – human skin metastatic melanoma,
BFP – biomembrane force probe,
BC3726 − *v-raf* transfected human non-malignant epithelial cell of ureter (HCV29) line,
BSA − bovine serum albumin,
ConA – concanavalin A, lectin from *Canavalia ensiformis,*
CaY − carboxypeptidase Y,
CHO – chinease hamster ovary cells,
DFS − dynamic force spectroscopy,
DNA – deoxyribonucleic acid,
Du145 – human androgen-independent prostate carcinoma,
ECM − extracellular matrix,
EDTA − ethylene-di-amine-tetraacetic acid
FN − fibronectin,
FWHM – full width at half maximum,
HWHM − half width at half maximum,
HCV29 – human non-malignant epithelial cells of ureter,
Hu456 − transitional cell cancer of urine bladder,
Hu609 − human non-malignant bladder epithelium,
ICAMs – immunoglobulin-like cell adhesion molecules,
LcH – lectin from *Lens culinaris*,
LNCaP – human androgen-independent prostatic adenocarcinoma,
MaxEr − maximum error,
NCAM – neural cell adhesion molecule,
PBS – phosphate buffered saline,
PC3 – human androgen-dependent prostate carcinoma,
PDMS − polydimethyl(siloxane),
PEG – poly(ethylene) glycol,
PSA – prostate specific antigen,
PSMA – membrane form of prostate specific antigen,
QCM − quartz crystal microbalance,
RGD – arginine-glycine-aspartate peptide sequence,
SD − standard deviation.
SFA – surface force apparatus,
sLex – sialo-Lewis x,
SMD – steered molecular simulations,
SNA – lectin from *Sambucus nigra*
T24 – transitional cell cancer of urine bladder,
WM35 – human primary cutaneous melanoma cell line.

***CONSTANTS:***
Avogradro's constant – $N_0 = 6.022 \cdot 10^{23}$ mol$^{-1}$,
Boltzmann's constant – $k_B = 1.381 \cdot 10^{-23}$ J/K,
The unified atomic mass (dalton, Da) $u = 1.661 \cdot 10^{-27}$ kg (mass of 1/12 of $^{12}$C atom).

# CHAPTER 1

# Introduction

Functions in living organisms depend on physical phenomena. One of them, adhesion occurs between an enormous number of different proteins. The physical contact enables cells to resist and transmit mechanical forces and to maintain the integrity of tissues and the whole organism. Moreover, cells use adhesion sites like fingers that allow them to feel their environment and collect information about such properties as the presence of binding sites and the presence of other cells, elasticity of substrates, and strength of forces acting on cells. Cell adhesion plays crucial role in many events governing the maintenance of various tissue structures and integrity where the interactions between cells themselves and also between cells and their environment are formed. Although these adhesive interactions seem to be stable, they should be considered as dynamic ones since in many cases the binding/unbinding events are intimately involved both in changes in cell arrangements responsible for various tissue structures and in their proper physiological functioning. The defensive role of the immune system is an example of the process where the interactions between single molecules are essential for organisms. Malfunctioning of the immune system can result in severe disorders, such as autoimmune diseases, hypersensitivities, or immune deficiency *(Lodish et al. 2004)*. Another example of the cell adhesion is a cell migration, which is dependent on the continuous formation and dissociation of specific bonds between the cell adhesion molecules and the cell environment *(Carlier et al. 2007; Geiger et al. 2001)*. All these biological functions of proteins depend on their direct *physical interactions* (i.e. contacts) with other molecules.

Cancer is a very complex disease involving multiple molecular and cellular processes arising from a gradual accumulation of genetic changes in individual cells. The most apparent morphological change occurring during the transition from a benign tumor to malignant and metastatic tumors is that cells change from highly differentiated normal cells to migratory and invasive phenotypes. Nowadays, about 90% of all cancer deaths are due to metastatic spread of primary tumors. Thus far, the criteria utilized to detect cancerous cells have mainly relied on a biological description, which is achieved on a morphological basis that may be complemented by a variety of other techniques, including genetic, chemical, and immunological methods applied in order to fine-tune diagnosis or therapy. Despite enormous efforts to develop better treatment protocols, our ability to cure solid tumors, such as those of the breast, prostate, cervix or colon, has not significantly improved in the past 30 years. Unequivocally, earlier diagnosis has been shown to be the most important factor in prognostic outcome *(Christofori 2006)*.

One of the key phenomena in metastasis includes adhesive interactions maintained by distinct type of adhesion molecules present on a cell surface. Cancerous cell aptitude for invasion and migration (clinically interpreted as tumor aggressiveness) has been associated with poor differentiation of the cell and the reduced adhesive interactions that characterize a vast majority of cancer cells.

This monograph presents the novel approach which aims to identify and diagnose cancerous cells through the implementation of the physics methods − Atomic Force Microscopy (AFM), with which one can characterize the intermolecular interactions in qualitative and quantitative way with a very high spatial and temporal resolution. The AFM measurements have been performed to answer the question whether an individual molecule or its part displays different binding properties in cancerous cells compared to normal ones. The data analysis has been improved by determination of additional parameters as rupture length, system spring constant, and unbinding probability. The proposed methodology of cancer identification at the level of individual cells gives the information, which is inaccessible by currently used techniques. Moreover, it will allow a quantitative description of cancer-related changes on individual cells.

## 1.1 Adhesion between cells

Cells adhere to their environment, i.e. to other cells or to the extracellular matrix (ECM)[1], at specialized adhesion sites (called *binding sites*) with the involvement of a large number of proteins that are molecules participating in almost all biochemical reactions in living cells *(Lodish et al. 2004)*. Proteins are designed to bind to other molecules, from ions to large protein or nucleic acids. The protein binding site is reserved for a specific[2] molecular interaction with certain physical properties that make such a binding favorable and reversible. The specificity of the binding site for a particular molecule (*a ligand*[3]) can vary depending on the structure of the protein. For example, a protein (*a receptor*) may be able to bind two different ligands and each of these ligands will then compete for the proteins binding site. Typically, these different ligand molecules will share some structural properties and thus both will be able to fit into the binding site on the protein (this is known as *a competitive binding*). In some cases, however, there may be more than one binding site on the single receptor. In consequence, two different or two similar ligands may be able to bind to such protein, one at each binding site.

[1] The extracellular matrix is the non-cellular component of an organism. It is a complex network of polysaccharides (e.g. hyaluronan acid) and proteins fibers (e.g. collagen or fibronectin) which are secreted by cells and serve mainly as structural elements *(Lodish et al. 2004)*.

[2] In this monograph, the term "***specific interaction***" is used for a receptor mediated adhesion where the binding sites of the interacting molecules are complementary. The term "***non-specific interaction"*** is reserved for the interactions where there is no such structural complementarity *(Lodish et al. 2004)*.

[3] The convention used in this monograph names i) ***a ligand*** as a molecule dissolved in solution or attached to the tip used in atomic force microscopy and, ii) ***a receptor*** as a molecule present in cell membrane or immobilized on a substrate surface.

Usually, biological adhesion on a cell level, is based on the formation of clusters containing a large number of adhesion receptors, which mediate contact to specific ligands, either carried by other cells or present in the extracellular matrix *(Bongrand 1999)*. The large number of receptors in *adhesion clusters* and their dense arrangement in the vicinity of ligands facilitates rebinding of broken bonds and stabilizes the clusters. This allows stable and long-living cell adhesion sites to be formed by weak bonds and prevents disintegration of the interactions. On the other hand, the existence of many weak bonds instead of a single strong bond prevents against failure of such individual bond. Therefore, it increases the flexibility of adhesion sites, and allows rapid rearrangement of the contacts in response to external stimuli *(Bongrand 1999)*. Figure 1.1 shows a single adhesion receptor present on a cell surface: an integrin molecule linked to actin filaments being a structural element of cellular scaffold *(Horwitz 1997)*. The integrin receptor is assembled in the plasma membrane and bound to its ligand (fibronectin) on the extracellular side. Inside the cell, different proteins attach the integrin receptor to the actin filaments.

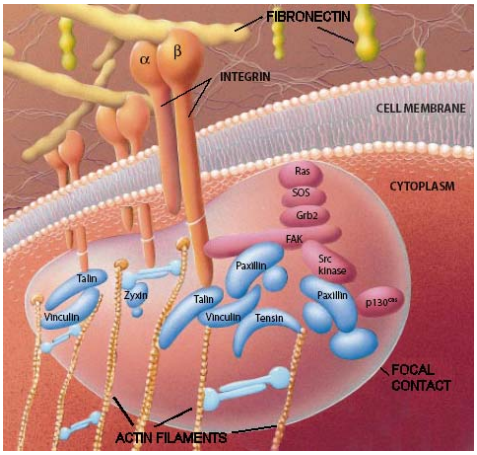


Figure 1.1. Illustration of an integrin (i.e. a cell surface adhesion receptor) anchorage in cell membrane and its linkage with actin filaments (adapted from *Horwitz, 1997*).

Adhesion clusters are usually assemblies of transmembrane proteins that are held in the plasma membrane of the cell by hydrophobic interaction. On the extracellular matrix side (outside the cell), they have a binding site for ligand molecules that may either be proteins or other molecules such as carbohydrates. On the cytoplasmic side (inside the cell), these receptors are very often linked to the cytoskeleton (*a cellular scaffold*). In many cases, association with distinct proteins strengthens and regulates these links. In that manner cells transmit and/or resist tension of tissues. The stability of adhesion clusters can be influenced by changes of the unbinding and rebinding probability through changes in the distance of a receptor and a ligand, and through conformational changes of both involved molecules, which alter the affinity of the bonds, or through changes in the number of receptors controlled for example by transport processes *(Geiger 2001)*. Also, mechanical forces (both external and/or internal) exerted on or out the cell are known to influence the bond dissociation. Such control mechanisms enable dynamic formation and destruction of adhesion clusters, as it happens for example during cell migration, where adhesion clusters formed at the leading edge of the cell have to be disintegrated at its rear side *(Goffin 2006)*.

Forces[4] between various molecules in living organisms are not different from those arising between any other molecules or surfaces *(Bongrand 1999; Israelaschvili 1992)*. They are Columb forces in origin and are usually non-covalent interactions with binding energies in the range of few units of thermal energy $k_BT$ (≅ 4.1 pN·nm at room temperature). Such weak bonds can be disrupted by thermal activation and they have finite lifetimes *(Evans 2001)*. Depending on the electron configuration of participating molecules, forces can be relatively long-ranged as for example van der Waals forces, or short-ranged ones resulting from the screening effect (screening acts only at direct contacts between molecules at specific binding sites).

For many biological functions, the interaction between cells involves the attachment of two complementary molecules characterized by their high specificity, which is strengthened by the complementary shape of the binding sites of both interacting molecules *(Lodish et al. 2004)*. This leads to the formation of a strong interaction (Figure 1.2a proteins A and B). Any variations lead to less stable complex and, in consequence, to a weaker interaction (Figure 1.2b, proteins A and C).

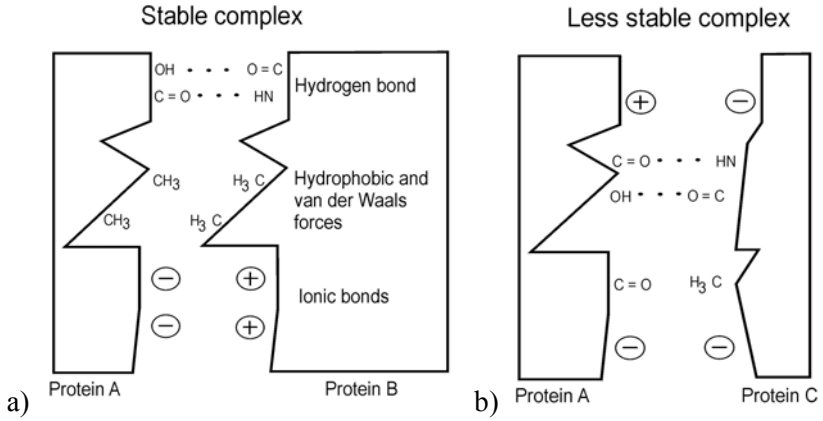


Figure 1.2. Binding between proteins. The complementary shape of the binding sites (a) together with the non-covalent interactions results in a strong adhesion. Lack of complementarity (b) leads to a less stable complex [adapted from *(Lodish et al. 2004)*].

Thus, the attraction is limited to microscopic sites, i.e. with no apparent long-ranged contribution from the van der Waals forces. These resulting attractive interaction is short–ranged and weak. It involves forces such as hydrophobic and electrostatic attraction, and hydrogen bonds that are a specific case of dipole–dipole interaction. The major part of the specific interaction results from hydrogen bonds which form a characteristic pattern on the receptor side recognized by ligands. The short range interaction and the dependence on the orientation of hydrogen bonds characterize a well-defined configuration of the two molecules at the ground state with the lowest energy. Small translation of rotation lead to an increase in energy because hydrogen bonds have to be disrupted. It

[4] The detailed description of different types of forces acting between molecules may be found in the book by J.N. Israelaschivili *"Intermolecular and surface forces"*, Academic Press, San Diego, 1992.

should be pointed out that bonds between molecules have been selected and optimized for their function as adhesion promoters. The structure of complex adhesion molecules has evolved to facilitate rapid and reliable association and dissociation *(Bongrand 1999)*.

The natural question arises why the molecule–molecule binding (referred to *a ligand–receptor binding*) is so important in biological systems and why it is so deeply investigated. Firstly, the binding between molecules is such that cells utilize to interact with huge variety of different types of molecules. Secondly, the binding is a basis for a great number of normal biological functions such as embryogenesis, cell growth, differentiation, enzyme catalysis, immunological response, etc., that are crucial for life. The loss or alteration of these interactions can affect cell functioning and can lead to many pathologies. Numerous diseases are related to the malfunctioning of the recognition processes. Investigations of the interaction mechanism are crucial for understanding the wide spectrum of biological processes present e.g. during inflammation, cancer metastasis or in the development of highly specific drugs *(Dubowchik et al. 1999)*.

## 1.2 Unbinding force measurements

Molecular bonds in cells usually have to operate under external forces. Thus, in order to understand the cell adhesion, it is crucial to investigate a bond failure under such conditions. Such studies have become valuable for biologists since they can deliver information about the structure of adhesion molecules and their binding properties that are inaccessible by other techniques. In particular, if such measurements are carried out on a surface of living cells in the conditions close to natural ones, they bring us to better understanding molecules' functioning in their normal conditions.

Many methods have been used to investigate the unbinding processes. Most of them enable studies where the unbinding involves a large number of interacting molecules. However, experiments, performed for single molecules, require observation methods with high spatial and temporal resolutions. Such methods encompass mainly: a biomembrane force probe with pipette suction *(Merkel et al. 1999)*, a hydrodynamic flow-based method *(Pierres et al. 1996)* magnetic *(Smith et al. 1992)*, and optical tweezers *(Kellermayer 2005)*, and also an atomic force microscopy (AFM, *Binnig et al. 1986*). Over last few years, AFM, invented in 1986, has become more and more applied in numerous scientific areas, especially in biology and medicine *(Pereira 2001; Simon et al. 2006; Hinterdorfer et al. 2006)*. Initially, the technique was discovered to explore structural details on solid material surfaces. Later on, it was used to image fine structural details on biological samples, in particular in liquid environment providing nearly physiological conditions for biological samples. However, not only the surface topography attracts biologists to AFM. Its great advantage is the possibility to deliver quantitative parameters that describe phenomena or features as adhesion, friction or sample stiffness *(Bhushan et al. 2007)*. These parameters can be

measured in different surrounding conditions: in ambient air, in vacuum or in liquids. Determination of physical properties of the investigated sample requires the atomic force microscope working in a contact mode, where the probing tip directly touches the investigated surface.

In particular, the AFM application to measure interaction forces between single molecules opens many possibilities to investigate biological, adhesion-related processes, with resolution allowing studies on a single cell and/or on molecule levels. The first AFM measurements were carried out for model systems with well-defined adhesive properties so that the forces acting within the binding sites could be accurately controlled. However, the most attractive feature of the AFM is the capability of measurements of the unbinding force between molecules present on a surface of living cells due to the fact that such measurement can be performed in conditions close to natural ones. It provides new insights into the force-induced unbinding of a single molecular pair. First experiments of this type were carried out for biotin-avidin complexes *(Florin et al. 1994; Izrailev et al. 1997)*. Avidin is a large, tetrameric molecule which can bind four biotin molecules with an unusually high binding energy of around ~ 20 $k_BT$. Using two of the binding sites, avidin was attached to the biotin-coated tip of an AFM-cantilever. The cantilever was brought into contact with a biotinylated agarose bead so that avidin could crosslink tip and bead. Retraction of the soft, elastic cantilever at a constant speed resulted in the linear increase of force acting on the bond. This experiment yielded a histogram of rupture forces for the biotin-avidin bond. The maximum of the distribution at around 160 pN was defined as the strength of a single avidin-biotin complex *(Florin et al. 1994)*.

Theoretical modeling of a force-induced bond rupture was initiated by steered molecular dynamic (SMD) method, performed also for the avidin-biotin binding *(Grubmüller et al. 1996; Izrailev et al. 1997)*. SMD simulates in atomic detail the force induced unbinding process of the molecules assuming the conditions of the real experiment: one end of the bond is trapped in a harmonic force field and the centre of this force field is moved outward at constant speed so that a linear force is exerted on the bond. In simulations, it is possible to follow movements of the two molecules with high resolution. Single hydrogen bonds and their formation and rupture upon translation of rotation of receptor and ligand can be observed.

So far, most of measurements of the interaction forces were performed for isolated molecules, such as different types of proteins or DNA strands, since the interpretation of the obtained results is straightforward *(Ikai 2002)*. Beside the abovementioned biotin−(strept)avidin complex, several other biological pairs have been investigated with the use of AFM. These studies encompass the interaction with cell adhesion molecules and with various types of immunoglobulins. The unbinding force was determined for several model systems, where the studied proteins were isolated. However, the direct comparison of its value, obtained for different complexes, is difficult

since the unbinding force depends strongly on the loading rate. The measured forces extend in a broad range of values. For example, the unbinding force between human albumin and its polyclonal antibody *(Hinterdorfer et al. 1996)* was of about 240 pN measured for the loading rate of 54 nN/s. At the other end of range one can place the interaction force measured for insulin–insulin complex, where the large unbinding force of 1345 pN was obtained for low loading rate of 7.4 nN/s *(Weisel et al. 2003)*. Therefore, the unbinding force can be used as a parameter characterizing a given molecular complex only under the assumption that all experimental conditions are more or less the same.

Once the measurements are performed for molecules present on a surface of living cells, the data interpretation is very difficult due to high complexity of such systems. In addition, the obtained strength of the molecules' interaction can give only partial information about the real interactions occurring between molecules in their native conditions where they interact either with its external environment or with neighboring cells in a very defined milieu. For example, the work by Lekka *et al. (Lekka et al. 2004)* compared the same type of interaction between the oligosaccharide moiety of the isolated or present in cell membrane proteins. The determined unbinding force was much larger for the isolated proteins (force was in the range of 800–950 pN) than in case where the similar oligosaccharide structure was a component of cell membrane proteins (116 ± 17 pN).

Parallel to the determination of the interaction strength, functionalization of the AFM tips has opened the possibility of the imaging where the modified tip is scanned over a surface (a so-called *affinity imaging*). The measured unbinding force contributes to a contrast of a recorded image, which arises from the biomolecular specific interactions. In work by Lekka *at al. (Lekka et al. 2005)*, the AFM was applied simultaneously as both chemical- and friction- force microscopes to study a typical carbohydrate–protein interaction. The former mode was realized by modifying the AFM tip and substrate surfaces with a pair of proteins recognizing each other, while the latter one was accomplished by recording the lateral force signal. Measurements were carried out for lectin concanavalin A (ConA) having the specificity to mannose and glucose units. As a complementary molecule, protein carboxypeptidase Y (CaY) was chosen since it possesses the covalently attached carbohydrate structure mainly composed of mannose units. Proteins were deposited on the sample surface using micro-printing with PDMS stamps[5] with periodically arranged holes. The surface topography of immobilized proteins (CaY or BSA) reflected the patterns of the used PMDS stamp. Figure 1.3a presents the surface topography of the CaY deposited on the modified glass surface.

[5] Micro-printing technique (μCP, *(Delamarche et al. 1997)*) is a technique applied to produce the well defined patterns of polymers (also biomolecules) on different substrates with the use of a polymeric stamp made of poly(dimethylsiloxane) (PDMS).

The friction force map obtained for ConA–CaY complex showed the same pattern, which corresponded to chemical diversity of the sample. The areas outside the circles were covered with the CaY while the interior of each circle corresponded to the silanized and glutaraldehyde treated glass surface.

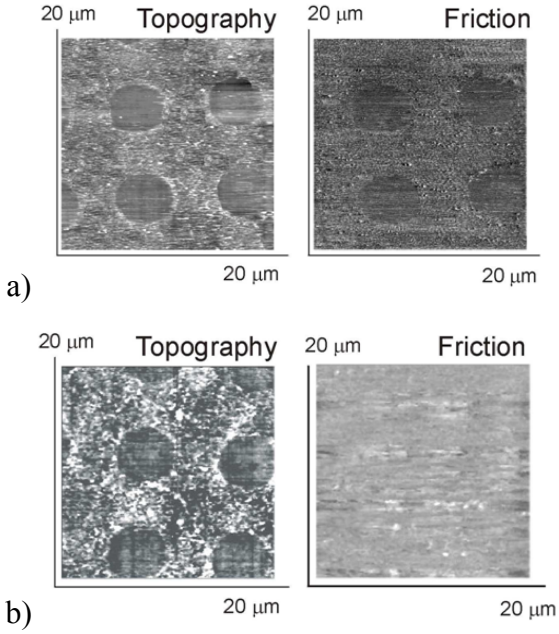


Figure 1.3. Surface topography (left) and friction force (right) images recorded at the same lateral loading rate of $1.4 \times 10^9$ pN/s, measured for (a) ConA−CaY and (b) ConA−BSA molecular complex measured in a buffer solution *(Lekka et al. 2005)*. Lack of contrast in friction force images, observed for ConA−BSA, confirms the specificity of the ConA−CaY interaction (a).

In order to verify that the observed for ConA–CaY complex was of specific character, measurements were performed for the ConA functionalized AFM tip and a BSA printed surface for which no specificity was expected (BSA molecules did not have attached carbohydrate structure). In this case, the friction force did not show any pattern while the surface topography still reflected similar pattern like in the case of the patterned CaY surface (Figure 1.3b).

The application of the affinity imaging to detect the presence of particular cells has been presented by Grandbois *et al. (Grandbois et al. 2000*). In these measurements, the sample was composed of two populations of erythrocytes coming from A and 0 blood groups. The erythrocyte surface was probed using the AFM tip modified with the lectin *Helix pomatia* that recognizes *N*–acetylgalactosamine terminated glycolipids characteristic for the group A. Using such modified AFM tip it was possible to distinguish cells between these two groups.

In the other work *(Yersin et al. 2007)*, the AFM was used for trafficking of single receptors at the surface of living neurons. The technique enables the simultaneous recording of the living cells

topography, their elastic properties, and of the distribution of AMPA[6]-type glutamate receptors. The results showed that on non-stimulated neurons, the receptors were located in stiff nanodomains with high elasticity modulus (relative to the remaining cell surface). Receptor stimulation provoked a permanent disappearance of these stiff nanodomains, followed by a decrease (53%) of the number of surface receptors. These results showed that modulation of receptor distribution is accompanied by changes in the local elastic properties of cell membrane.

The presented examples demonstrate a great potential of the AFM technique based on the affinity imaging. Such measurements can distinguish between different types of receptors and provide their location. This may be very useful either in the investigations of cell affinity alterations due to drugs used in the cancer treatment or in the studies of membrane receptors expression of different types of cancers. Figure 1.4 presents the typical distribution of sialic acid residues on surfaces of living non-malignant and malignant bladder cells.

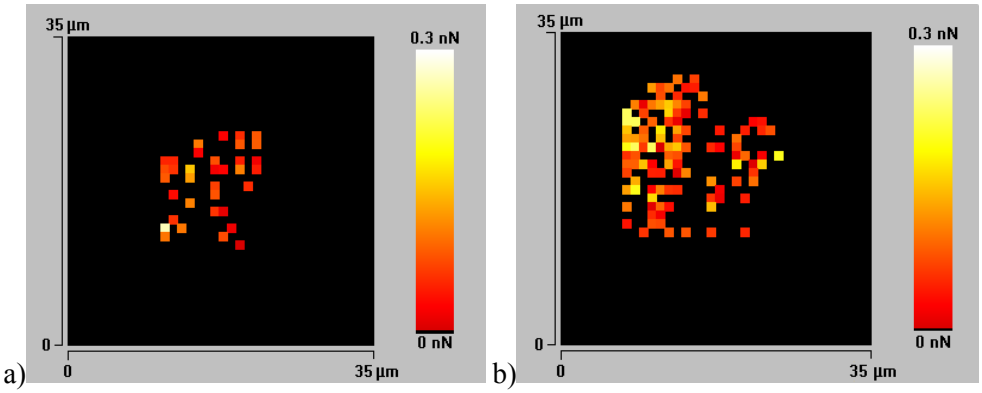


Figure 1.4. The distributions of sialic acids residues on the surface of (a) non-malignant HCV29 and (b) malignant T24 bladder cells. The central part of a cell (~20 µm diameter) was probed, each spot has the same size of ~1 µm. Black color denotes no adhesion events.

These results confirmed the non-homogenous distribution of the binding sites on both cell surfaces. The number of adhesion events was larger in case of cancerous cells what showed the larger amount of sialic acid residues on cancerous cells. The unbinding force reached higher values strongly suggested the multiple unbinding events, i.e. the simultaneous rupture of a few bonds. This indirectly indicates the presence of groups (clusters) of more than one mannose-type ligands.

## 1.3 Detection of malignant alterations in cancerous cells by AFM

It is obvious that novel techniques are in the limelight if they are able to bring more precise, local information about cancerous changes as early as possible. The atomic force microscopy is one of such candidates since it has many advantages that make it a valuable tool in biology. The main

[6] AMPA -amino-3-hydroxy-5-methylisoxazole-4-proprionic acid.

feature is the possibility to measure biological objects directly in their natural environment, such as buffer solutions or culture media.

The cells transformed oncogenically differ from normal ones in many ways. Variations in any aspects such as cell growth, differentiation, interactions of cells with neighboring cells and/or with extracellular matrix, and organization of cell cytoskeleton and several others have been already described[7]. Poor differentiation of the cell cytoskeleton can result in the larger deformability of cancerous cells. Low stiffness of cancer cells may be caused by a partial loss of actin filaments and/or microtubules, and therefore by lower density of the cellular scaffold *(Ben-Ze'ev 1997; Yamazaki et al. 2005)*. There are rather few methods capable to assess cell mechanical properties. Historically, the first technique was the micropipette aspiration *(Drury et al. 1999; Hochmuth 2000)*. Other researchers have employed the magnetic bead rheology *(Bausch et al. 1999)*, microneedle probes *(Zahalak et al. 1999)*, acoustic microscopes *(Kundu et al. 2006)*, and the manipulation of beads attached to cells with optical tweezers *(Sleep 1999)*. Among these techniques, the atomic force microscopy is able to detect most of malignant changes with a very high resolution, being applied either in imaging mode or as the technique providing information about the mechanical properties of living cells (i.e. their ability to deform and to adhere) in a quantitative manner.

### *Cell ability to deform*

The cell elasticity determined via AFM is a very local feature, showing large discrepancy in the Young's modulus[8] measured on a population of cells as well as on a single cell. It has been reported that cells *in vitro* have the Young's modulus values in the range of 1–100 kPa *(Radmacher 1997; Sokolov 2007)*, which encompasses different types of investigated cells, including vascular smooth muscle cells, fibroblasts, bladder cells, red blood cells, platelets, and epithelial cells. Since different cell types are measured, the large modulus variation is fully justified. Despite the lack of absolute value of the Young's modulus, the obtained relative change of the elastic modulus is sufficient to describe the alterations in cancerous cells. One of the first measurements on a cancer cell line was performed in 1993. The human lung carcinoma cells were measured and the obtained Young's modulus value varied from 13 kPa to 150 kPa *(Weisenhorn et al. 1993)*. Later on, in 1998, some studies showing that the vinculin–deficient F9 mouse embryonic carcinoma cells had slightly lower Young's modulus (2.5 ± 1.5 kPa) than the wild–type cells (3.8 ± 1.1 kPa) were presented. The authors attributed these changes to the altered actin cytoskeletal organization *(Goldmann et al.*

[7] The comparison of properties of cancerous and normal cells can be found in the book by I.Damjanov "*Pathology for the health-related professions*", W.B.Saumders Company, Philadelphia, 1996.

[8] The review on the use of the Young's modulus for characterization of biological samples may be found in the book by B.Bhushan, H.Fuchs, *"Applied Scanning Probe Methods II",* Springer, Berlin, Heidelberg New York, 2006, *in Chapter 7 by M.Lekka, A.Kulik "Quantitative nanomechanical measurements in biology"*.

*1996)*, indicating an important role of vinculin as an integral part of the cytoskeletal network. Lekka *at al*. reported in 1999 the first comparative studies of the mechanics of non-malignant and malignant cells *(Lekka et al. 1999a)*. They show that the Young's modulus of three human cancerous bladder cell lines (T24, Hu456, BC3726) is one order of magnitude lower than that for the reference cells. These measurements were confirmed in 2005 by Guck *et al. (Guck et al. 2005)* and by Park *et al. (Park et al. 2005)*. In the former paper, the authors showed that the cell deformability is sensitive enough to monitor changes during the progression of mouse fibroblasts and human breast epithelial cells from normal to cancerous cells. The latter showed a much wider distribution of the Young's modulus (0.34–4.95 kPa) of normal fibroblasts than the malignantly transformed cells. Having in mind the diagnostic application of cell elasticity, the finding of the correlation between the degree of malignancy of different melanoma cell lines and Young's modulus values is essential for the use of AFM in cancer research. Such correlation was found for melanoma cells *(Lekka et al. 2007* where the most malignant cell lines had the smallest Young's modulus (Figure 1.5).

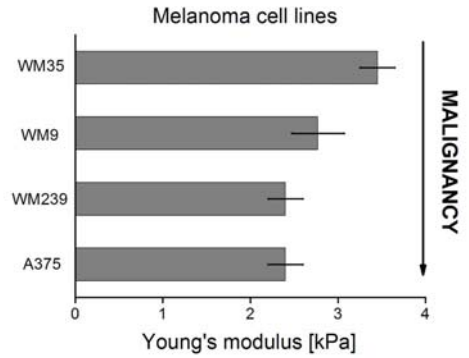


Figure 1.5. The correlation between the decrease of Young's modulus with the increase of malignancy of melanoma cells *(Lekka et al. 2007)*

The observed differences in the Young's modulus value enabled tracing the alterations within cell populations due to the drug action. This was demonstrated in studies showing the correlation between cell stiffness and glycolytic activity as a function of various chitosan deacetylation degrees (defined as a ratio of the number of amino groups to the sum of amino and acetyl groups). The increase of Young's modulus was associated with the decrease of glycolytic activity in cancerous cells. The modulus value was unaffected for the reference cells, what indicated the cancer-specific action of chitosan *(Lekka et al. 2001)*.

In general, malignant cells respond either more elastically (softer) or less viscously to the applied stress. This is because metastatic cells must be squeezed to go through the surrounding tissue matrix when they make their way into the circulatory systems where they are directed to establish distant settlements *(Farina et al. 1998)*. These findings suggest that cell stiffness can be used as a marker and also as a diagnostic parameter for the underlying disease. Therefore, the measurements of Young's modulus of cells can in future help to determine the range of cytoskeleton changes and allow quantifying them. The cancerous alterations linked with cell stiffness seem to be relatively

straightforward and non-specific. They are induced in the whole volume of cells, and therefore are easier to be measured by different techniques.

*Cell ability to adhere*

The cancerous transformation changes the adhesive properties, therefore, a natural direction for the studies is the determination of changes in cell's adhesive interactions through measurements of unbinding forces between particular molecules that are well-established (as potential) markers of the disease. The expression of different types of molecules can be studied using several other methods. The most popular are the immunodetection of blotted proteins (i.e. Western blot technique) and fluorescence based methods (fluorescence microscope or flow cytometry). In the former method, the presence of a given interaction can be detected and used for estimation of the molecular mass of the formed complexes. However, these experiments deliver only qualitative information related to bond strength. Furthermore, the cell membrane is usually blocked in order to prevent non–specific antibody binding. This step is not needed in the AFM measurements since the specific interaction is a discrete one, manifesting as a periodicity in the force histogram. The fluorescence-based methods require fluorescent-labeled molecules. Again, they are not needed in AFM, where if there are no specific requirements, the native protein is immobilized using a rather simple protocol. Applying fluorescence, the detection of bound complexes is performed relatively easy. However, the quantitative information about their number (or density), and about the strength of interaction is indirect. These parameters can be estimated only by measuring fluorescence intensity. Therefore, the AFM measurements of the unbinding forces between single molecules are of great interest for many biologists, since in contrast to standard biochemical or cell biology methods, this technique can be used not only for the detection of molecules on the cell surface but also it gives additional information about the physical properties of the studied interaction. The technique offers a convenient way to measure forces involved in specific interactions by detection of the unbinding events between the AFM tip functionalized with one type of molecules (a ligand) probing its complementary partner (a receptor) which can be either immobilized on the substrate or present on a surface of the cell plasma membrane. So far, the AFM technique has been mostly applied to study the interaction of different molecular complexes for isolated molecules in buffer conditions *(Zlatanova et al. 2006)*. However, some attempts have been also focused on studies of receptors present on the living cell surface. Such measurements require that the force to uproot the receptor from the cell membrane is higher than the force necessary to rupture the molecular bonds *(Ikai 2004)*. This assumption has been justified by several studies *(Oesterhelt et al. 2000; Afrin et al. 2004)*. Depending on the way of the data collection, one can distinguish two groups of measurements: static and dynamic ones. The static force spectroscopy when performed at well-defined experimental conditions can provide useful information about the strength of the

interaction of different types of molecules present on a surface of living cells. In that manner the interaction between integrins[9] present on living osteoclasts and their different ligands was quantified *(Lekenkari et al. 1999)*. The studied ligands had a common RGD (Arg-Gly-Asp) sequence which was recognized by integrins with high affinity. The obtained unbinding force varied from 32 pN to 97 pN, demonstrating that the context of RGD sequence within a protein considerable influences the unbinding force value.

Several studies have been focused on differences between normal and cancerous cells where the AFM technique has been shown to be complementary to other biochemical methods *(Laidler et al. 2005; Lekka et al. 2006)*. Using AFM, the characterization of the expression of cell surface molecules in different cancerous cells can be used to show either the antigenic identity of receptors, or their dissimilarities, or alterations of the binding site within the same receptor type. Thus, for example, the presence of the same surface molecule, i.e. the membrane form of prostate specific antigen (mPSMA[10]) has been shown in three cancerous prostate cells, without and with the induced expression of mPSMA by the chosen growth factors *(Laidler et al. 2005)*. These studies showed that there were rather a few PSMA molecules present in the plasma membrane of all investigated cell lines. Moreover, the calculated unbinding force of a single antibody–mPSMA complex present on prostate cells, regardless of growth factors treatment (or lack of treatment), was in the range of 45–64 pN. The differences of single-molecule interactions in the living cancerous cells have been demonstrated by Lekka et al. in carbohydrate[11] recognition *(Lekka et al. 2006)*. This work proposed the AFM as a method to interrogate both the identity of the complex carbohydrates as well as their relative number on the cell surface. The unbinding force, determined for the same molecular ligand, suggested slightly dissimilar structure of the binding sites of the same receptor present on cell surface. For the other lectin probe (agglutinin from *Phaseolus vulgaris*) much larger unbinding force indicated a distinct structure of the binding site in cancerous cells. The unbinding probability confirmed a higher content of both sialic acids and mannose-containing carbohydrates in cancerous and reference cells.

The unbinding force measured by AFM is not a fundamental property of a single ligand-receptor complex but it depends on how fast the external force applied to a single bond changes in time (i.e. on loading rates). The studies of the unbinding force as a function of loading rate bring the information on the properties of the energy landscape of the interacting molecules. Such studies, called *dynamic force spectroscopy*, were applied to investigate the single-molecule

[9] Integrins are cell surface receptors responsible for the interactions with extracellular matrix (outside the cell), see *Chapter 2* for more details.

[10] PSA – prostate specific antigen is nowadays used for the detection of prostate cancers. Its membranous form (mPSMA) is more specific for oncogenic alterations, and therefore, can be used as a better cancer marker.

[11] Complex carbohydrates (i.e. glycans) belong to a class of molecules present on the cell surface (for more details see *Chapter 2*).

interactions on a living cell surface. The most common integrin receptor is the $\alpha_5\beta_1$ integrin, which interacts with a fibronectin (FN). An important intrinsic property of the $\alpha_5\beta_1$−FN interaction is the dynamic response of the complex to a pulling force. The AFM measurements carried out for this interaction revealed two distinct regimes during unbinding: a fast loading rate and a slow one, both characterize the inner and outer activation barriers of the complex, respectively. The use of genetically changed fibronectin showed that both inner and outer activation barriers were suppressed by the mutation *(Li et al. 2003)*. In other studies, the adhesion mediated by another integrin ($\alpha_4\beta_1$) has been investigated. The mechanical strength of the interaction allows resisting the large shear forces imposed by the bloodstream *(Zhang et al. 2004)*. The employed single-molecule dynamic force spectroscopy showed that the dissociation of the $\alpha_4\beta_1$ from its ligand complex involves overcoming of least two energy barriers: a steep inner barrier and a more elevated outer barrier. The inner barrier grants the complex the tensile strength to withstand large pulling forces (> 50 pN). The outer barrier of the complex was stabilized by integrin activation. Together, these findings can provide a molecular explanation for the functionally relevant kinetic properties of the studied interaction involving $\alpha_4\beta_1$ integrin. Recently, Taubenberger *et al.* characterized early steps of integrin-mediated cell adhesion to a collagen type I by using single-cell force spectroscopy *(Taubenberger et al. 2007)*. In agreement with the role of $\alpha_2\beta_1$ integrin as a collagen type I receptor, the $\alpha_2\beta_1$-expressing Chinese hamster ovary (CHO)-A2 cells spread rapidly on the matrix, whereas $\alpha_2\beta_1$-negative CHO cells adhered poorly. Probing CHO-A2 cell detachment forces over a contact time range of 60 s revealed a nonlinear adhesion response. During the first 60 s, cell adhesion increased slowly, and forces associated with the smallest rupture events were consistent with the breakage of individual integrin–collagen bonds. Above 60 s, a fraction of cells rapidly switched into an activated adhesion state marked by up to 10-fold increased detachment forces. Elevated overall cell adhesion coincided with a rise of the smallest rupture forces above the value required to break a single integrin–collagen bond, suggesting a change from single to cooperative receptor binding. Transition into the activated adhesion mode and the increase of the smallest rupture forces were both blocked by inhibitors of actomyosin contractility.

## 1.4 Overview of the monograph

The present monograph demonstrates the applicability of AFM to study the expression of different types of molecules on the surface of living cells, with the emphasis on application of the AFM to detect cancerous alterations. The results, which will be presented here, show that the quantities obtained *via* AFM are reliable parameters describing the expression of molecules on a surface of living cells. The developed analysis was applied to characterize the alterations in cancerous cells.

The analysis of the interaction forces performed by AFM allows the quantitative determination of: *i)* the static properties of a single molecular complex where its strength of interaction and stiffness of the studied complex can be obtained, *ii)* dynamic properties, on the basis of which the kinetic properties of the unbinding process can be delivered. They are described by two parameters: dissociation rate constant and the position of the energy barrier in the energy potential, and *iii)* properties of adhesion clusters, where the inter-relation between single complexes can be characterized, in particular the mechanism of the unbinding can be obtained.

The full quantitative description of a given type of molecules has been developped using following quantities extracted from AFM measurements:

- ***the unbinding force*** which is directly measured by AFM. The stronger unbinding force means the more difficult rupture of the molecular complex, and thereby the more stable complex formed. On the other hand, when a certain ligand type recognizing the specific structural fragment of its receptor is immobilized on the AFM probe, any variation of the force value indicates the alteration in the structure of the receptor-binding site.
- ***the rupture length*** which determines a distance at which molecules separate. Its value is characteristic for a given bond type and can be used in order to distinguish the bond properties. When a spacer is applied to attach molecule to the AFM probe surface, the length of the spacer will enlarge the rupture length. Also, when interacting molecules are embedded in a membrane of a living cell, the rupture length can contain the contribution originating from stretching of the cell membrane.
- ***the effective spring constant*** that takes into account two types of springs in series: a cantilever spring constant and a stiffness either of a single molecular bond participating in the rupture event or of a whole system composed of a receptor embedded in the cell membrane.
- ***the unbinding probability***, which corresponds directly to the number of molecules that are present on the surface of living cell. The unbinding probability can be related to the density of surface receptors.

A major part of the experiments was carried out with the use of a home–built atomic force microscope, working at the Institute of Nuclear Physics, Polish Academy of Sciences in Kraków. Crucial importance for all performed studies was the access to cell lines obtained from the Chair of Medical Biochemistry at the Jagiellonian University Medical College in Kraków. Part of the measurements was carried out using atomic force microscopes working at the Institute of Physics of Complex Matter (Ecole Polytechnique Federale de Lausanne) in Lausanne, Switzerland. All measurements and data analysis have been performed by the author.

The monograph is divided into several parts:

− *Chapter 2* contains the introductory description of the structure of the studied molecules present on a surface of living cells.

− *Chapter 3* describes the basis of the theory on the force-induced rupture of molecular bonds for both single and multiple adhesion events.

−*Chapter 4* presents the main issues that are related to the atomic force microscope working in force spectroscopy mode. Due to the importance of the quantitative data delivered by AFM, the large part of this monograph is devoted to the calibration procedure. A brief description of the AFM tip functionalization is provided as well.

− *Chapter 5* is related to the data processing since, apart from the experimental difficulties with a proper sample preparation and the measurement in liquid conditions on a living cell surface, the way of data processing and their proper interpretation is still under development. Only careful data analysis and independent verification allow the exact determination of the unbinding force. Therefore, the large part of this work describes the different aspects of the data processing that are important for proper data interpretation.

− *Chapter 6* presents the obtained results of studies on the expression of different types of molecules on a surface of cancerous cells. This chapter includes results obtained in a search of differences of N-cadherin expression. This biological system is relatively simple since it involves the recognition based on a typical antigen-antibody interaction that is unambiguously defined if monoclonal antibodies are used. Characterization of the more complicated system, where the specific interactions are not well defined, is demonstrated for the specific glycan recognition. To enable comparison with studies on N-cadherins, the results obtained for measurements performed on the surface of bladder cells have been chosen.

− *Chapter 7* includes summary and main conclusions related to the study of the expression of cell surface molecules in the context of alterations in cancerous cells.

# CHAPTER 2

## Molecules on a cell surface

All living organisms are built up of cells – the basic units of living matter. Every cell, in order to carry out all living functions, has to preserve its integrity, to limit and/or to control the contacts between its interior and the surroundings. Inside the cell proceed many highly specialized, complex, and very often quite contradictory processes localized in subcellular organelles. The structure enabling these functions is called *a biological membrane*. Each biological membrane is composed mainly of complex lipids and proteins (Figure 2.1).

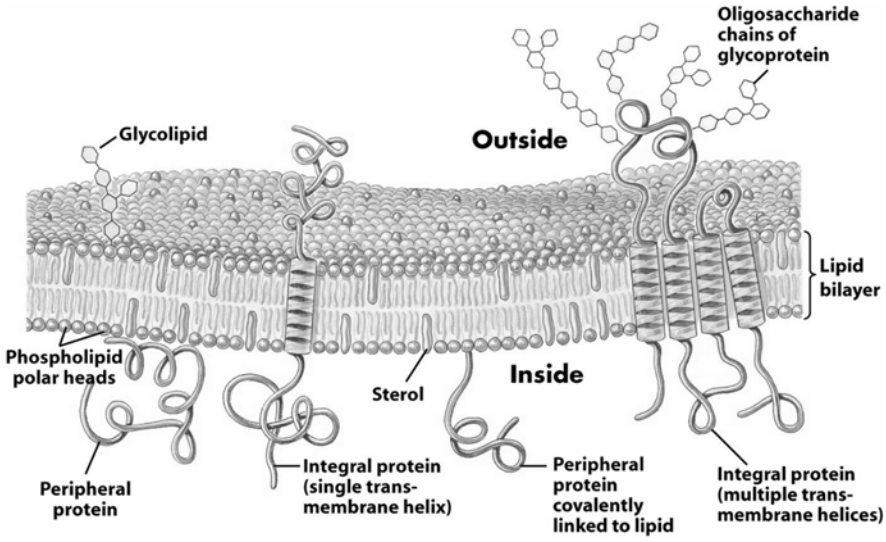


Figure 2.1. Fluid mosaic model of a plasma membrane (image was taken from *Nelson et al. 2005*).

The lipids, due to their amphipathic (i.e. partly hydrophobic and partly hydrophilic) properties, form – in water or water solutions – a sheet-like structure called *a lipid bilayer*, which is an impermeable barrier for the majority of solutes present in biological fluids. Consequently, a lipid bilayer physically separates the interior of a cell from its surrounding. Simple and complex ions, hydrophilic molecules (such as glucose), and even some hydrophobic compounds such as fatty acids cannot pass through most membranes. Therefore, to enable communication between a cell and its surrounding, additional molecules must be present in the plasma membrane. These are the numerous specialized proteins that serve as pumps, carriers, receptors, etc., enabling a more or less selective recognition of solutes and their translocation in and out the cell. Interaction between a plasma membrane receptor and its ligand usually triggers a complex sequence of events inside the cell, known as signal transduction that more or less affects cell behavior: proliferation, motility, apoptosis, or metabolism *(Lodish et al. 2004)*.

There are many types of membrane proteins. It is important to remember that they can move laterally in the cell membrane due to the fluid nature of the whole structure. Thus, they should move to place where their function is required. Membrane proteins can be divided into three main classes: integral, peripheral, and lipid anchored proteins. The *integral proteins* are fully incorporated into the cell membrane and contact both the inside and the outside of the cell. The *peripheral proteins* are proteins of the cytoplasmic surface of the membrane that are non-covalently bound to the polar head group of the lipid bilayer or to an integral membrane protein. The *lipid anchored proteins* are membrane proteins that are covalently bound either to a phospholipid or a fatty acid that is embedded in one of the leaflets of the lipid bilayer *(Lodish et al. 2004; Lipowsky et al. 1995)*. Many of the integral membrane proteins, on the extracellular side of the membrane, contain one (rarely) or more oligosaccharide components (due to the origin called also *carbohydrate moieties*). An individual oligosaccharide chain covalently bound to a protein is called *a glycan* and such proteins are called *glycoproteins*.

Adhesion of biological cells is based on clusters containing a large number of adhesion receptors, which mediate contact to specific ligands either carried by other cells or present in the extracellular matrix. These clusters are assemblies of transmembrane proteins that are held in the plasma membrane of the cell by hydrophobic interaction. On the cytoplasmic side (i.e. inside the cell), receptors can be linked to the actin cytoskeleton. A binding pocket on the extracellular side allows specific interaction with appropriate ligands.

## 2.1 Cell surface adhesion molecules

Cell–cell and cell–extracellular matrix protein interactions require adhesion molecules that are present as integral plasma membrane proteins, and are exposed to the extracellular environment. All adhesion molecules are glycoproteins classified into four main families participating in the intercellular interactions: cadherins, integrins, selectins, and immunoglobulin–like superfamily. The interactions between them can be divided into two classes: homophilic (with the same partner) and heterophilic (a complementary distinct ligand is needed). They are variously expressed in different cells of the same organism and often by the same cell at various stages of their development and in various metabolic circumstances. All adhesion molecules mediate numerous contacts (interactions) between cells and their surroundings i.e. other cells and proteins embedded in the extracellular matrix. The structural arrangement of protein molecules determines cell interactions (its strength, lifetime, association and/or dissociation constants, etc.) with more or less specifically recognized ligands, antibodies, and other proteins at the physicochemical level.

*Cadherins*

The most important adhesion molecules are cadherins. They are involved in formation of cell–cell adherent junctions that are critical for the maintaining of tissue architecture, cell polarity, limiting cell movement, proliferation, and also in the transformation and invasion of cancer cells *(Lodish et al. 2004; Leckband et al. 2006)*. Cadherins constitute a superfamily of transmembrane glycoproteins located in the plasma membrane. They provide strong intercellular adhesion in a $Ca^{+2}$ dependent manner. Cadherins are divided into a few subgroups. The most typical members are: i) *E-cadherin* – mostly expressed in epithelial tissue of various organs and recognized as one of the suppressors of cancers, ii) *N-cadherin* – mainly found in neural tissue and many cells at their fetal stage of development, but also common to many metastatic tumors and therefore known as a tumor inducer, iii) *P-cadherin* – found initially in the placenta. Classic cadherins appear in single polypeptide chains of different lengths (about 730 amino acids) and different molecular weights. They are composed of i) a large N-terminal extracellular domain (mediating homophilic type cell adhesion), ii) a short transmembrane domain, and iii) a highly conserved C-terminal cytoplasmic domain. The latter one interacts with cytoplasmic skeleton proteins as α-, β-catenins and plakoglobin (γ-catenin) and through them with the actin cytoskeleton. This seems to be a key event in the interaction between extracellular domains of E-cadherin and intracellular cytoskeletal proteins as well as signaling between cells and their surroundings.

*Integrins*

The most diverse group of adhesion molecules are integrins – heterodimers composed of α and β type subunits. There are at least 18 well recognized α–type and 9 β–type subunits. Extracellular domains of the αβ complexes participate in bivalent metal ion–dependent interactions with various extracellular matrix proteins, such as fibronectin, vitronectin, laminin, collagens, and other numerous cell receptors belonging predominantly to the immunoglobulin superfamily. It is worth to mention that metal ions play a critical role in the ligand binding function of all integrin heterodimers. It has been shown that many (but not all) integrins require an arginine-aspartate-glycine (RDG) sequence in their ligands. The presence of such amino acid sequence has been ascertained for the interaction with e.g. fibronectin, vitronectin or collagen I. However, it is still unclear whether this is the only signal recognized by integrins. It is now a well-accepted concept that the physiologic role of integrins involves more than adhesion. Upon binding their ligands, integrins activate members of intracellular signalizing pathway cascades, transducing in and out signals that can stimulate or regulate motility and invasiveness, cell growth, and survival. The expression of integrins depends on the tissue of origin and the degree of differentiation. Cancer

cells very often switch the types of expressed integrins, favoring the ones that transmit growth signals *(Lodish et al. 2004; Plow et al. 2002).*

### *Immunoglobulin–like superfamily*

Among the adhesion molecules there are proteins belonging to the immunoglobulin superfamily. Its members (called also *immunoglobulin-like cell adhesion molecules, ICAMs*) possess a common structural motif, an immunoglobulin fold composed of about 70–110 amino acids that form 7–9 β plated sheets[12], stabilized by disulphide bonds *(Lodish et al. 2004; Lipowsky et al. 1995).* They function as cell adhesion and signaling receptors that transduce extracellular signals from neighboring cells or the extracellular matrix to the intracellular signaling machinery. Most of the members of this superfamily participate in the cell-cell recognition, immunological processes, and cancer metastasis.

### *Selectins*

Concerning the adhesion events, one of the most important biological functions of carbohydrates is their recognition by selectins, a family of adhesion proteins, which belong to a very broad and highly diversified group of plant and animal proteins called lectins *(Varki 1994; Lipowsky et al. 1995)*. These proteins are classified basing on similarities in specificity of their carbohydrate–recognition domains. Selectins are animal lectins usually present on non-adhesive blood cells (leukocytes, platelets) and on endothelial cells remaining in close and constant contact with them. Being crucial elements of the intercellular recognition system between circulating cells and the alignment of blood vessels, the selectins participate in the function of the defense system. Three members of the selectin family have been recognized. They are *L-selectin* (constitutively expressed on leukocytes), *P-selectin* (mainly expressed on platelets but also on endothelial cells), and *E-selectin* (inducible endothelial cell protein). All selectins are glycoproteins with a $Ca^{+2}$-dependent carbohydrate recognition domain at their N-termini, followed by a single epidermal growth factor domain, a variable number of regulatory domains, a single transmembrane polypeptide, and a fairly short C-terminal cytoplasmic domain. Selectins mediate the cell-cell contacts by binding *via* their lectin domain, to a carbohydrate-containing counter-receptor on target cells. Like other mammalian lectins, the selectins bind selectively but with low affinity to particular oligosaccharides. One of them is sialyl-Lewis x (sLex)[13] attached to glycoproteins and glycolipids

[12] A secondary structure of proteins is governed by the local inter-residue interactions mediated mainly by hydrogen bonds. The most common secondary structures are α–helice (a right-handed coiled conformation, resembling a spring) and β–sheet (an elongated plate-like structure, in which the peptide carbonyls point in alternating directions relative to the plane of the sheet) *(Lodish et al. 2004)*. See *Appendix 1* for the structure of α-helice and β-sheet.

[13] Sialyl LewisX (sLex) – a tetrasaccharide carbohydrate usually attached to O-glycans on the surface of cells.

on most leukocytes and some endothelial cells. The results of numerous studies strongly suggest that one of the key factors in metastasis is the presence on tumor cells of a high density sLex structure, and ligands of E– and P– selectins. The whole complex sequence of consecutive recognition events is mediated by oligosaccharide-lectin interaction, followed by the aggregation of platelet and tumor cells. This may finally lead to the attachment of tumor cells to the endothelium, extravasation, and colonization of a tissue.

## 2.2 Glycans

Glycans are complex carbohydrates composed of single sugar units that are usually referred to the carbohydrate moiety attached either to proteins or to lipids. Depending on the bond structure, there are two types of glycans: O- and N-linked ones *(Goochee et al. 1991)*. The O-linked glycans (*O-glycans*) are linked to the hydroxyl group of serine[14] (Ser) or threonine (Thr) side chain. Usually they are short and not significantly branched oligosaccharides, composed of few monosaccharide residues such as *N*-acetylgalactosamine, galactose, *N*-acetylglucosamine, fucose, and *N*-acetylneuraminic acid called also sialic acid *(Mechref et al. 2002)*. The N-linked glycans form the bond with an amide group of the side chain asparagine (Asn). Oppositely to O-glycans, *N-glycans* are often much larger (longer, more branched) and contain *N*-acetylglucosamine, mannose, galactose, fucose, *N*-acetylgalactosamine, and *N*-acetylneuraminic acid. Their size varies between 6–15 monosaccharide units arranged in 2 to 5 antennae structures *(Mechref et al. 2002)*.

The glycans fulfill many important structural and functional roles. They are responsible for increased solubility and stability of a number of proteins, e.g. as in the case of blood plasma proteins. Oligosaccharides differ from proteins and nucleic acids in a few characteristics: they are usually highly branched and their monomeric units are bound by variety of bonds. Due to the branching and numerous alternative linkages, these types of oligosaccharides are able to carry more information than other biological molecules. Therefore, their varying structural motives serve as a part of a recognition system as in antigen–antibody and receptor–hormone reactions, bacterial infection, cell–cell, and cell–extracellular protein interactions. The most important 'role of glycoproteins' from the point of view of their presence in plasma membranes, is that they form parts of: (i) antigenic determinants which create individuality of a cell, and (ii) cell–cell and cell–extracellular matrix proteins recognition systems *(Goochee et al. 1991)*.

## 2.3 Molecules on a cancer cell surface

During oncogenic transformation cells undergo modifications that can alter their surface structures by changing both the expression of molecules at the cell surface and the level of protein

[14] One of amino acids building up the proteins. List of amino acids and their abbreviations is included in *Appendix 1*

glycosylation[15]. Such structural alterations of the cell surface usually result in modified or reduced interactions either with a neighboring cell or with the extracellular matrix. The loss of these interactions promotes motility and detachment of tumor cells at the primary tumor site (*Hanahan et al. 2000*). On the other hand, these changes enable to establish of new adhesive interactions in distant locations during the formation of the secondary tumor site (*Conacci-Sorrell et al. 2000*).

Many proteins participating in normal biochemical processes are glycosylated, i.e. they have attached oligosaccharide moieties. It has been reported for many tumors that the plasma membrane oligosaccharides are altered during cancer transformation. The distinct pattern of protein glycosylation influences tumor cell invasion and adhesion, and thereby leads to disturbances in cell's interaction with the extracellular matrix and/or neighboring cells. Changes in the expression and the structure of oligosaccharides seem to be a characteristic feature of the malignant transformation *(Kannagi et al. 2004)*.

Since molecules or their structural parts are responsible for the adhesion, they are not only important for normal cell functioning but also involved in pathological processes. Distinct methods have been applied to study the role and properties of various cell adhesion molecules in malignant transformation, with the emphasis on the use of such molecules to identify cancerous cells or to monitor patient response to treatment.

It has been reported in many papers *(Lindblom et al. 2000)* that adhesion molecules undergoes characteristic changes during oncogenic transformation. Some examples of such changes are presented below:

- *Cadherins*

  Many epithelial cancers are associated with the loss of the E-cadherin–mediated intercellular adhesion what may lead to tumor cell migration *(Sung et al. 2007)*. The loss of E-cadherins can be accompanied by its replacement with N-cadherin at intercellular contacts, what promotes cell migration in, for example, breast cancer *(Hazan et al. 2000)*. In many cancers, N-cadherins can be treated as an indicator of tumor development. However, the replacement of E-cadherin by N-cadherins cannot be generalized for all tumor types. For instance, Arenas and co-workers observed a decreased expression of N-cadherin in prostatic cancer *(Arenas et al. 2000)*.

- *Integrins*

  Cadherins are not the only cell adhesion molecules that play a critical role in tumor progression. These are integrins which mediate the adhesive interaction with the extracellular

[15] Glycosylation is the process or result of addition of carbohydrate structures to proteins and lipids.

matrix and thereby they influence the cell growth, differentiation, or migration. The malignant transformation is also characterized by altered interactions with extracellular matrix what is the consequence of changes in the integrins expression on cell surface, often associated with the modification of their structure. Some integrins are either overexpressed (such as $\beta_1$ integrins) or no longer expressed, whereas others become phosphorylated, affecting remarkably their cytoskeletal and extracellular binding properties *(Brakebusch et al. 2005)*.

- *Other cell adhesion molecules*

  Also other types of cell adhesion molecules are affected by oncogenic transformation. As an example, it has been shown that the neural cell adhesion molecule (N-CAM) in various cancer types shows changes of the isoforms from the embryonic 140 and 180 kDa to the adult 120 kDa *(Mareel et al. 2003)*. However, the significance of such alteration in tumor progression is not fully understood so far. It may be based on the distinct sialylation[16] of the various N–CAM isoforms.

Some of the present alterations in cell adhesion molecules can be used as indicators of cancerous state. However, the drawback is that frequently the same molecules are present in both normal and cancerous cells, as it takes place for prostate specific antigen (PSA) used for the detection of prostate cancer *(Allsbrook et al. 1992; Catalona et al. 1994)*. Its elevated level can indicate prostate cancer but there are also other causes of the higher lever of the PSA antigen that are not related to cancer. Therefore, the quantitative description of the differences in the adhesive interactions between single proteins performed cancerous cells may help the development of methodological approaches to the treatment of cancer.

[16] Sialylation is the process or results of addition of oligosaccharides composed of sialic acids to proteins and/or to lipids.

# CHAPTER 3

# Models for molecule unbinding

The main aim of the studies of molecular, biological systems is to identify the physical mechanisms and properties of molecules establishing their functions. The bond dissociation can be considered as a particle moving over an energy barrier of a one-dimensional energy landscape, which is determined by the structure of the binding pocket of the two interacting molecules *(Orsello et al. 2001)*. Figure 3.1 schematically presents one-dimensional energy landscape $U(x)$ as a model for a single molecular bond interaction as a function of a reaction coordinate $x$ which, in this case, represents the distance between two interacting molecules, e.g. distance between a ligand and a receptor. The bound state ($\Delta G_0$, a deep minimum appearing at small distances, $x_{bound}$) is separated from the unbound one by a transition state ($\Delta G_a$) represented by an energy barrier with height $E_b$ located at the distance $x_b$.

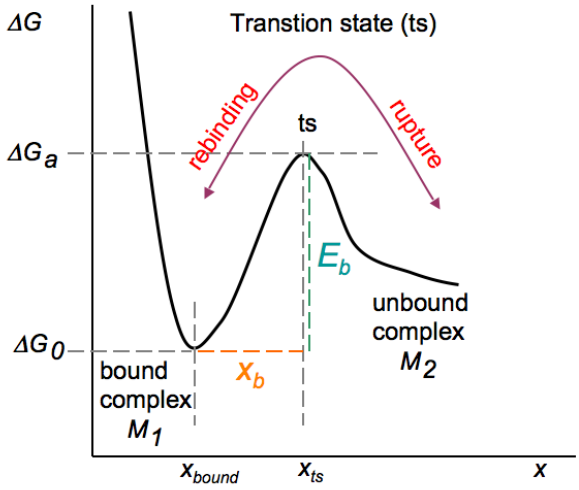


Figure 3.1. Scheme of an energy landscape of the unbinding process of two interacting molecules as a function of the reaction coordinate $x$. For the molecule composed of only two atoms the reaction coordinate is the distance between these two interacting atoms.

The first approach describing the unbinding process approximates it as a chemical reaction of two reactants $M_1$ and $M_2$ described by

$$M_1 \underset{k_0}{\overset{k_{on}}{\Leftrightarrow}} M_2 \qquad \text{and} \qquad \frac{dM_1}{dt} = -k_{on}M_1 + k_0 M_2 \,. \tag{3.1}$$

This reaction is assumed to be a first–order kinetics because the rate of change depends linearly on the concentration of reactants what takes place for many processes involving proteins *(Dembo et al.*

*1988)*. Consequently, such reaction proceeds through an intermediate state (called also activated state) present as an energy barrier with the height $E_b$. If the transition has a free energy $\Delta G_a$ then the rate constant for the transition can be determined from the Van't Hoff – Arrhenius law. According to it, the rate for a barrier crossing (i.e. *dissociation rate constant*, $k_0$) is exponentially dependent on the height of the energy barrier and on temperature $T$. Later on, it was realized that escape from a bound state could happen only *via* noise-assisted hopping events. The theory of Brownian motion was therefore the starting point for the Kramer's theory *(Kramers 1940)*. The rate of escape from the state of a local stability (i.e. a bound state) along a preferential path over the confining barrier *via* a saddle point in the energy potential is driven by thermal forces $F$, which in turn depend on temperature $T$ and the damping $\gamma$ *via* the fluctuation-dissipation theory. This saddle point approximation allows to solve the integrals and the expression for the dissociation rate reads:

$$k_0 = \gamma_D \cdot e^{-\frac{\Delta G_a - \Delta G_0}{k_B T}} = \gamma_D \cdot e^{-\frac{E_b}{k_B T}} \tag{3.2}$$

where $\gamma_D$ is the frequency of attempts, $E_b = \Delta G_a - \Delta G_0$ is the height of the barrier relative to the bound state, $k_B$ is the Boltzmann's constant. The dissociation rate constant $k_0$ is the inverse of the bond lifetime, $\tau_0$

$$\tau_0 = \frac{1}{\gamma_D} \cdot e^{\frac{E_b}{k_B T}} \tag{3.3}$$

In the transition state theory, the prefactor $\gamma_D$ is the natural vibration frequency of the bond, which is of the order of $\gamma_D \sim 5 \cdot 10^{13}$ s$^{-1}$ for C-C bonds *(Hängii 1990)*. In this case, the corresponding activation barriers and bond lifetimes would be: for 30 $k_BT$ – 0.2 seconds, for 40 $k_BT$ – 1.3 hour and for 50 $k_BT$ more than 3 years. In the Kramer's theory, the attempt frequency $\gamma_D$ is governed by viscous damping $\gamma$ and thermal length scale ($L_{th}$).

The rupture and rebinding events correspond to transitions of the Brownian particle over the energy barrier. The probability distribution $p(x, v, t)$ at time $t$ for the coordinate $x$ and the velocity $v$ of a particle diffusing freely in the potential $U(x)$ can be described by the Klein-Kramer's equation *(Kramers 1940; Hängii 1990)*

$$\frac{\partial}{\partial t} p(t,x,v) = \left( -\frac{\partial}{\partial x} \cdot v + \frac{\partial}{\partial v} \cdot \frac{U'(x) + m \cdot \gamma \cdot v}{m} + \frac{\gamma \cdot k_B \cdot T}{m} \cdot \frac{\partial^2}{\partial v^2} \right) \cdot p(t,x,v) \tag{3.4}$$

where $m$ is the mass of a moving particle, $\eta$ is the friction coefficient of the particle in a fluid, $U(x)$ is a metastable, nonlinear potential represented, for instance, by the function $U(x) = -\frac{1}{2}x^2 + \frac{1}{4}x^4$.

Within the Kramer's rate theory, the escape form the bound state to unbound one can happen only *via* noise-assisted hopping events driven by thermal fluctuations. If the thermal energy $k_BT$ is much

smaller than the respective barrier height, the random forces are acting only as a small perturbation, and can be neglected. The system will stay at the deep minimum for a long time, until finally it accumulates enough energy to hop over the energy barrier to the unbound state. Such events are very rare but still may occur within finite time. However, if the thermal energy is comparable with or even larger than the barrier height, the particle can move almost freely from the bound to unbound states.

There is assumed here that the unbinding reaction takes place on a time scale much longer than the relaxation times of all other degrees of freedom of the system, so that the friction coefficient can be considered as independent of time. In the limit of strong friction ($\eta \gg 1$), the inertial term can be neglected with comparison to the thermal one. In addition, force and velocity follow a Maxwell distribution, which is independent of $x$:

$$p(v) \sim e^{-\frac{m \cdot v^2}{2 \cdot k_B T}} \tag{3.5}$$

Then, the Klein-Kramer's equation is replaced by Smoluchowski equation:

$$\eta \frac{\partial}{\partial t} \rho(x,t) = \frac{\partial}{\partial x} U'(x) \cdot \rho(x,t) + k_B T \cdot \frac{\partial^2}{\partial x^2} \rho(x,t) \tag{3.6}$$

where $\rho(x, t)$ describes the spatial distribution of overdamped Brownian motion of a particle in the external potential $U(x)$. The above replacement is valid when the potential $U(x)$ and the spatial distribution $\rho(x,t)$ are constant on the thermal length ($L_{th}$) scale ($\sqrt{k_B T m}/\eta$). The thermal length scale dependence on the protein mass for the thermal energy of 4.1 pN·nm and $\eta \approx 4 \cdot 10^{-10}$ kg/s *(Hummer et al. 2001)* is presented in Figure 3.2.

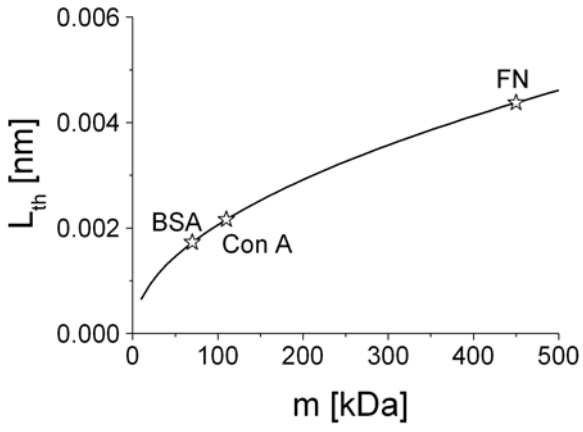


Figure 3.2. Thermal length-scale ($L_{th}$) as a function of a protein mass with marked three examples of proteins (stars): albumin from bovine serum (BSA), concanavalin A (ConA), and fibronectin (FN).

The values of thermal length calculated for albumin from bovine serum (a protein with molecular mass of 70 kDa), and much larger protein, fibronectin from human plasma (~ 450 kDa) are 0.0017 and 0.0044 nm, respectively. These values are very small in comparison with the typical distance between the bound and the transition states that is in the range of 0.5 nm *(Bell 1978)*.The interaction

potential with a single energy barrier is valid for a certain class of molecules such as various antigen–antibody pairs *(Evans 1999)*. However, some molecular interactions are represented by the interaction potential possessing two or more energy barriers as for example streptavidin–biotin complex *(Evans 1999)*. The thermal fluctuations are the driving force for all molecular bonds, i.e. they help to overcome the energy barrier between bound and unbound states.

### 3.1 Force–induced single bond dissociation

In many biochemical processes, the bond rupture is induced by external forces that modify the interaction potential. According to the transition state theory *(Kramers 1940)*, the effect of the force on the reaction rates is that it tilts the free energy diagram (Figure 3.3).

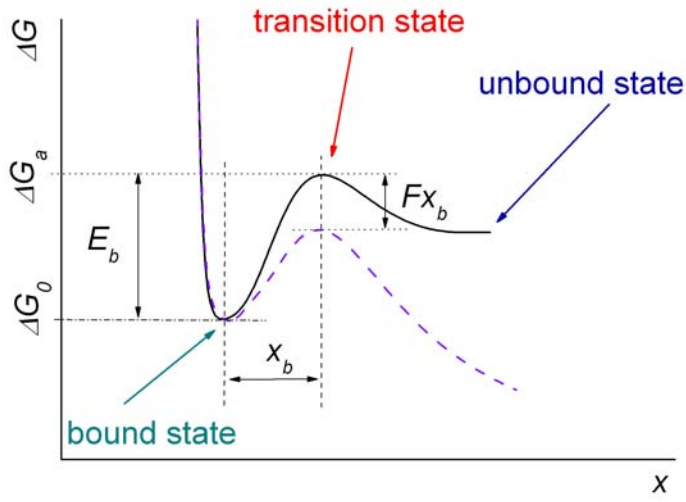


Figure 3.3. Schematic representation of an energy landscape of two interacting molecules (i.e. ligand-receptor complex, black line). The applied external force $F$ (as it is in the case of measurements by means of atomic force microscopy) lowers the height of the energy barrier, resulting in easier bond disruption (dashed line). The transition state is characterized by a barrier height $E_b$ and its distance from the bound state $x_b$ (termed also *an energy barrier position*).

If the position of the energy barrier is between the bound and unbound states then a negative external force (*a push*) will slow down the reaction since it will lead to a rise of the energy barrier height whereas a positive external force (*a pull-off force*) will accelerate the reaction. If the position of the transition state is the same or close to the bound state, the force will have a little influence on the association rate constant. If the position of the energy barrier will be comparable with the unbound state, then the force will have no influence on the dissociation rate constant.

The Kramer's model assumes that the motion of the ligand proceeds in the strong friction limit ($\eta >> 1$) along a reaction coordinate $x$ and is governed by the one-dimensional Langevin equation

$$\eta \frac{\partial}{\partial t} x(t) = -\frac{\partial}{\partial x} U(x) + F(x,t) + \sigma \cdot N(t) \qquad (3.7)$$

where $F(x, t)$ is the external force applied to the ligand and $\sigma N(t)$ is a stochastic force of an amplitude $\sigma$ and a zero mean. One way to apply external forces to a protein–ligand complex is to pull off the ligand, forcing it to move from its initial position in the binding pocket, and allowing the ligand to explore new contacts along its unbinding path. For a constant pulling velocity $v$ and assuming the external potential $U(x) = \frac{K(x - x_{bound})^2}{2}$ (where $K$ is the stiffness of the pulling complex), the external force applied to the ligand can be expressed as a function of single reaction coordinate $x$

$$F = K(x_{bound} + v \cdot t - x) \tag{3.8}$$

The force corresponds to the ligand being pulled by a harmonic spring of stiffness $K$ with its end moving with velocity $v$.

If the protein structure is very rigid and the transition from bound to unbound states over the energy barrier is associated with displacement in the direction of the acting force, the energy of the transition state will be decreased by an additional term generated by the potential of the acting force $F$. Therefore, the height of the energy barrier is lowered by $-Fx_b$ where $x_b$ is the distance between the bound and unbound states. This implies that

$$k_{off} = \gamma_D \cdot e^{-\frac{E_b - Fx_b}{k_B T}} = k_0 \cdot e^{\frac{Fx_b}{k_B T}} \tag{3.9}$$

For the first time, the above equation was presented by Bell in 1978 *(Bell 1978)*. The model shows that bond rupture forces are dependent on the intrinsic lifetime of the bond, the temperature, and on the measurement time. It is valid if the energy landscape under the applied force is the sum of the original potential (in the absence of force) and the (linear) potential defined by the applied force with a fixed distance $x_b$ between the bound and unbound states along the reaction coordinate and unbinding path.

The Equation (3.9) does not account for the stochastic nature of a single bond rupture, and the model cannot predict the actual distributions of measured bond strengths around the average value as they are experimentally observed. These statistical fluctuations arise from random fluctuations of the system in its equilibrium state. In Bell's theory, all features of the energy landscape are put into one parameter – the distance $x_b$. To overcome this limitation, Evans & Ritchie introduced a different model for the description of the bond rupture under an external force, based on Kramer's theory *(Evans 1999)*. It is still assumed that all possible reaction paths are focused onto one by the application of an external force. Therefore, the energy landscape can be sketched one-dimensionally along the reaction coordinate.

From the first–order of the kinetic theory *(Hängii 1990; Tees et al. 2001)* for the irreversible unbinding of single bonds, the probability that a single bond breaks in the time interval (*t, t + dt*) is

$$p(t+dt) = p(t)\cdot\left(1 - k_{off}(t)\cdot dt\right) \tag{3.10}$$

and therefore

$$\frac{dp(t)}{dt} = -k_{off}(t)p(t) \tag{3.11}$$

Taking into account the Equation (3.9) one can determine the probability density function *p(t, F)* of a single bond dissociating in the time interval (*t, t + dt*) as a function of force, *F*, is

$$p(t,F) = k_{off}(F(t))\cdot e^{-\int_0^t k_{off}(F(t'))dt'} \tag{3.12}$$

The first term represents the probability of dissociation in the next short time interval, *dt*, whereas the exponential term describes the probability of the bond survival up to time *t*.

The first experiments reporting the unbinding of single bonds were performed at fixed pulling velocities and spring constants. It is now generally accepted, that the rupture force of an isolated bond is not only dependent on the shape of the unbinding potential and temperature, but also on the force loading rate: any non-covalent bond will fail under any level of pulling force if held for sufficient time. Therefore, with the bond dissociation process being a non-equilibrium dynamical process, the bond strength (as well as adhesion strength) can be expected to be time and loading rate dependent. This has been shown in several experiments by employing the dynamic force spectroscopy (DFS) technique where the applied force–loading rate was varied over a few orders of magnitude *(Fritz et al. 1998; Nishizaka et al. 2000; Kienberger et al. 2005)*.

Depending on the relation between the breaking external force *F* and time (and thus the dissociation rate on time), several solutions for probability distribution can be obtained. The simplest solution assumes that the external force *F* is not dependent on time. In that case, the probability that a single bond will be broken at time *t* is as follows

$$p(t,F=const) = k_0\cdot e^{\left(\frac{x_b\cdot F}{k_B\cdot T} - k_0\cdot e^{\frac{x_b\cdot F}{k_B\cdot T}\cdot t}\right)} \tag{3.13}$$

However, in most pulling measurements, the applied force changes linearly in time

$$F(t) = k_{syst}\cdot v\cdot t \tag{3.14}$$

*w*here $k_{syst}$ is the effective spring constant accounting for the AFM cantilever and the single bond spring constants, and $v$ is the tip retraction velocity. In that case, the probability distribution is expressed by the following equation

$$p(t,F) = \frac{k_0}{r_f} \cdot e^{\frac{x_b \cdot F}{k_B \cdot T}} \cdot e^{-\frac{k_0 \cdot k_B \cdot T}{x_b \cdot r_f} \cdot \left( e^{\frac{x_b \cdot F}{k_B \cdot T}} - 1 \right)} \tag{3.15}$$

where $r_f = k_{syst} v$ is the loading rate, describing how fast the force changes in time during bond rupture. The equation was normalized according to $\int_0^\infty p(F)dF = 1$.

The Equation (3.15) shows that the probability distribution of the unbinding force depends on the loading rate $r_f$ (Figure 3.4). The higher loading rate shifts the maximum of the distribution towards larger unbinding force values and, in addition, broadens the force distribution.

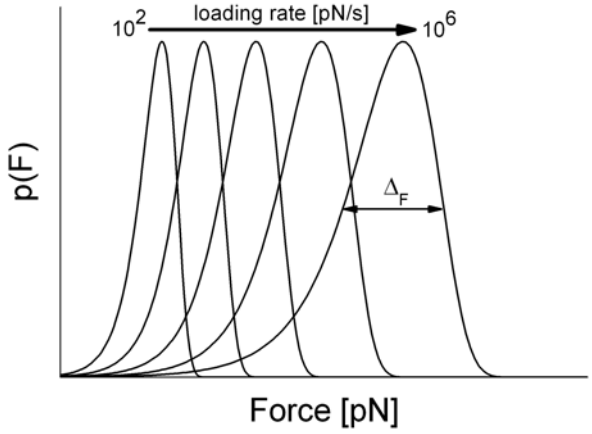


Figure 3.4. Probability distributions as a function of an unbinding force calculated for different loading rates (from 100 pN/s to $10^6$ pN/s).

The curvature ($1/\Delta^2_F$) of the distribution local at the maximum $F_{max}$ provides a measure of the spread ($\Delta_F$) in the distribution given by the equation:

$$\frac{1}{\Delta_F^2} = \left[ -\left( \frac{1}{p(F)} \right) \cdot \frac{\partial^2 p(F)}{\partial F^2} \right] \tag{3.16}$$

The maximum of the distribution (the most probable unbinding force), defined by the condition $dp(F)/dF = 0$ is located at

$$F_{unb} = \frac{k_B \cdot T}{x_b} \cdot \ln\left( \frac{x_b \cdot r_f}{k_0 \cdot k_B \cdot T} \right) \tag{3.17}$$

From the above equation, one can observe that at loading rates below the characteristic rate $r_f = k_0 \cdot \frac{k_B \cdot T}{x_b}$ (for $F_{unb} = 0$), the spontaneous dissociation is faster than the force application and the maximum of the unbinding force distribution is located at zero. The Equation (3.17, *(Evans 1998; Neuert et al. 2006)* can be rewritten as follows

$$F_{unb} = \frac{k_B \cdot T}{x_b} \cdot \ln\left(\frac{x_b}{k_0 \cdot k_B \cdot T}\right) + \frac{k_B \cdot T}{x_b} \ln(r_f) \tag{3.18}$$

This form clearly shows the linear dependence of the most probable unbinding force on the logarithm of the loading rate $ln(r_f)$.

The effect of the loading rate on the unbinding force was observed by AFM for many distinct pairs of molecules, bringing deeper insight into molecular mechanism of the bond breaking. The example of such study is shown in Figure 3.5.

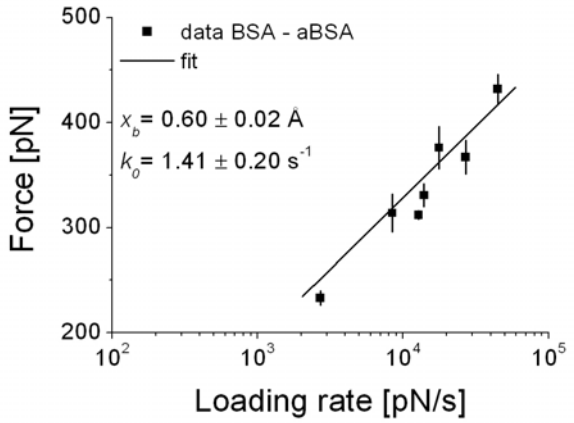


a)

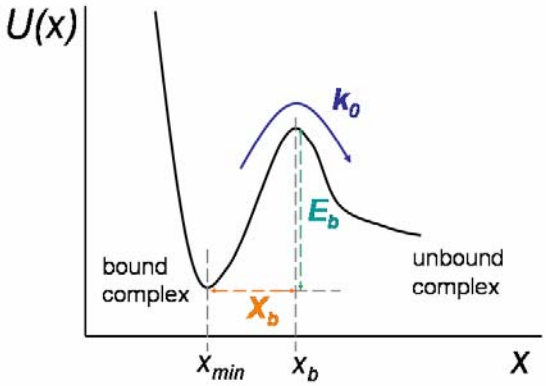


b)

Figure 3.5.a) The dependence of the most probable unbinding force on the logarithm of the loading rate measured for the interaction between the albumin (BSA) and its antibody (aBSA) *(Grybos 2005)*. b) The single line corresponds to the energy landscape with only one energy barrier characterized by two parameters: its height $E_b$ and position $x_b$.

In this case, the interaction force acting between the typical antigen–antibody complex represented by albumin and its monoclonal antibody (BSA−aBSA complex) was measured as a function of the loading rate *(Grybos 2005)*. The obtained relation was fitted with a single line, bringing thus information that the interacting potential of two molecules possessed only a single energy barrier at the position of 0.060 ± 0.002 nm from the minimum energy (i.e. bound state). The corresponding dissociation rate constant was of 1.41 ± 0.20 $s^{-1}$, corresponding to the bond lifetime of 0.71 s. Such linear dependence of the most probable unbinding force on the logarithm of the loading rate has been commonly observed for most of antigen–antibody interactions.

### *3.1.1 Hierarchic crossing through the energy barriers*

In almost all molecular complexes investigated so far, the dependence between the unbinding force and the logarithm of the loading rate was represented either by a single line, indicating as mentioned, the presence of only one energy barrier in the interaction energy landscape. However, kinetic processes that involve complex molecules, such as proteins, may exhibit multiple local maxima and minima in the interaction potential along the reaction coordinate. In such cases, the plot of the most probable unbinding force and logarithm of the loading rate shows a sequence of lines with different slopes, each corresponding to the position of a particular energy barrier.

Apart from biotin–(strept)avidin complex, the measurements of the unbinding force as a function of the loading rate were extensively applied to study the selectin interactions, since during rolling, these types of bonds are exposed to the action of the external forces *(Izrailev et al. 1997)*. Selectins are present on the surface of leucocytes which, upon activation, interact with ligands present on the endothelium. AFM measurements were performed in search of ways of identification of the interactions between selectins (P, E, and L, see *Chapter 2*) and their ligand sialyl Lewis X (sLex). The sLex ligand is an oligosaccharide containing two sugars, sialic acid and fucose, participating at distinct degree in interactions with different types of selectins. That ligand is present in the structure of the endothelial protein. The dependence between the unbinding force and the logarithm of the loading rate showed two linear sections for each selectin type (P, E, and L) and their sLex ligand what indicates that the unbinding process involves overcoming of two energy barriers, located at different distances from the energy minimum (bound state). In addition, results showed that the inner barrier (detected at high loading rates) is governed by the interaction between fucose and $Ca^{++}$ ion, whereas the lower loading regime corresponds to the outer barrier in interactions dominated by sialic acids.

Another example of the unbinding force dependence on the logarithm of the loading rate *(Gryboś et al. 2004)* is presented in (Figure 3.6). The measurements were carried out for two molecules: albumin and ethylene-di-amine tetraacetic acid (EDTA). The observed two linear segments indicated

existence of two barriers (inner and outer ones) in the corresponding energy landscape. For each of them a separate set of the Bell model parameters would be determined.

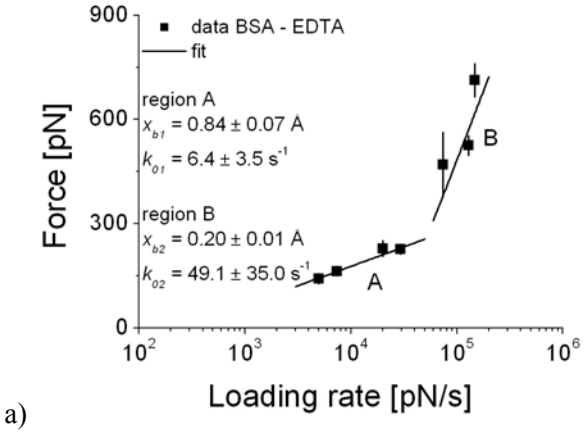


a)

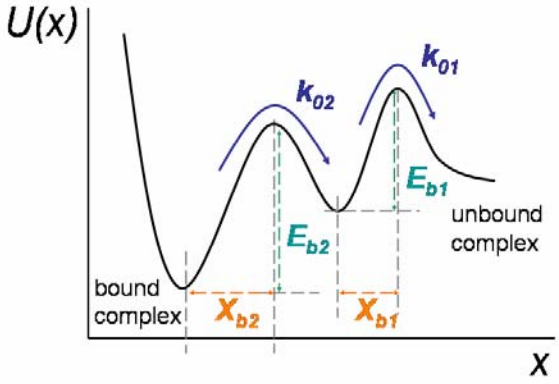


b)

Figure 3.6. a) The force versus loading rate dependence measured for BSA–EDTA complex showing two segments of linear dependencies *(Gryboś et al. 2004)*. b) The corresponding energy landscape possessing two energy barriers (outer and inner ones), each represented as a line in Figure 3.6 a).

The region A (Figure 3.6a) corresponds to the outermost energy barrier characterized by $x_{01} = 0.084 \pm 0.007$ nm and $k_{01} = 6.4 \pm 3.5$ s$^{-1}$. The inner energy barrier (region B, Figure 3.6a) is located at the distance of $x_{02} = 0.020 \pm 0.001$ nm from the bound state and the dissociation rate constant is $k_{02} = 49.1 \pm 35.0$ s$^{-1}$. The extrapolation of the different linear segments to $F = 0$ differs by the amount related to the relative differences in the magnitude of the individual energy (the absolute values of multiple activation barriers can no longer be calculated directly). During the unbinding the complex stays for 0.020 s in the first transition state (inner barrier) and for 0.156 s in the second transition state (outer barrier).

For such a hierarchic crossing, each $i$-th barrier is described by its own dissociation rate constant ($k_0^i$) and a position of the energy barrier ($x_b^i$). The Kramer's kinetic rate theory can be extended to

model the escape over a series of barriers under force *(Evans et al. 2001)*. Then, the overall unbinding rate is a sum of dissociation rates ($k_{off}$) needed to transit each individual barrier

$$\frac{1}{k_{off}(F)} = \sum_{i=1}^{N} \frac{1}{k_{off}{}^{i}(F)} \tag{3.19}$$

or taking into account that the lifetime of a bond in each transition $t_o{}^{i}$

$$k_{off}(F) = \left( \sum_{i=1}^{N} t_0^i \cdot e^{-\frac{x_b^i \cdot F}{k_B T}} \right)^{-1} \tag{3.20}$$

In case when the system must overcome a series of still higher activation barriers before final dissociation, the dissociation kinetics at low pulling forces (low loading rate) is governed by the properties of the outermost barrier. With the increase of the loading rate, the outermost barriers are suppressed, and the dissociation is governed by the inner activation barriers *(Zhang et al. 2004)*.

### *3.1.2 The height of the energy barrier*

The AFM measurements performed with variable loading rates together with the application of Bell model deliver parameters that enable to describe the kinetics of the unbinding process, i.e. the position of the energy barrier and the dissociation rate constant, but the absolute value of the height of the energy barrier cannot be determined. This should be determined using other techniques, such as quartz microbalance *(Lebed et al. 2006)*, surface plasmon resonance *(Homola 2003)* or calorimetry *(Jelesarow et al. 1999)*. However, these techniques base on the measurements in a certain volume, where a large number of molecules associate and dissociate. That's why, the data obtained from the AFM measurements are so very valuable: the unbinding phenomena may be characterized at a single molecule level. Such situation is very close to natural conditions where it takes place for receptors embedded in the cell membrane. Despite the lack of the absolute value of the barrier heights, they can be quantitatively estimated according to

$$\Delta(\Delta G) = \Delta G_1 - \Delta G_i = k_B T \cdot \ln\left(\frac{k_{0i}}{k_{01}}\right) \tag{3.21}$$

where $k_{01}$ is the dissociation rate constant of the unbinding of a single bond while $k_{0i}$ is the rate describing the escape over of the *i*-th barrier.

The Equation (3.21) can be applied to estimate the differences of the energy heights in the simultaneous unbinding of the consecutive bonds under the assumption that the association constant ($k_{on}$) remains unchanged during bond formation (it is true for the same bond type). In this case, $k_{0i}$ is the rate constant of the simultaneous failure of *i*-bonds.

## 3.2 Multiple bond disruption

Adhesion between biological cells is mainly based on clusters containing a large number of adhesion receptors that mediate contact to specific ligands, either carried by other cells or attached to the extracellular matrix. When an attachment is realized by several bonds, each characterized by a single energy barrier potential, during a rupture of the cluster of bonds, several scenarios can be distinguished concerning the distribution of the force applied to single bonds. Assuming their uncooperative failure (i.e. when force drops to zero, each attachment behaves as a time separated dissociation event with no dependence on the previous unbinding process), the dissociation of a molecular complex can proceed in two extremes, characterized by either consecutive or simultaneous rupture of bonds, described by a "zipper–like" or "parallel–like" models, respectively.

In the "zipper–like" model of the bond rupture, the whole force is exerted on the first bond and as soon as it breaks, the next bond is loaded. This model is frequently used for modeling of RNA or DNA unzipping *(Strunz et al. 1999; Cocco et al. 2001)* but it can also be used for a sequential rupture of multiple bonds as it takes place in leukocyte rolling *(Tees et al. 2002)*.

In the "parallel–like" model, the breakage of several bonds at the same time require the application of the force being the product of the number of ruptured bonds times the value of the force needed to break a single bond alone *(Williams 2003)*.

The cluster of bonds can be modeled as a "new type" of a single bond with the barrier being the sum of the energy barriers of each participating individual bond *(Strunz et al. 1999)*. A deterministic model for the non-equilibrium dissociation of a cluster of bonds under the external force has been already described within the frame of the Bell model *(Bell 1978)*. This model is mainly used to study very specific problems, as abovementioned example of leukocyte rolling *(Tees et al. 2002)*. Recently, the Bell model has been extended to the case when a linear loading is applied during rupture of a bond *(Seifert 2000; Evans et al. 1997)*, which is the case of measurements carried out by the atomic force microscopy.

### *3.2.1 Sequential bond rupture – the "zipper-like" model*

In the "zipper-like" model (Figure 3.7), the applied external force breaks each bond separately, one after another, like in a zipper *(Williams 2003)*.

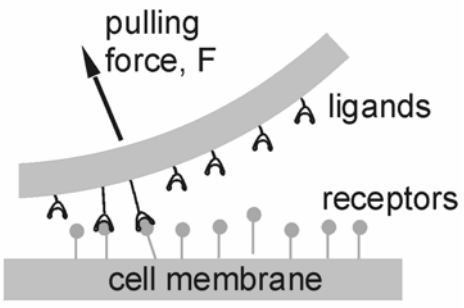


Figure 3.7. Schematic representation of the consecutive unbinding of *N*-bonds – the "zipper-like" model.

Assuming that all individual bonds dissociate through the same single–barrier potential, described by the dissociation rate constant $k_0$ and by the position of energy barrier $x_b$, one can calculate the overall dissociation rate constant of the failure of $N$ bonds. In this model, each bond fails under the same value of the external force, $F$, and the failure of the $N$-th bond is identical to that of the single bond

$$k_{off}(F) = k_0 \cdot e^{\frac{x_b \cdot F}{k_B \cdot T}}. \tag{3.22}$$

Thus, the overall dissociation rate of all identical $N$ bonds (calculated from the Equation (3.20)) is the following

$$k_{off}{}^{N}(F) = \left( \sum_{i=1}^{N} \frac{1}{k_0} \cdot e^{-\frac{F \cdot x_b}{k_B \cdot T}} \right)^{-1} = \frac{k_0}{N} \cdot e^{\frac{x_b \cdot F}{k_B \cdot T}} \tag{3.23}$$

The most probable unbinding force for $N$ bonds ruptured sequentially, $F^{Z}_{unb}$, can be determined from the corresponding unbinding probability density (Equation (3.12)) by setting the condition $dp(F)/dF = 0$

$$F^{Z}_{unb}(N) = \frac{k_B \cdot T}{x_b} \cdot \left( \ln(r_f) + \ln\left( \frac{x_b}{k_0 \cdot k_B \cdot T} \right) + \ln(N) \right) \tag{3.24}$$

Finally, after inserting the Equation (3.17) for the single bond failure

$$F^{Z}_{unb}(N) = F_{unb} + \frac{k_B \cdot T}{x_b} \cdot \ln(N) \tag{3.25}$$

Hence, many attachments rupture like in a zipper, resulting in a force value larger than that needed to break one bond by the factor $G$ defined as

$$G = \frac{k_B \cdot T}{x_b} \cdot \ln(N) \tag{3.26}$$

The relation between its value and the number of bonds simultaneously ruptured is presented in Figure 3.8.

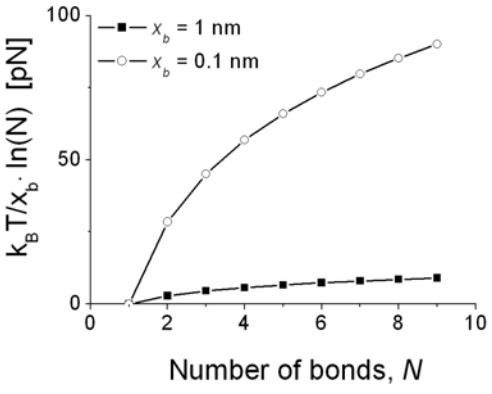


Figure 3.8. Factor $G$ (Equation (3.26)) as a function of the number of simultaneously broken bonds calculated for $x_b$ = 1 nm and $x_b$ = 0.1 nm in the "zipper-like" model ($k_BT$ = 4.1 pN·nm)

For $x_b$ = 1 nm the influence of the $G$ factor is negligible as even, for relatively large number $N$, its value is comparable with thermal fluctuations of the cantilever (~10 pN for 10 bonds). However, the measured $x_b$ values are usually lower: for different types of molecular complexes, the position of the energy barrier was reported from 0.08 to 0.55 nm *(Zhang et al. 2004; Kienberger et al. 2005)*. For $x_b$ = 0.1 nm, the contribution of the $G$ factor to the unbinding force cannot be neglected since its value (28 pN and 100 pN for 2 and 10 bonds simultaneously ruptured) is comparable with the unbinding force measured for some types of the single complexes *(Zhang et al. 2004; Sulchek et al. 2005)*.

In pull–off measurements of the bond failure, the most probable unbinding force is determined from the force histogram. If single bond failures are independent of each other, then only one peak is present in the force histogram. When the simultaneous unbinding of the certain number of the same bonds is observed, the histogram contains several maxima. When the rupture process follows the "zipper–like" model, the resulting distance between two subsequent bonds is $\frac{k_B \cdot T}{x_b} \cdot \ln\left[\frac{i+1}{i}\right]$, and therefore decreases with $i$.

### *3.2.2 Simultaneous bond rupture – the "parallel-like" model*

The analytical description of "parallel-like" model describing the simultaneous rupture of $n$−bonds has been presented by Williams *(Williams 2003)*. During such unbinding, the external force is equally shared between all participating bonds. The dissociation rate of rupture of all $N$ identical uncooperative bonds is the following *(Williams 2003)*

$$k_{off}{}^{N}(F) = \left( \sum_{n=1}^{N} \frac{k_0}{n} \cdot e^{\frac{-x_b \cdot F}{n \cdot k_B \cdot T}} \right)^{-1} . \tag{3.27}$$

As a consequence, for large number of bonds, the rupture force may be approximated by

$$F_{unb}^{P} \sim N \cdot F + N \cdot \frac{k_B T}{x_b} \cdot \left( \ln\left( \frac{k_B T}{x_b} \right) - \ln\left( F_{unb}^{P} \right) \right) \tag{3.28}$$

where $F_{unb}{}^{P} < N \cdot F$.

In AFM measurements, when few bonds are simultaneously ruptured ($N$ is small), the measured force is a sum of those characteristic for the single, separate bonds. Moreover, very often, the cooperative character of the unbinding is observed. Therefore, the "parallel-like" model reported by Williams *(Williams 2003)* was modified for such a case *(MLekka unpublished data)*. Thus, the

applied external force breaks simultaneously a certain group of $N$ bonds where each bond fails under the same value of the force (all bonds are identical, i.e. the dissociation proceeds through a single energy barrier ($E_b$ and $x_b$) with the same unbinding rate $k_0$). In this case, the applied external force $F$ is a product of the number of simultaneously ruptured bonds $N$ by the value of the force needed to break a single bond (Figure 3.9).

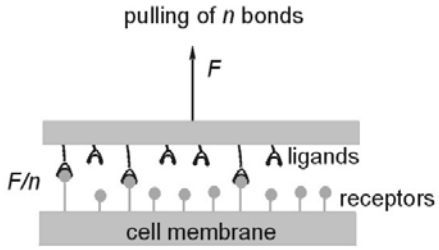


Figure 3.9. Scheme of the simultaneous rupture of cooperative $N$-bonds – the "parallel–like" model.

When multiple bonds act as cooperative bonds, the lifetime of the composite bond is a sum of the individual bond lifetimes. Thus, the unbinding rate for breaking of $N$ bonds, determined from the Equation (3.20), is the following

$$k_{off}{}^{N}(F) = \frac{k_0}{N} \cdot e^{\frac{x_b \cdot F}{N \cdot k_B \cdot T}} \tag{3.29}$$

The probability density function $p(t, F)$ describing $N$ single bonds dissociating in the time interval $(t, t + dt)$ is

$$p(F) = \frac{k_0}{N} \cdot e^{\frac{x_b \cdot F}{N \cdot k_B \cdot T}} \cdot e^{-\frac{k_0 \cdot k_B \cdot T}{x_b \cdot r_f} \cdot \left( e^{\frac{x_b \cdot F}{N \cdot k_B \cdot T}} - 1 \right)} \tag{3.30}$$

The corresponding most probable unbinding force, $F^{P}{}_{unb}$, can be determined by setting the condition $dp(F)/dF = 0$

$$F^{P}_{unb}(N) = \frac{N \cdot k_B \cdot T}{x_b} \cdot \left( \ln(r_f) + \ln\left( \frac{x_b}{k_0 \cdot k_B \cdot T} \right) \right) \tag{3.31}$$

Analogously, after inserting the Equation (3.17) for a single bond failure, finally, one can get

$$F^{P}_{unb}(N) = N \cdot F_{unb} \tag{3.32}$$

Thus, many attachments ruptured under the shared force result in the force value being the product of the number of ruptured bonds and the force value needed to break one bond. The distance between two subsequent maxima, corresponding to the failure of the *i–th* and *(i+1)–th* bonds is equals to $F_{unb}$.

# CHAPTER 4

# Force spectroscopy

The studies of interaction between molecules, in general, assume the equilibrium binding. Kinetic measurements are carried out using such techniques as surface plasmon resonance *(Homola 2003)* or quartz crystal microbalance *(Lebed et al. 2006)*. In these techniques, interaction forces are indirectly inferred or calculated from the applied molecular model. However, such calculations are feasible for small molecules only and they become more complicated and less precise for large proteins. Since the main goal of biophysical studies is to determine forces acting between molecules and to use this information to monitor (or even manipulate) the function and structure of proteins, therefore, the development of techniques that can directly and quantitatively measure molecular forces is of a great importance.

There are several techniques that allow detection of molecular interactions with very high force resolution (at the order of nano– and piconewtons) that can be applied to recognize phenomena occurring between single molecules (e.g. proteins or other types of molecules). Among them, a surface force apparatus (SFA, *Helm et al. 1991; Leckband et al. 2000*), a biomembrane force probe (BFP, *Merkel et al. 1999)* and an atomic force microscope (AFM, *Binnig et al. 1986*) are the most popular ones. The first, atomic force microscope, was constructed in 1986 in IBM laboratory in Zurich. Initially, AFM was applied to study a surface topography in ambient or in vacuum conditions, but later on this technique was found to be very useful for biologists, since it enables measurements in liquids, at nearly physiological conditions. First, the most straightforward use of the AFM were studies of surface morphology of various biological samples, starting from single proteins and through imaging of living cell surfaces. However, the AFM ability to determine such properties as stiffness, adhesion, or friction, registered simultaneously with sample topography, makes it to be widely applied to characterize mechanical properties of biological samples in quantitative way.

Determination of the mechanical properties by means of AFM usually is carried out in the force spectroscopy mode, where so-called *force curves* are recorded. The force curve is the dependence between a cantilever deflection (that is converted into force) and a relative sample (or scanner) position, which can be transformed to a tip–sample distance. The interaction forces can be obtained from the analysis of the retraction part of the force curve recorded during the AFM tip withdrawal from the surface. The value of the interaction force between molecules measured in a single AFM measurement depends on such factors as number of bonds formed within the tip–surface contact area, properties of the surrounding media, concentrations of ions in a buffer, etc. Therefore, the

unbinding force of a single pair of molecules is usually determined by analyzing a large number of recorded force curves.

## 4.1. Atomic force microscope (AFM)

The idea of the AFM operation is straightforward (Figure 4.1). A sharp delicate probing tip, mounted at the end of a compliant cantilever, is placed almost parallel to the investigated surface and then moved over it, performing a raster scan. The cantilever senses forces acting between the tip and the sample surface, what results in its deflection that is usually recorded using the optical system: the laser beam is focused at the cantilever end and then, after reflection, is detected by a position sensitive photodiode. The position of the beam spot brings information on the cantilever displacement $z$ that can be converted into force $F$ using Hook's law:

$$F = k \cdot z \tag{4.1}$$

where $k$ is the cantilever spring constant.

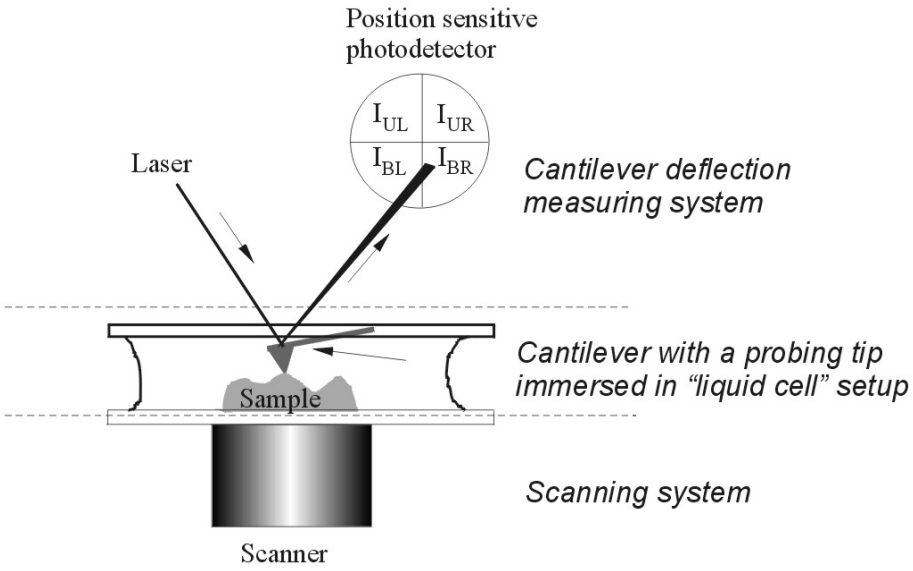


Figure 4.1. Basic elements of an atomic force microscope (AFM).

There are three basic elements that are common for all types of the atomic force microscopes (Figure 4.1): i) cantilever with a tip, ii) system that detects the cantilever deflection and iii) scanning system.

### *4.1.1 Cantilevers*

Usually, cantilevers are made of silicon or silicon nitride. Each cantilever is mounted on the rectangular chip, which can contain one or more cantilevers with different spring constants (see Appendix 2). The probing tip is located at the free end of the cantilever.

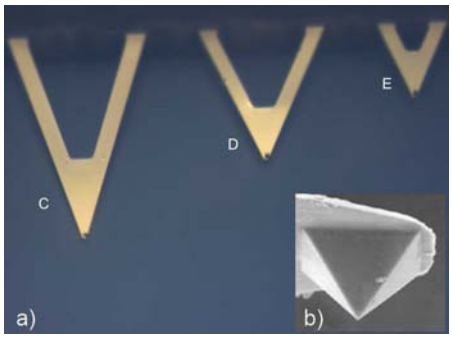


Figure 4.2. Silicon nitride cantilevers: a) three types of cantilevers (C, D, and E) with the corresponding spring constants of 0.01 N/m, 0.03 N/m and 0.1 N/m. b) The image of the four-sided pyramidal AFM tip with the radius of curvature of 50 nm.

Usually, tip has a shape of a four–sided pyramid with the height in the range of few microns. The radius of tip end curvature characterizes the tip and varies typically from a few nm to 50 nm. (Figure 4.2).

### *4.1.2 Deflection measuring system*

The most popular method of the deflection measurement uses an optical system, where the laser beam is focused at the end of the cantilever. After reflection, the laser beam is detected by a position sensitive detector (a photodiode) whose surface is divided into four quadrants. The cantilever deflection causes the reflected beam spot to move within the active area of the photodetector, thus changing photocurrents of the quadrants. The cantilever deflections are measured by signals in perpendicular (*A–B signal*) and parallel (*C–D signal*) directions to the sample surface, which are obtained from the following formula (Figure 4.1)

$$(A-B)\ signal = \left[\left(I_{UL}+I_{UR}\right)-\left(I_{BL}+I_{BR}\right)\right], \tag{4.2}$$

$$(C-D)\ signal = \left[\left(I_{UL}+I_{BL}\right)-\left(I_{UR}+I_{BR}\right)\right], \tag{4.3}$$

where $I_{xy}$ is the current of a single quadrant ($U$ = up, $B$ = bottom, $L$ = left, $R$ = right). Knowing the mechanical properties of the cantilever and the photodetector sensitivity, it is possible to estimate the value of the normal and lateral forces that cause the cantilever to bend. The measured signal is normalized, in practice, to the total recorded signal $(A+B)\ signal = \left(I_{UL}+I_{UR}+I_{BL}+I_{BR}\right)$ in order to avoid the influence of variations of laser intensity.

### *4.1.3 Scanning and positioning system*[17].

The sample is mounted on a holder fixed to a piezoelectric scanner. The scanner has a form of a tube with outer surface segmented (parallel to tube axis) into four electrodes. The tube interior wall serves as an internal electrode. The voltage applied to the electrodes causes the mechanical deformation of a tube. Equal voltages applied to all external electrodes cause scanner tube elongation (or shortening), resulting in Z movement. The voltages of opposite signs, applied to opposite segments, cause tube bending in X or Y directions what enables XY scanning. Usually, the piezoelectric scanner is mounted on the coarse positioning system facilitating a convenient and rapid sample exchange.

## 4.2. Force spectroscopy mode

In the *force spectroscopy mode*, AFM measurements of interaction forces require the recording of so-called *force curves*, while the scanning is disabled. The force curve links the cantilever deflection and the relative sample position (recorded in *Z*-direction i.e. perpendicularly to the investigated surface) and it is usually converted into a function of force versus tip–sample distance.

### *4.2.1 Force curve*

The force curve consists of two parts: the one recorded during approaching of the tip to the sample surface (*an approach curve*) and the other one, collected during opposite motion (*a retract curve*). The character (shape) of the force curve depends on physical and chemical properties of the two interacting surfaces. The Figure 4.3 shows the ideal curve (red line – approach, black – retract). Regardless of the sample type, several features are present in all curves.

*Base line (A)*

When the cantilever is away from the surface of a surface, its deflection should be zero since there is no detectable interaction force. Actually, due to thermal vibrations, the cantilever oscillates around its free position, reflecting the noise present in a particular AFM system. During the approach (red line) if both the tip and the surface are charged with the same sign, at close distances − prior to the contact − the cantilever can be repulsed from the surface. It is represented by the slight raise in the baseline, as it is visible in Figure 4.3 (A).

[17] The detailed description of the scanning and positioning system of the AFM working at IFJ PAN (Krakow, PL) can be found in PhD thesis by J.Lekki “Scanning force microscopy studies of implanted silicon” (1995, Krakow, PL).

*Jump–in (B)*

The presence of attractive forces between the tip and a surface is reflected by a jump–in, i.e. the moment when the cantilever is suddenly attracted. At this moment, the gradient of the attractive force is larger than the cantilever spring constant.

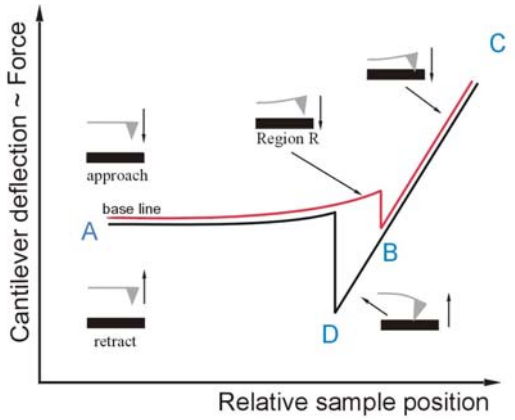


Figure 4.3. An ideal *force curve* between the end of the AFM tip and the hard surface. Arrows indicate direction of movement of the AFM cantilever *(*adapted from *Lekka 1998)*.

*Contact (C)*

When the tip is in a contact with the sample surface, the electron clouds of atoms of both the tip and the sample are overlapping and repulsing. The further approach results in the cantilever bending (up to the certain maximum value, point C), which character depends on the material properties of the investigated sample (linear or not). During separation of the two surfaces, the interacting repulsive force decreases.

*Pull–off (D)*

During retraction, the tip does not separate from the surface exactly at the same point where it started to touch the surface. Forces that are responsible for such behavior arise from adhesive properties of investigated surfaces. In further retract when the elastic force of the cantilever exceeds the gradient of the adhesive force, the tip is rapidly separated from the surface. The point D corresponds to the maximum value of the force (a so-called *pull-off force*). Further separation yields in cantilever fluctuations around its free position (base line).

*Unbinding of single and multiple bonds*

The shape of the force curve observed during the unbinding of discrete molecular bond is slightly different (Figure 4.4). However, the basic characteristics remain the same. Analogously to Figure 4.3, when the AFM probe with attached ligands is far away from the receptors, forces acting on the cantilever are negligible (A) and thus there is no cantilever deflection. Then, the cantilever and surface come to a contact, and the further movement manifests here as a bending of the cantilever. At the moment when the cantilever deflection reaches a certain maximum (point C), the retraction starts.

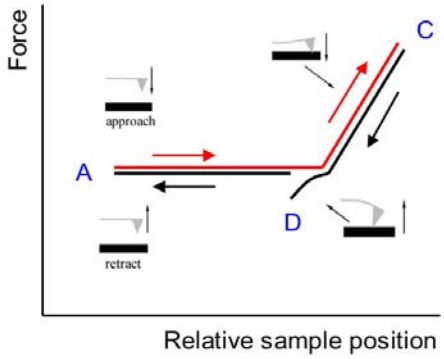


Figure 4.4. An ideal *force curve* characteristic for the interaction between a single pair of ligand and receptor molecules. Similarly as in Figure 4.3, red line denotes approach and the black one – retract.

During the reverse motion, the deflection of the cantilever decreases. However, the point of separation is rarely identical with the contact point. If any prolonged interaction between the ligands and receptors occurs, then the attractive forces still cause the cantilever attachment to the surface. Only when the cantilever spring constant exceeds the force gradient of the bond the AFM probe detaches from the surface, i.e. bonds holding the cantilever attached to the surface receptors are broken (point D). At this moment, the cantilever returns abruptly to its initial position where it oscillates around its free position (base line).

The character of the force curves changes depending on how many bonds are formed within the contact area between the ligand-modified tip and the receptor-covered surface. The disruption of multiple bonds can proceed through several mechanisms. The two simplest ones are cooperative and independent adhesion (Figure 4.5).

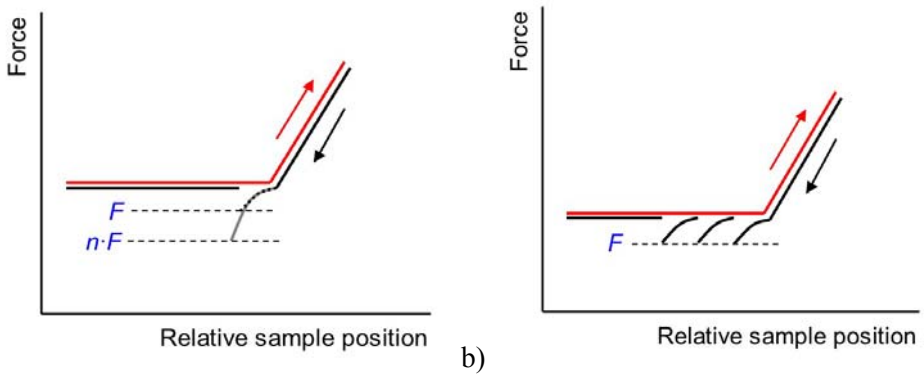


Figure 4.5. Multiple bonds unbinding showing cooperative (a) and independent (b) adhesion.

In cooperative adhesion multiple ligand-receptor complexes break simultaneously, leading to the larger unbinding force (being the product of a force of the single bond $F$ and the number of bonds $n$ ruptured at the same time). The resulting force curve has a similar shape with larger unbinding force (Figure 4.5a). When molecular bonds act independently, the rupture proceeds sequentially and the detachment force has a similar value as that of a single molecular complex. The force curve

will show a saw-tooth pattern with unbinding events of the similar rupture length and the unbinding force value (Figure 4.5b).

### *4.2.2 Force versus sample-distance conversion*

In the force spectroscopy, the raw dataset represents usually a photodetector response versus a voltage applied to the piezoelectric scanner. Both these quantities have to be converted into the dependence between a force (in nN) and a relative surface (or scanner) position (in nm). Next, the data are converted into the force and tip-sample distance values.

*The tip-sample distance*

The relative scanner (or sample) position recorded during the AFM measurement is not a distance between a tip and a sample *(Cappella et al. 1999)*. A sample (or an AFM tip) is moved along Z-axis (this is related to the piezoelectric scanner displacement, $Z$) and the cantilever deflection $d_C$ is recorded. Thus, displacement $Z$ is a distance between the sample surface and the "rest" cantilever position (Figure 4.6).

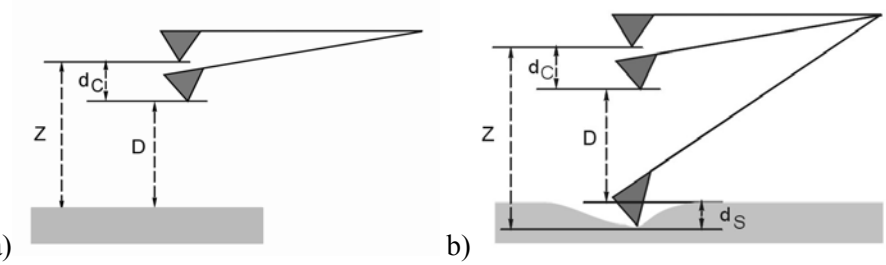


Figure 4.6. The tip–sample distance in AFM. $D$ is the actual tip-sample distance, $Z$ is the distance between the sample and the cantilever "rest" position. The difference between them takes into account the cantilever deflection $d_C$ and depth of the sample deformation $d_S$.

If the sample is non-deformable, the tip–sample distance, $D$, can be calculated as follows

$$D = Z - d_c . \tag{4.5}$$

However, if the sample surface undergoes deformation, the resulting cantilever deflection will be smaller as compared with a hard sample and then the calculation of the tip-sample distance should consider it. The equation should be rewritten into

$$D = Z - (d_c + d_S) \tag{4.6}$$

where $d_S$ is the depth of the sample deformation.

*Force determination*

The force is usually calculated using the formula (4.1), which requires the knowledge of the cantilever spring constant $k$ and the photodetector sensitivity *PSDcal*

$$F_{[nN]} = k_{[N/m]} \cdot PSDcal_{[nm/V]} \cdot d_{[V]} \tag{4.7}$$

where $d$ is the measured cantilever deflection.

The determination of the true force acting on molecule should take into account the contribution from the hydrodynamic drag force, $F_{drag}$,, which is usually present in AFM measurements since the cantilever experiences a force arising due to viscous friction with the surrounding liquid *(Butt et al. 2005),* like any object moved through a solution (see *Annex 7*). Thus, hydrodynamic drag acts always in the opposite direction to the cantilever movement. Thus, the force measured by AFM ($F = kx$) is a sum of the true force acting on molecule ($F_{true}$) and the hydrodynamic force ($F_{drag}$). Its value is smaller when cantilever approaches the surface and larger when cantilever is withdrawn from the surface.

### *Force detection limit*

The detection limit value of the unbinding force is linked with the cantilever spring constant, $k$, by the following formula *(Gittes et al. 1998)*:

$$F_{MDL} = \sqrt{k \cdot k_B \cdot T}, \tag{4.8}$$

where $k_B$ is the Boltzmann constant, and $T$ is the temperature. Table 4.1 presents the theoretical force detection limit calculated for typical cantilevers.

Table 4.1. Force detection limit of cantilevers typically used for various biological applications, estimated for the room temperature of 23°C.

| | |
|---|---|
| $k$ = 0.01 N/m | $F_{MDL}$ = 6.6 pN |
| $k$ = 0.03 N/m | $F_{MDL}$ = 11.4 pN |
| $k$ = 0.1 N/m | $F_{MDL}$ = 20.9 pN |
| $k$ = 0.5 N/m | $F_{MDL}$ = 46.7 pN |

Depending on the cantilever spring constant, the detection limit changes significantly and inappropriate choice of the cantilever may make impossible measurements of the interaction force between single molecules.

Experimentally, the force detection limit is usually determined from the noise fluctuations of the base line i.e. the horizontal parts of the force curve recorded far away from the investigated surface, where the interaction forces are negligible (Figure 4.7).

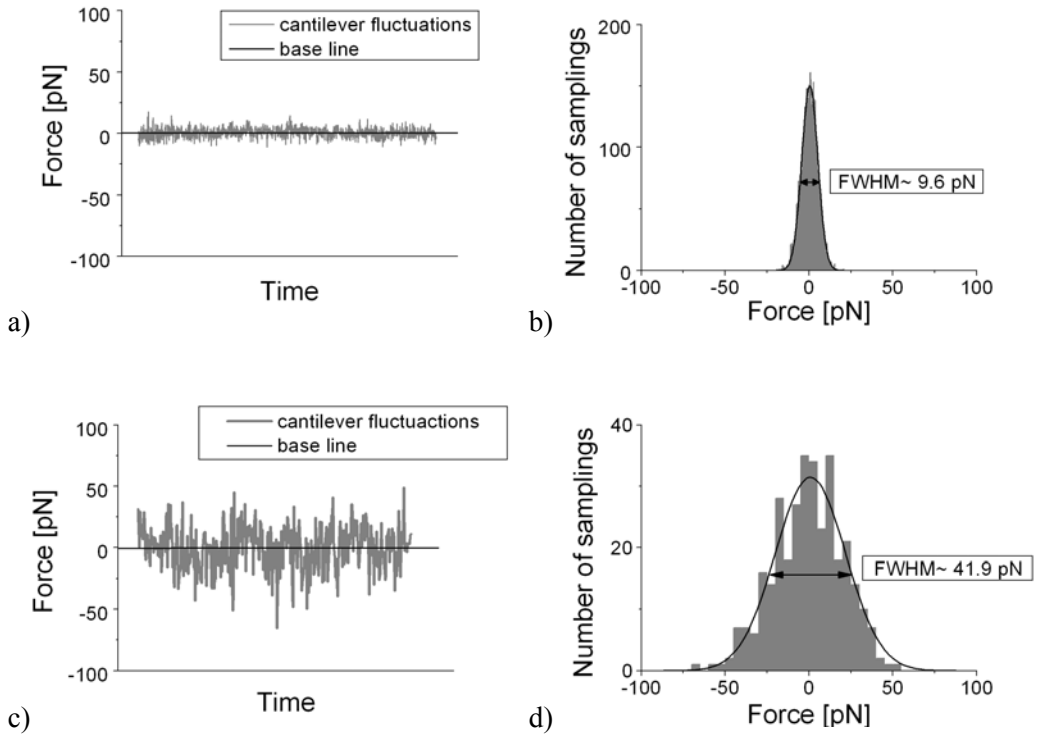


Figure 4.7. a) & c) Cantilever fluctuations around the base line measured in PBS buffer for two randomly chosen cantilevers, both with the nominal spring constant value of 0.01 N/m, functionalized with the antibody against prostate specific membrane antigen. b) & d) The corresponding histograms of the cantilever fluctuations. FWHM defines the range of fluctuations.

To quantify the cantilever fluctuations, their histogram can be fitted with the Gauss function. The determined full width at half height (FWHM) can be used as an estimate of the force detection limit. Figure 4.7 b&d presents the cantilever fluctuations around the base line measured in PBS buffer for the cantilever with the nominal spring constant of 0.01 N/m, functionalized with the antibody against prostate specific membrane antigen. The FWHM value in this particular experiment was ~10 pN. However, in similar experiment (Figure 4.7 c&d) even though the same cantilever type was used, the FWHM value was much larger (41.9 pN), indicating much higher noise level. Apart thermal excitations, there are many possible sources for the cantilever fluctuations. They may be induced due to: i) the quality of the surface of the liquid-cell setup, ii) transparency of the buffer used in experiment, iii) the fact that the sample or its fragments may detach from the surface, and also, iv) the quality of the procedure for cantilever functionalization.

### *4.2.3 Elements that should be calibrated separately*

The conversion of the force curve into the dependence between the force and the tip-sample distance and also the determination of the interactions forces requires that some microscope's elements have to be calibrated (or at least checked).

*Scanner linearization*

Since the true scanner displacement is very crucial for all calculations, the piezoelectric scanner nonlinearity and hysteresis should be checked. In commercially available AFMs, scanner linearization is frequently an integral part of their hardware. Real displacements of the sample in all three axes are measured using optical, capacitive, or other methods. A simple way to verify the precision of the scanner performance is to measure a force versus relative sample position curve on a stiff, non-deformable surface and to verify whether the approach curve is identical (overlaps) to the retraction one and if it is represented by a straight line. If it is true, the piezoelectric scanner is hardware-linearized. If not, the piezoelectric scanner should be linearized off-line. Among several methods of scanner linearization, the method of *z*-calibration proposed by Jaschke and Butt *(Jaschke et al. 1995)* is very straightforward and does not require any additional equipment (Figure 4.8a). However, it can be applied only to AFMs having an optical detection system. In this method, a mirror is placed in the sample position in such a way that the inclination of a mirror is the same as the inclination of a cantilever. The slightly unfocused laser beam produces two reflected beams: from the back of cantilever and from the mirror surface. When the mirror moves up and down, the optical path lengths of a beam fractions change and the resulting interference signal varies (Figure 4.8b). The measured distances between subsequent maxima reflect the scanner nonlinearity

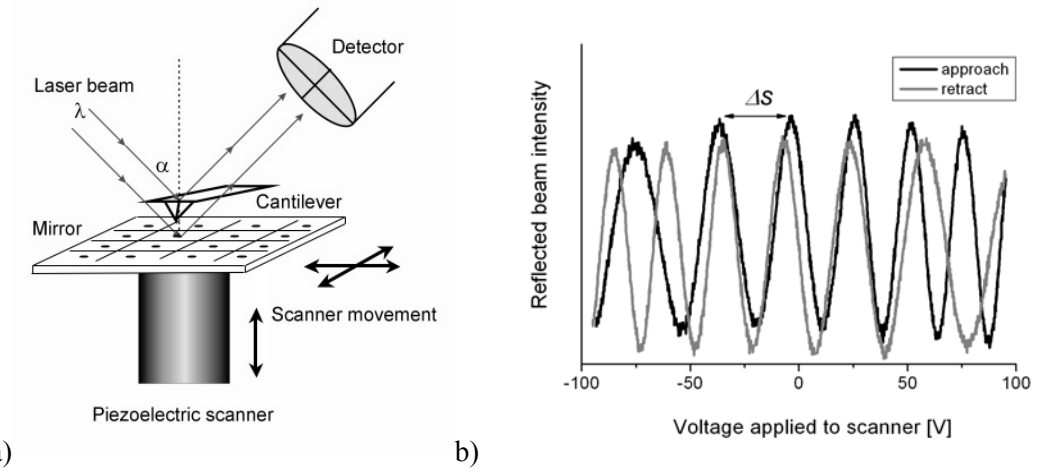


a) b)

Figure 4.8. a) Schematic representation of the method proposed by Jaschke and Butt applied for the piezoelectric scanner calibration at each location (black dots) on a mirror surface. b) Reflected beam intensity as a function of the voltage applied to the scanner recorded in both direction of scanner movement: to and from the mirror and the distance ($\Delta s$) is between two subsequent interference maxima *(Lekka et al. 1999)*.

Using the Bragg law it is possible to calculate the true scanner extension

$$\Delta s = \frac{n \cdot \lambda}{2 \cdot \sin\alpha}. \tag{4.9}$$

where λ is the wavelength of the laser beam, α is the angle of the incident beam and *n* is the number of interference maxima. In case of the linearized scanner, the two traces of the reflected intensity, recorded during the up and down movement of the scanner, should overlap. If not the relation between the determined positions of the maxima and the applied voltage should be quantified. The scanner nonlinearity and hysteresis can be described by a polynomial function – usually a quadratic approximation is sufficient *(Lekka et al. 1999b)*:

$$True\ scanner\ extension = H_Q \cdot (applied\ voltage)^2 + H_L \cdot (applied\ voltage) \qquad (4.10)$$

where $H_Q$ and $H_L$ are quadratic and linear coefficients.

To demonstrate the effect of the scanner hysteresis and non-linearity, the intensity of the interference signal was recorded along a single scan line within the scanner surface close to the scanner centre (open squares) and away from it (black dots). Two different scan sizes were chosen i.e. 2.5 μm and 30 μm. Figure 4.9a&b presents the changes of the linear coefficient $H_L$ describing the scanner nonlinearity while Figure 4.9c&d – the quadratic one, $H_Q$. In general, the variations of the linear coefficient are smaller (up to 10 % for the case when calibration was performed away from the scanner centre, for a large scanned area). The quadratic coefficient, $H_Q$, deviates more strongly – up to 40 %. The most reliable and accurate AFM data can be obtained when the measurements are performed in the middle of the scanner and with a small scan size.

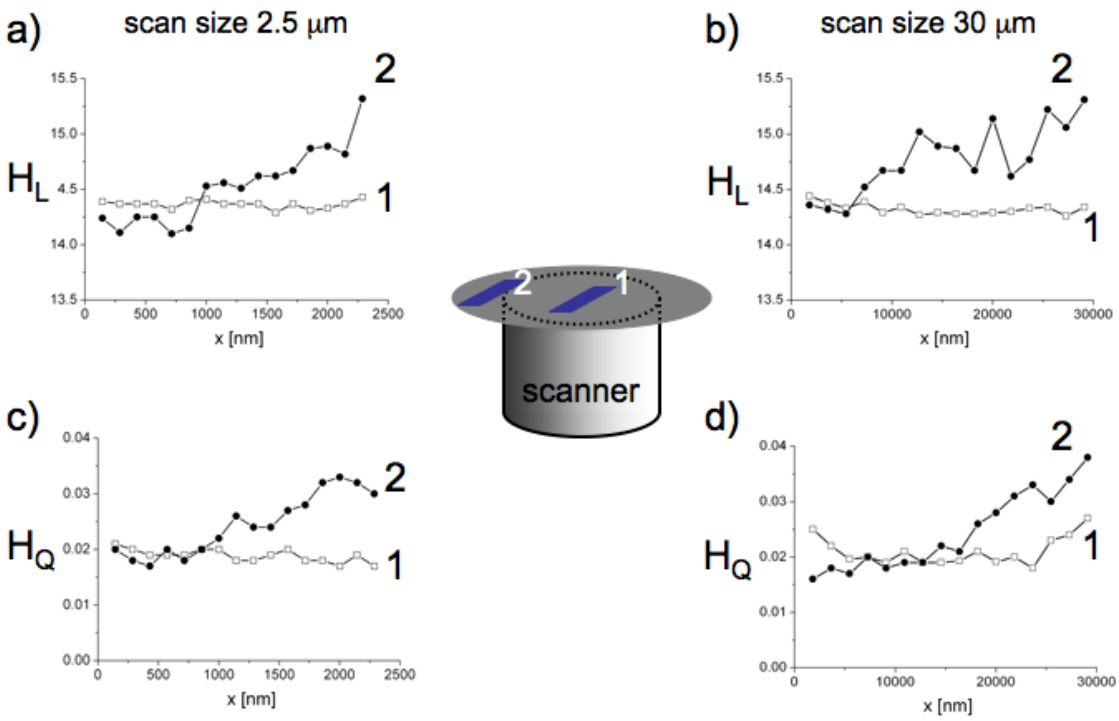


Figure 4.9. Dependence of the scanner nonlinearity coefficients on a relative position of the sample surface with respect to the scanner centre (EBL#2 from Staveley Sensors (see Appendix 2). a) & c) scan size of 2.5 μm. b) & d) 30 μm.

In that case the determination of the true piezoelectric extension is minimally burden by the scanner non-linearity and hysteresis. The obtained mean values of the non-linearity factors are $H_Q = 15.6 \pm 0.8$ nm/V and $H_L = 0.037 \pm 0.003$ nm/V$^2$.

In commercial devices, the scanner linearization is usually performed automatically without the action of the external user. Taking into account the ageing of piezoelectric materials with time, the linearity of scanner should be measured from time to time since the incorrect parameters influence not only the true scanner displacement but also the photodector sensitivity used for the force determination.

*Photodetector sensitivity calibration (PSDcal)*

In most AFM systems, the deflection of the cantilever is recorded using the optical system composed of a laser and a photodetector. In order to calibrate the cantilever deflection in the force spectroscopy mode, the force curve should be recorded on stiff, non-deformable surface, where after the contact with the surface the deflection directly reflects the position of the sample. In many biological applications, where the force spectroscopy mode is involved in the cell elasticity measurements, the commonly applied cantilevers have the spring constant in the range of 0.01 N/m ÷ 0.1 N/m and the typical loading force value does not exceed 30 nN *(Lekka et al. 1999a; Ikai et al. 2003)*. Assuming that the typical silicon nitride cantilever of a paraboloidal shape (with the tip radius of 20 nm) indents the flat surface with the load force of 30 nN, the resulting indentation depth is merely of 0.2 nm for glass (this estimation is performed assuming Hertz mechanics of contact *(Sneddon 1965)*. Therefore, in this range both glass and mica surface can be used as hard, non-deformable samples. Figure 4.10 presents the typical force curve (only the approach part is shown) recorded on a glass surface used as a reference curve for photodetector sensitivity calibration.

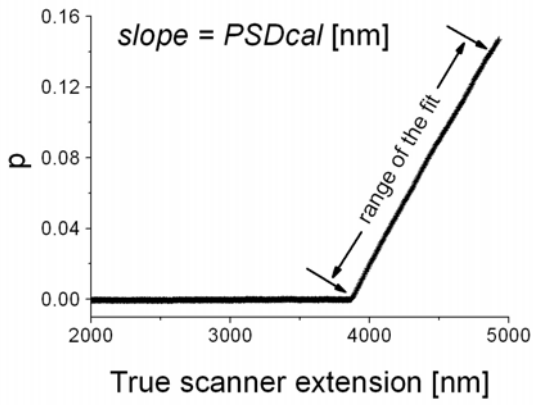


Figure 4.10. Typical force curve recorded on a glass surface with the cantilever $k$ = 0.01 N/m (only approach part is shown). The *PSDcal* coefficient was determined as a slope of the fitted line (range marked by arrows).

The *Y-axis* is the cantilever deflection *(A–B) signal* normalized to the recorded total signal *(A+B) signal* according to

$$p = \frac{(A-B)\,signal}{(A+B)\,signal}. \tag{4.11}$$

The *PSDcal* coefficient was determined as an inverse value of the slope obtained from the linear fit to the region where after the contact with the surface the deflection directly reflects the position of the sample. The obtained value reflects the properties of the optical system used for the cantilever deflection. However, one should keep in mind that it changes not only from one AFM system to the other but also from one measurement to another. Fortunately, for a particular AFM system, careful cantilever treatment (especially, during liquid exchange), and proper settings of the optical system, its value does not change much. Figure 4.11 shows the distribution of the *PSDcal* values obtained for the three different types of cantilevers used in the measurements presented in this monograph.

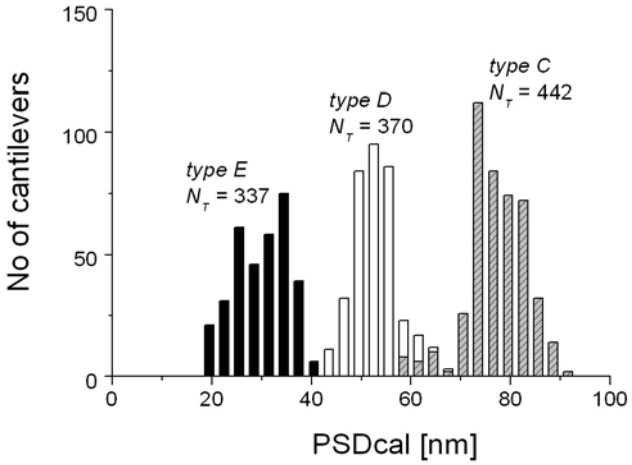


Figure 4.11. The distribution of the *PSDcal* coefficients determined for the three different cantilever types. Cantilevers of type C, D, E were used for the measurements presented in this monograph. $N_T$ is the total number of cantilevers analyzed.

The photodetector sensitivities (determined from Gaussian fit for each cantilever type C, D, E, with the corresponding nominal values of the spring constants given by the producer, equal to 0.1, 0.03 and 0.01 N/m were 30.5 ± 6.4 nm, 52.4 ± 4.1 nm, and 77.3 ± 5.7 nm, respectively. The half width of the distribution at half-maximum height (HWHM), used as an error estimate, was below 10% of the central value for 0.01 N/m & 0.03 N/m cantilevers and 20% for $k$ = 0.1 N/m. Values much lower and much larger than (*mean* ± *HWHM*) may indicate broken cantilevers. Therefore, in such case, the cantilever must be exchanged.

*Spring constant determination*

The knowledge of the spring constant of the cantilever is crucial for the force calibration. Sometimes, its value can be analytically calculated when the geometry and materials constants are given. It is relatively easy to do this if the used cantilever has a rectangular shape *(Green et al. 2004)*. However, in case of triangular shaped cantilevers, the calculations are far more complex.
One can estimate the spring constant for the triangular cantilever approximating its shape as a doubled rectangular cantilever. However, such approach does not precisely estimate the elastic properties of the cantilever. The most complete analytical description of the cantilever bending was proposed by Neumeister *et al. (Neumeister et al. 1994;* see Appendix 3*)*. In order to avoid these calculations several methods for the spring constant calibration has been delivered. Among them, the most popular one uses the measurement of the resonant frequency ($\omega_{meas}$) of thermally excited cantilever. In the most convenient way one assumes that the actual mass of the cantilever is equal to the nominal one. Then the following equation can be applied:

$$k = \frac{k_N \cdot \omega_{meas}^2}{\omega_N^2}, \tag{4.12}$$

where $\omega_N$ and $k_N$ are the nominal values of the thermally excited resonant frequency and the spring constant of the cantilever, respectively. Figure 4.12 presents the example of the resonant frequency spectrum obtained on the basis of the noise measurement of the thermally excited cantilever and the applied fast Fourier Transform.

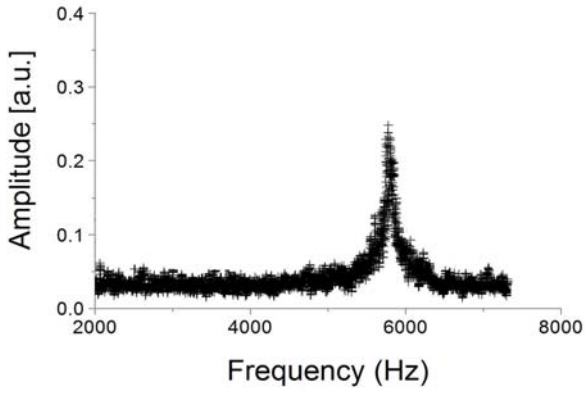


Figure 4.12. Resonant frequency measured for the thermally excited cantilever. The obtained resonant frequency is 5.8 kHz what corresponds to the calculated cantilever spring constant of 0.007 N/m

For cantilevers undergoing the same production conditions the distribution of the resonant frequency is narrow what enable to determine the resonant frequency. Very often, its value is smaller than the minimal value given by manufacturer (see Appendix 4). A detailed, more precise procedure of the spring constant determination has been proposed by Sader[18] *(Sader et al. 1995)*. In

[18] The Sader method of the cantilever spring constant determination has been published in Sader *et al. Rev. Sci. Instrum.* **66** (1995) 3789.

this method, the $k$ value is determined from the cantilever resonant frequency $\omega_{meas}$ according to the following equation

$$k = M_e \cdot m \cdot \omega_{meas}^2, \tag{4.13}$$

where $M_e$ is the effective mass, $m$ is the mass of the cantilever calculated by multiplying the density of the silicon nitride (2.8 g/cm$^2$) by the volume of the cantilever. This method delivered similar values as those when using the Equation (4.11), i.e. 0.007 N/m for the cantilever with nominal spring constant of 0.01 and 0.025 N/m for the cantilever with the nominal spring constant of 0.03 N/m. The observed small discrepancy between the values comes from the errors in the estimation of the cantilever mass which takes into account all geometrical dimensions of the cantilever. Therefore, the true value is burden by many factors, mainly the value of the cantilever thickness. The large discrepancy of the spring constants is not disturbing the calculations if all cantilevers used have the similar resonance frequency.

*Scanner velocity determination*

The retraction velocity (describing how fast two molecules are separated) is essential for the determination of the loading rate value, since the measured unbinding force depends on how fast the applied rupture force changes in time *(Evans 2001)*. In AFMs, the separation is realized by the movement of the piezoelectric scanner. Therefore, scanner nonlinearity influences strongly the values of the retraction velocity. Only if a hardware linearization is provided, the force change in time can be assumed linear.

How strongly the scanner non-linearity influences the determination of the retraction velocity can be demonstrated for the apparatus working at the IFJ PAN. It operates using a non-linearized piezoelectric scanner (Figure 4.13).

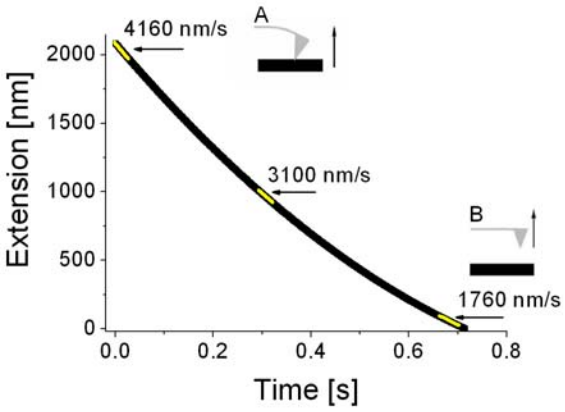


Figure 4.13 Relation between the scanner elongation and time (scanner type EBL#2). Arrows indicate the temporary speed.

The temporary speed calculated from the tangential (marked by arrows) decreases with time during retraction (from point A to B). Two extreme values of the velocity correspond to the loading rates of 41600 pN/s and 17600 pN/s. For example, the unbinding force measured for the

antigen–antibody pair composed of bovine albumin and the monoclonal antibody (for data from *Gryboś 2005*) changed by about 15 % – from 376 ± 20 pN (17640 pN/s) to 432 ± 14 pN (44700 pN/s).

In offline data processing, the averaging of the retraction velocity manifests in broadening of the force distribution. The other consequence of the lack of accurate knowledge of the loading rates causes a large distribution of points in the relation between the unbinding force and loading rate. Therefore, knowing the exact value of scanner retraction velocity in the moment when unbinding of two molecules occurs significantly improves the quality of the force histogram as shown on the Figure 4.14 a&b).

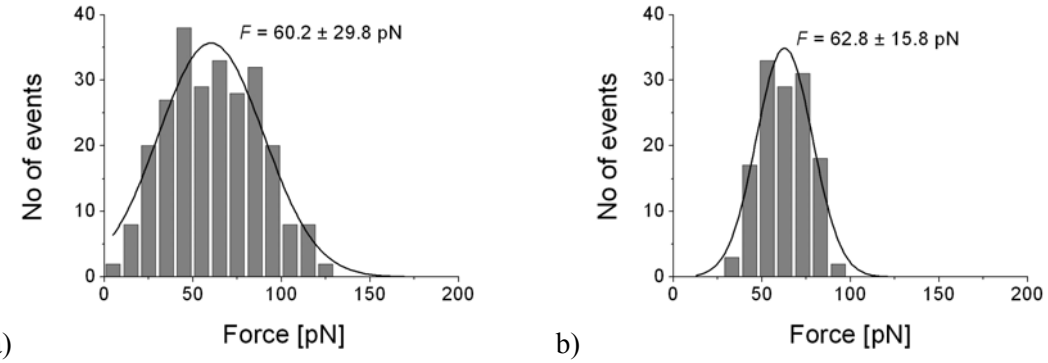


Figure 4.14. Force histograms before (a) and after (b) the determination of the exact value of the retraction velocity. The same set of data is shown on both histograms.

The effect of the inappropriate determination of the retraction velocity is slightly visible in the unbinding force value where the relative change of the unbinding force was of about 4%. Such error lies within the experimental uncertainties originating from the AFM measurements. The influence of the retraction velocity was clearly visible in the width of the force histogram. After exact determination of the retraction velocity the width of the force histogram decreases almost two times. However, one should point out that the retraction velocity is not the only factor influencing the width of the force histogram. The other factors are, for example, the noise level (and thereby the force detection limit) and the physics of the unbinding process (i.e. the dependence on the loading rates).

## 4.3 Tip and surface functionalization

Studies of the expression of various molecules present on the living cell surfaces require the use of protocols of the AFM cantilever functionalization with complementary molecules that are recognized by the cell surface molecules. The molecules of interest can be broadly grouped into nucleic acids (DNA, RNA), proteins (antibodies, enzymes, and receptors), small molecules (e.g. peptides, metabolites), and other biomolecules (e.g. carbohydrates, lipids). The attachment of those

molecules depends on their surface properties, on the solid surface used as a substrate, and/or on the liquid medium. In most cases, surface of molecules will display a higher level of complexity than the substrate or the liquid medium. They exhibit not only an overall charge and hydrophobicity, but also a heterogeneous distribution of surface-exposed groups. In addition, during measurements the attached molecules should preserve their biological activity unchanged.

### *4.3.1. Tip functionalization*

There are two popular protocols that either directly or indirectly immobilize proteins on the surface of the AFM tip (Figure 4.15).

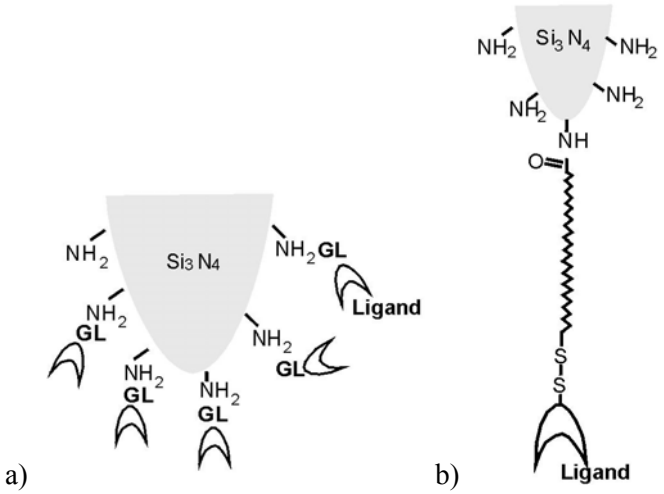


Figure 4.15. Two ways of the AFM probe surface modification: a) direct method where the desired ligand is attached through crosslinking agents as glutaraldehyde (GL), and b) indirect one where ligands are attached through a polymeric spacer.

In the first protocol, the glass or mica surface is silanized using e.g. 3–amino-propyltriethoxylsilane, which enriches the surface with amino groups *(Allen et al. 1999)*. Next, the silanized surface is activated using crosslinking agent such as glutaraldehyde. The choice of agents depends on proteins to be deposited. Both homo- and bifunctional agents can be employed in the protocol. Afterwards, proteins are delivered. Such protein immobilization enables direct deposition of proteins on the surface. However, for some purposes, this procedure may not be desired since it blocks protein reorientation. To avoid it, another method was developed *(Hinterdorfer et al. 1996)*. In this method, protein molecule is attached to the AFM probe using a polymeric spacer. A common spacer is, e.g. polyethylene glycol, PEG. Its amino group is used to bind PEG onto a gold-coated surface of the silicon nitride tip. A thiol group located at the end of the PEG molecule attaches a ligand *via* a covalent bond.

*Immunoglobulins*

Regardless of the method chosen for the cantilever modification, the final results should assure the attachment of reacting functional molecules. The most common way of studying molecular interactions uses immunoglobulins (or in the other words *antibodies*) as probes. These molecules are synthesized by lymphocytes, highly specialized immune system cells involved in the differentiation between self and non-self structures which leads to specific and nonspecific interactions, and suppression of the latter ones *(Davies et al. 1990)*. Antibodies recognize with a high affinity fragments of various structures, such as simple or complex proteins, carbohydrates, nucleic acids, etc. Such structures, due to their ability to trigger immune response, are called antigens. Regions of antigens, which bind to antibodies, are known as antigenic determinants (or epitopes). The interaction between an antigenic determinant and its specific antibody is an excellent example of intermolecular interaction, irrespective of whether the antigenic determinant is of a solely protein, protein/carbohydrate or other origin. Furthermore, such binding is determined by typical intermolecular weak forces such as hydrophobic, electrostatic, and van der Waals forces *(Leckband et al. 2001)*. The characteristic feature of large antigen molecules is that they induce the activation of many antibody-producing B lymphocytes in the immunized animal. This polyclonal mixture of resulting antibodies (called *polyclonal antibodies*) may then recognize variety of epitopes on the antigen. A homogeneous population of antibodies (i.e. *monoclonal antibodies*) can be raised by fusion of B lymphocytes with immortal cell cultures. Both groups of antibodies have its own specificity of application in different studies. The polyclonal antibodies, since they react with multiple epitopes on the antigen, will be more tolerant of minor changes in the antigen, e.g., heterogeneity of glycosylation, or slight denaturation, than will monoclonal (homogenous) antibodies. The latter ones are more vulnerable to the loss of epitope through chemical treatment of the antigen. Specificity of monoclonal antibodies makes them extremely efficient for binding of the antigen within a mixture of related molecules, such as in the case of affinity purification.

### *4.3.2. Surface modification*

Mechanisms of immobilization of biological molecules can be divided into two major categories: ***adsorption*** and ***covalent binding***. Adsorption relies on non–covalent interactions – mainly electrostatic, van der Waals, and dehydration of hydrophobic interfaces *(Israelaschvili 1992)*. It has a purely physical nature and therefore displays varying levels of reversibility. Such way of molecule immobilization results in their random orientation and relatively weak attachment, what may significantly elongate the time of measurement. The covalent binding of specific molecule functional groups to functionalized surfaces, by definition involves formation of essentially irreversible chemical bonds between the molecule and the substrate surface. Therefore, it results in a very strong attachment and, in certain instances, enables the oriented molecule

deposition. A variety of side groups can be easily used for covalent binding – most common ones are amino, carboxylic, hydroxyl, and thiols groups. However, in many cases the covalent binding is enabled only after additional functionalization of the surface and/or biomolecule *(Zlatanowa 2006)*. Very often, it is realized using crosslinkers such as glutaraldehyde. In biological applications, the most common AFM probes are made of silicon or silicon nitride. Biomolecules are usually immobilized on glass, mica, and gold. Therefore, immobilization requires a development of an appropriate protocol of the attachment.

The diversity and complexity of proteins can make their deposition very difficult. Proteins have many different structures, contain heterogeneous hydrophobic and charged domains, are extremely fragile with respect to their biological activity, and can have multiple interaction sites. Additional complications arise when a correct orientation of the bound protein is required, for example to increase the number of functional groups exposed to the buffer. The immobilization protocols that have been used so far apply both mechanisms of immobilization, i.e. adsorption and covalent binding. The appropriate protocol of the protein deposition should therefore be tailored to the specific protein used.

### *Adsorption*

The adsorption of proteins depends on two main features: their surface charge and their hydrophobic domains. Both properties enable a certain degree of control of protein deposition, however, they can result in randomly oriented molecules. The electrostatic adsorption seems to be sufficient to assure a relatively strong attachment, but it does not have permanent nature and it can be strongly affected by changes of solution pH and ionic strength. Therefore, there are a limited number of proteins that can be immobilized in this manner. When the hydrophobic attraction is chosen as a main source of adsorption, stronger and less reversible interaction is expected. On the other hand, it may result in loss of functional activity due to partial denaturation, as the protein unfolds to expose hydrophobic interior portion to the hydrophobic surface.

### *Covalent binding*

Covalent binding is quite often used since proteins present a variety of functional groups, including amino, carboxyl, hydroxyl, and thiol that can be readily used for such binding to the different surfaces possessing complementary chemical groups. However, more care should be taken into account in order to avoid chemically induced denaturation of protein during the attachment process. There are many strategies for crosslinking of available functional groups. Most of them use a specially designed crosslinkers, for both attachment and physical separation of protein from the surface, thereby allowing more of the protein functional domains to be exposed to the buffer. Covalent binding generally produces a higher concentration of proteins than the adsorption.

Proteins can be also better oriented by additional techniques, such as i) the use of antibodies that bind proteins leaving the antibody binding sites free, ii) the use of biotinylation which enriches proteins with the binding site specific to streptavidin-coated surface, iii) cysteine thiol production in the protein fragment far from the binding site, allowing its deposition on gold coated surface, or iv) using the sugar binding molecules that bind to the oligosaccharide's moieties of proteins.

*Cell lines*

The application of AFM in studies of mechanical properties of living cells requires the appropriate cell preparation, i.e. cells should be well attached to the substrate (usually it is a glass coverslip, see Figure 4.16a) forming a dense but single monolayer. Apart from that, the way of cell preparation is similar as for other methods. Sometimes reagents such as fibronectin, collagen or poly-L-lysine have to be used to improve adhesive properties of the substrate in order to attach cells. However, one should remember that reagents might influence the mechanical properties of living cells what can be detected by the measurements of cell stiffness[19] *(*Figure 4.16b, *Lekka et al. 1999a; Lekka 2007)*.

a)

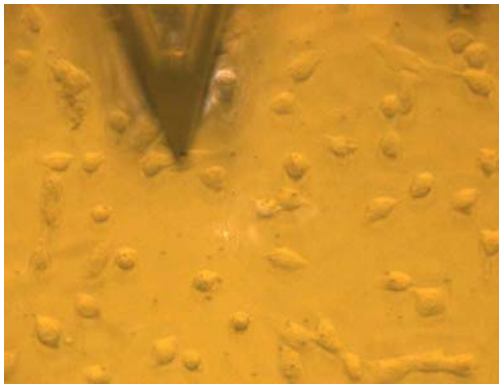

b)

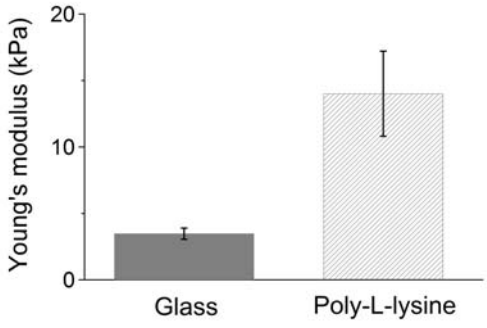


Figure 4.16 a) HCV29 cells on glass coverslip prepared for AFM measurement. b) The Young's modulus value of WM35 melanoma cells determined for cells growing on a glass and poly-L-lysine coated surfaces in culture media (RPMI 1640 supplemented with 10 % of fetal calf serum.

[19] Cell stiffness determination is described in *Appendix* 6.

The Young's modulus value determined for WM35 melanoma cells (primary cutaneous melanoma cell line from a radial growth phase) was different depending on the used substrate: pure glass surface carrying negative charge in water solution and poly-L-lysine (0.01 % v/v) coated glass carrying positive charge on its surface. As one can see, the cell stiffness can undergo 3-fold change, thereby indicating the reorganization of cell cytoskeleton. Since the organization of cytoskeleton defines the surface location of adhesion receptors that are connected with the cytoskeletal elements, it is important to keep substrate properties constant during the whole experiment.

## 4.4. Inhibition of binding sites

In AFM studies, the proper control of the experiments proving that the observed interaction comes indeed from the investigated molecular pairs must be carried out. One way of control experiments is to use standard biochemical methods such as fluorescence microscopy *(Lebed et al. 2006)* or immunolabbeling *(Goffin et al. 2006)*. However, very often these methods are not sensitive enough to prove the specificity of the interaction. Therefore, apart from them, the common way of keeping control is to block the studied interaction by adding to the solution the same type of molecules, as those attached to the tip surface (Figure 4.17a).

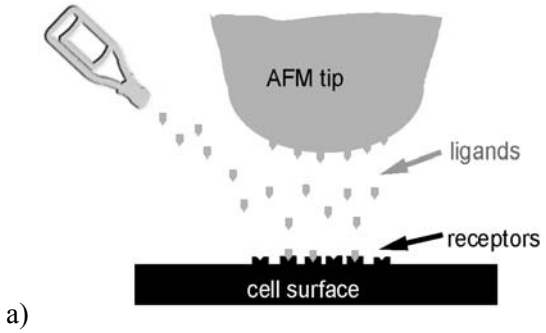


a)

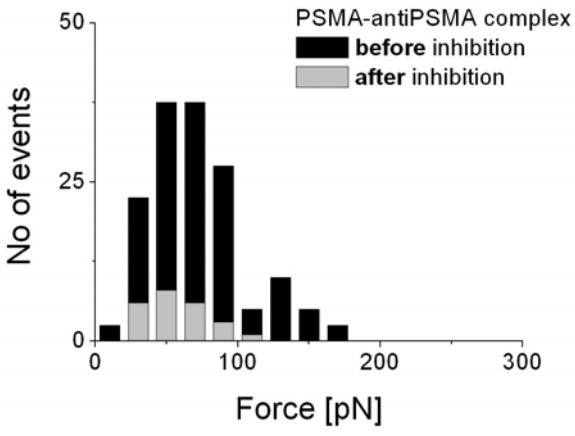


b)

Figure 4.17 a) The idea of the inhibition of binding sites on cell surface. b) The distributions of the unbinding events before (black columns) and after (grey columns) the inhibition of the interaction between the prostate specific membrane antigen (PSMA) and its monoclonal antibody (anti-PSMA, *Laidler et al. 2005* ).

These free molecules bound to the binding sites make them inactive during probing with the functionalized AFM tip. Such experiment can be parameterized by *the unbinding probability*, defined as a ratio between the number of the unbinding events to the total number of force curve recorded. This quantity is proportional to the number of binding sites of receptor molecules (or to the receptor number if only one binding site is present on its surface). The inhibition of binding sites results in the lower number of events (and thus smaller event probability) that can be attributed to the unbinding of ligand–receptor complex. Therefore, the comparison of the estimated probability, before and after the inhibition of binding sites, proves the specificity of the studied interaction. The example of the binding site inhibition is presented in Figure 4.17b. The prostate specific membrane antigen, present on the surface of prostate cells, was blocked with its monoclonal antibody added to the buffer *(Laidler et al. 2005)*. Thus, the antibody molecules attached to the AFM probe did not interact with the complementary antigen and the resulting number of the unbinding events decreased. Some unbinding events were still observed, since not all antigens were recognized and blocked by the antibody molecules. Such measurements show the origin of the measured interaction force.

# CHAPTER 5

# Data analysis

New class of experimental techniques, such as laser optical tweezers, the biomembrane force probe, and the atomic force microscope, enable measurements of interaction forces at molecular level not only for isolated single molecules but also for receptors embedded directly in a plasma membrane of living cells. Together with the development of these new techniques, novel analytical methods are the challenge for many experimentalists willing either to more precisely describe the force–induced unbinding or to parameterize the observed differences between investigated samples.

The qualitative and quantitative description of the expression of adhesion molecules is possible after the analysis of a large number of recorded force curves. During the contact of functionalized tip with receptors covering the substrate, bounds are formed randomly. Therefore, the first step of the analysis is a selection of the appropriate subset of data with force curves possessing a characteristic jump related to the unbinding of two molecules. Then, an unbinding event is quantitatively characterized by three parameters: the unbinding force, the rupture length and the system spring constant.

## 5.1 Force curve selection

First step of data selection is based on the examination of the character of the recorded force curves. The easiest work is to take the decision whether the unbinding event was registered or not (Figure 5.1).

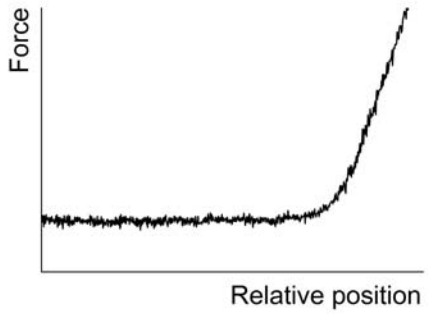


Figure 5.1. The retraction part of the force curve with no unbinding event.

When an adhesion event is present, it is registered as a jump present on the retraction part of the force curve. If the shape of such jumps has no common features for a large number of recorded curves, it can be only attributed to non–specific interactions e.g. electrostatic attraction present between any charged surfaces. The additional indication of such case is no change in the slope of

the curve in the repulsive ($k_c$, reflecting the cantilever stiffness) and adhesive part where the system spring constant, $k_{syst}$, has only the contribution from the cantilever stiffness (Figure 5.2).

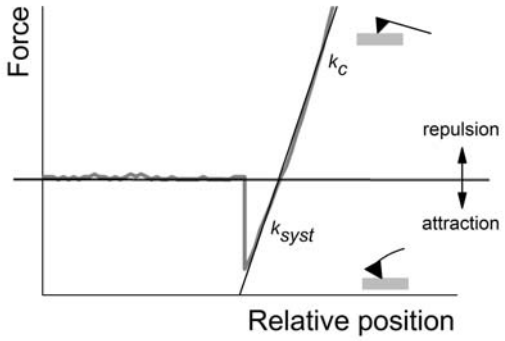


Figure 5.2. The retraction part of the force curve showing the non-specific adhesion.

More accurate examination of the curve shape is required when unbinding events of similar shape occur with visible change of the system spring constant. As the analysis of the interaction forces is mostly reliable for the unbinding of single molecules, all curves displaying the complex bond rupture should be disregarded when more than one bond was formed,

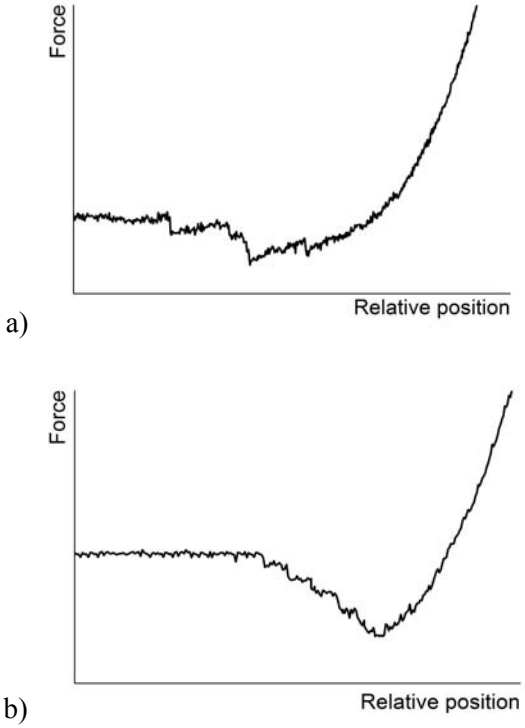


Figure 5.3a&b. Retraction curves recorded during the separation of the functionalized AFM tip from the cell membrane. Two distinct shapes of the unbinding events can be observed.

Two different shapes of curves with multiple unbinding events can be observed: those with almost separate events (Figure 5.3a) and those with step–like structure (Figure 5.3b). It is worth to notice that those force curves showing a characteristic jump observed during approach should be excluded

from the analysis. Most probably, such behavior indicates the cell membrane punching (Figure 5.4).

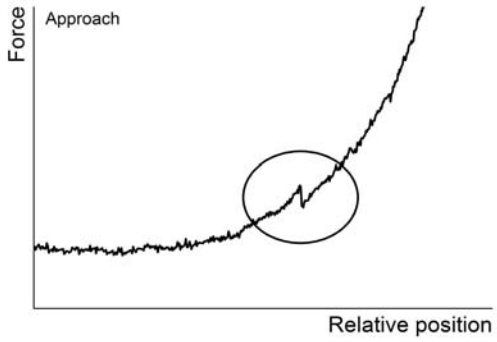


Figure 5.4. Curve recorded during the approach of the AFM tip towards the cell membrane. The characteristic jump most probably indicates the punching of the membrane. Such force curve also should not be used in the analysis *(Lekka et al. 2006)*.

To complete the picture, the examples of curves showing a single specific unbinding event are presented in Figure 5.5.

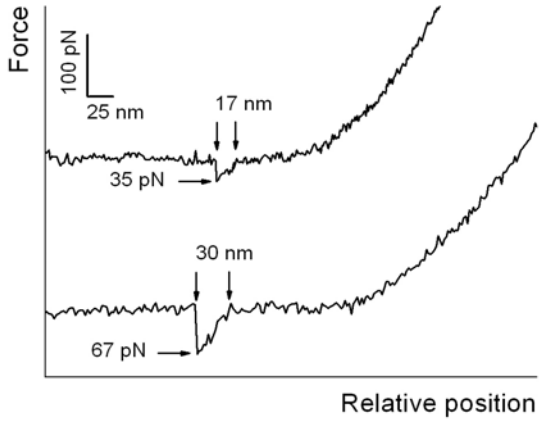


Figure 5.5. The retraction part of the force curves recorded on a surface of living HCV29 bladder cells probed with cantilever functionalized with monoclonal antibody against N-cadherin. Curves demonstrate the single unbinding events occurring between N-cadherin and its monoclonal antibody *(Lekka, unpublished data)*.

From such single unbinding events two parameters can be obtained: the unbinding force values and the distance at which two molecules were separated.

## 5.2 Parameters derived from a single force curve

In order to quantitatively characterize the specific interaction between a pair of molecules, three parameters are determined: an unbinding force, a rupture length which together with bond stiffness reveals the stiffness either of a formed bond or of a whole system composed of a bond and a pulled cell membrane. An additional parameter determined on the basis of the performed overall

measurements, is an unbinding probability that is related to the density of receptors present on the substrate surface or in the cell membrane.

### *5.2.1. The pull-off force and force histogram*

*The pull-off force delivered from a single force curve*

The value of the unbinding force needed to separate the two interacting molecules is delivered from the analysis of the retraction part of the force curve. However, it should be pointed here that in AFM only a so-called *pull-off force,* can be measured (Figure 5.6).

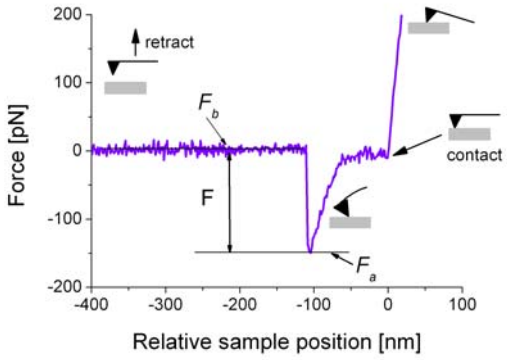


Figure 5.6. Example of the force curve recorded for the interaction occurring between the antigen−antibody complex.

It is defined as a difference between the force $F_b$, corresponding to the free cantilever position (when the interacting force is negligible) and the maximum value of the force $F_a$

$$F = |F_a - F_b| \tag{5.1}$$

The pull-off force value measured for two surfaces, bearing the complementary proteins that interact in a specific way, is usually a superposition of two components: *i)* discrete, short–range component, dominating within the binding sites, that is related to the bond of the single molecular pair, and *ii)* component originating from long–range, distance–depended forces, dominating outside of the binding site. Depending on the conditions, either one of them dominates or their values are comparable. In addition, the non-specific force is not constant but changes in the response of the properties of the environment surrounding the molecules of interest. Very often, it is difficult to separate between the specific forces from the non-specific interaction since the strength of the latter one can be comparable. For example, the determined non-specific forces *(Lekka et al. 2004)* ranged from 60 pN to about 400 pN, what was significant in comparison with the measured specific interaction forces (240 ± 160 pN for ConA–ASA, 370 ± 110 pN for ConA–CaY and 180 ± 130 pN

for PAP–aPAP pairs). For a complementary protein embedded in the plasma membrane, the non-specific force was 60 ± 30 pN for ConA-PC3 cells. Such low value can be explained by the overall interactions present on the cell surface, not involved in the molecular recognition phenomenon.

Studies demonstrating the difference between the pull-off force measured by AFM and the single bond force were reported by Lekka *et al. (Lekka et al. 2002).* In this work, the adhesion force was measured between the bare silicon nitride cantilevers and two surfaces carrying opposite charges: mica, bearing the negative charge *(Pashley 1981),* and glass covered with poly-L-lysine, which is positively charged in water due to the presence of amino groups. The surfaces were immersed in $CaCl_2$ aqueous solution in the range of concentration varied from 0 to 100 mM. Figure 5.7 presents both the measured pull-off (a) and single−bond (b) forces as a function of calcium dichloride concentration.

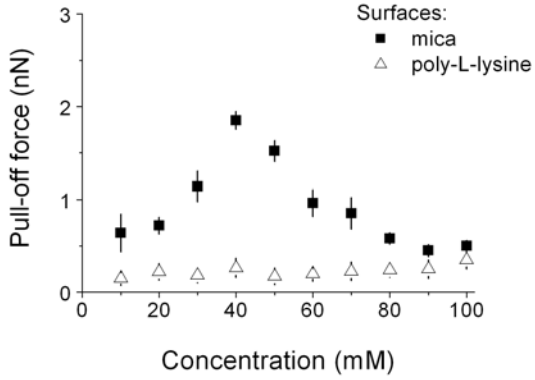


a)

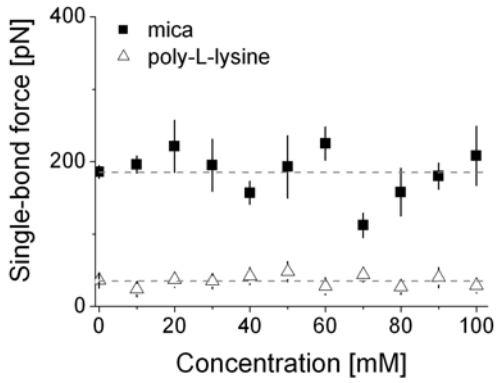


b)

Figure 5.7. The pull-off (a) and single−bond (b) forces as a function of $CaCl_2$ concentration measured between the bare silicon nitride cantilever and two surfaces: the mica and the glass covered by poly-L-lysine. Grey lines denote the average[20] values (185 ± 33 pN and 35 ± 8 pN, respectively).

The measured pull-off force for mica surface increased up to 40 mM concentration of $CaCl_2$. Further increase of calcium concentration resulted in the drop of the measured force. The poly-L-

[20] The average value was calculated as a mean from all concentrations (from 0 mM to 100 mM).

lysine covered glass showed distinct behavior − the pull-off force was independent of the salt concentration and almost constant in the range of the experimental error. However, the force needed to break single bond, determined following the method reported by Han et al. *(Han et al. 1995),* did not follow the pull−off force behavior. For both cases, the determined value of the unbinding of the single was independent of the calcium chloride concentration.

*Force histograms*

To quantify the unbinding force, many force curves must be collected and analyzed using histograms. The force histogram is created using the bin size reflecting the minimum value of the detected force (see section 3.2.3 *Force detection limit* for more details). Shape of the histogram is characteristic for the studied pair of molecules and depends on the number of molecules present within the contact area. The histograms can show either only one peak that can be directly attributed to a single bond rupture (Figure 5.8a) or multiple peaks that correspond to the case when simultaneous rupture of one or more bonds takes place (Figure 5.8b). The most probable unbinding force is usually determined by fitting the Gaussian functions to the maxima present in the histogram of the measured rupture force. Unbinding force is calculated as a centre of the fitted Gauss distribution and the corresponding error is a standard deviation determined from the half width of the peak at its half maximum height. Such fitting procedure gives the position of the maximum with reasonable reliability but it does not describe fully the shape of the force histogram.

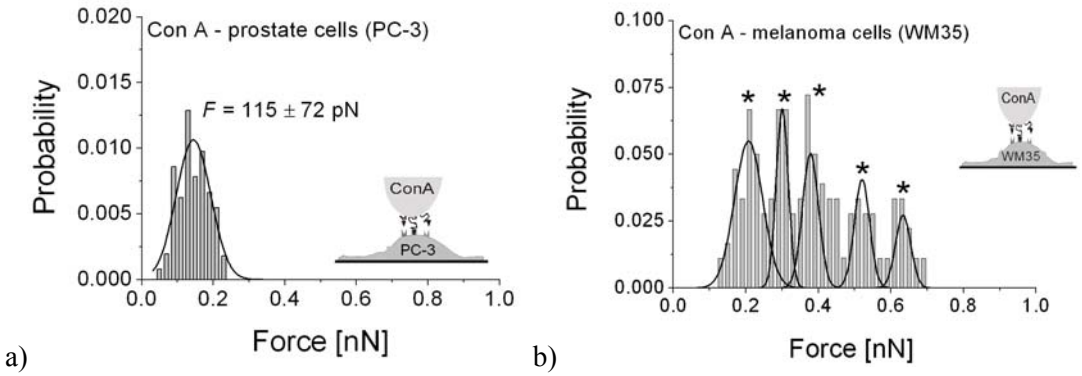


a) b)

Figure 5.8. Force histograms showing a) only one peak attributed to the specific interaction between mannose-type glycans present on the surface of prostate (PC-3) cells probed with AFM tip functionalized with lectin ConA *(Lekka et al. 2005)*, b) multiple peaks observed in the interaction occurring between the same glycan type present on the surface of melanoma cells (WM35) probed with ConA. The solid line is a Gaussian fit used for determination of the unbinding force *(Lekka, unpublished data)*.

The shape of the histogram is determined by the stochastic nature of the unbinding process. It can be analytically described by the probability density function

$$y(x) = a \cdot e^{b \cdot x} \cdot e^{-c \cdot (e^{b \cdot x})} \tag{5.2}$$

where $a$, $b$, and $c$ are parameters of the fit, see Equation (3.15) fitted to the unbinding force histogram obtained at the given loading rate value. Since the probability function is determined by the two parameters describing the bond dissociation: the energy barrier $x_b$ and the dissociation rate constant $k_0$, the fit delivers the estimates of those parameters. They are calculated according to

$$x_b = b \cdot k_B T \tag{5.3}$$

$$k_0 = \frac{x_b r_f \cdot c}{k_B T} \tag{5.4}$$

The errors can be obtained in the standard way:

$$\Delta x_b = k_B T \cdot \Delta b \tag{5.5}$$

$$\Delta k_0 = \sqrt{\left|\frac{r_f c}{k_B T}\right|^2 \cdot (\Delta x_b)^2 + \left|\frac{x_b r_f}{k_B T}\right|^2 \cdot (\Delta c)^2} \tag{5.6}$$

As an example, the probability distribution of the unbinding force obtained for the specific interaction between concanavalin A (ConA) and carbohydrate moiety of carboxypeptidase Y (CaY), measured at the loading rate of 8500 pN/s, was fitted with the Equation (5.2) (Figure 5.9).

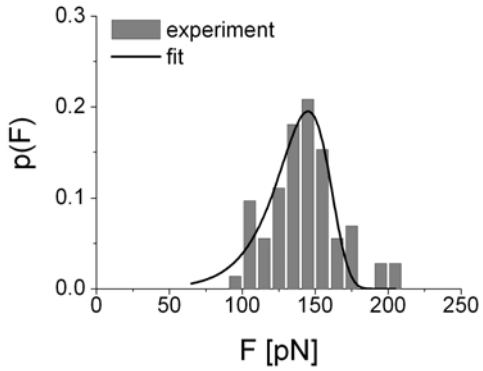


Figure 5.9. The probability distribution *p(F)* of the unbinding force obtained for the interaction between concanavalin A and carbohydrate moiety of carboxypeptidase Y. Measurement were performed in Tris-buffered saline (supplemented with Ca and Mg ions that are crucial for lectin recognition). The solid line is the theoretical fit of the Equation (5.2) to the experimental data.

The dissociation rate constant and the position of the energy barrier, determined form the fit, were in a reasonable agreement with the data reported by Lebed *et al*. *(Lebed et al. 2006)*, obtained using two independent methods: the quartz crystal microbalance and the AFM working in a dynamic force spectroscopy mode. The dissociation rate constant was of 0.137 ± 0.029 $s^{-1}$, placed between 0.095 ± 0.002 $s^{-1}$ (QCM measurements) and 0.170 ± 0.060 $s^{-1}$ (AFM measurements). The fitted

position of the energy barrier was 0.23 ± 0.01 nm, what is in good agreement with the reported value of 0.229 ± 0.004 nm.

The Bell model's parameters determined in that manner enable the reconstruction of the energy landscape during the rupture of interacting molecules. However, it should be pointed out that the absolute value of the energy barrier height can be determined if the association rate is known. Therefore, such way of the potential reconstitution delivers the relations with respect to one reference barrier. The energy barrier height reported by Lebed *at al*. was of 13.3 $\cdot k_B T$. The obtained on the basis on the presented way of data analysis energy barrier height was only slightly smaller (13.1$\cdot k_B T$) while its width values agreed very well.

*Relation between the force and the number of ruptured bonds*

A common way to determine the unbinding force attributes the position of the first peak in the histogram to the unbinding event of a single molecular complex. However, for the case discussed, this simple approach is reliable only under assumption that the unbinding probability is lower than about 30 % *(Tees et al. 2001)*. In that case, rather few molecular bonds are expected to be formed. When multiple peaks are observed in a force histogram, they are usually attributed to the formation (and rupture) of more than one bond within the contact area of the AFM probe and the surface. Thus, the first peak corresponds to the unbinding event involving the rupture of one bond; the second one is related to the simultaneous unbinding of two bonds (thus, the force value at the second maximum is doubled), etc. Such force histogram can be translated into the relationship of the unbinding force determined for each consecutive peak and the peak number (i.e. number of bonds), and the linear dependence is expected if only one type of interaction is present (Figure 5.10). The peak number is equal to the number of ruptured bonds when the center of the first force peak agrees with the force value obtained from the slope.

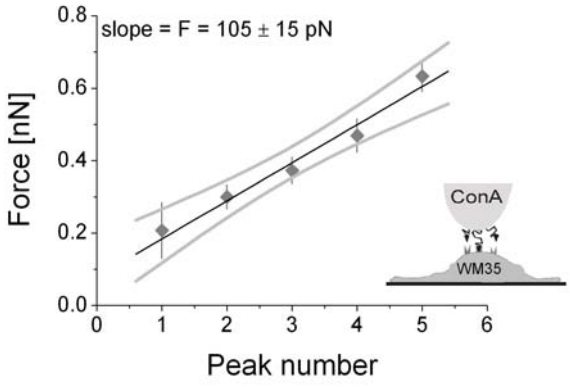


Figure 5.10. Linear regression fitted to the unbinding force as a function of the number of succeeding peaks observed in the histogram (Figure 5.8b) obtained for melanoma WM35 cells probed with lectin ConA. Data points correspond to centers of Gaussians fitted to each single peak present in force histogram while error bars represent their standard deviations. The 95% confidence bands are marked as grey lines.

The unbinding force for a given individual lectin–glycan complex, i.e. ConA − mannose–type glycans, determined from the slope of the fitted line, was 105 ± 15 pN. This value is in agreement with those obtained to unbinding ConA from the same glycan type probed on the prostate cells (115 ± 72 pN, *Lekka et al. 2004*). Therefore, the position of the first peak (~200 pN) can be attributed to the simultaneous rupture of two single complexes, what was confirmed by the large number of mannose-type glycans *(MLekka, unpublished data)*.

In order to statistically evaluate the obtained differences between cell lines, for each fitted line the confidence bands of 95% were calculated. They estimate the certainty of the shape of the fitted line and the assumed confidence level implies a 95% chance that the true regression line fits within these bands (grey lines in Figure 5.10). This approach works reasonably well when the regression curve is calculated basing on more points, what in our studies corresponds to cases where histograms were composed of five maxima.

### *5.2.2. The rupture length and its histogram*

If the bond is formed, the AFM probe withdrawal generates bending of both interacting molecules. The rupture length is an unbinding distance $L^*$ calculated after the conversion of the force curve into the force versus tip−surface distance function. The value of the rupture length, $L$, is determined from the following equation:

$$L = L^* - \frac{F}{k_c} = |L_k - L_c| - \frac{F}{k_c} \tag{5.7}$$

where $k_c$ is the cantilever spring constant, $F$ is the unbinding force. $|L_k - L_c|$ is the distance between the moment when cantilever starts to bend ($L_c$) and the moment when molecules unbind ($L_k$) as it is shown at Figure 5.11.

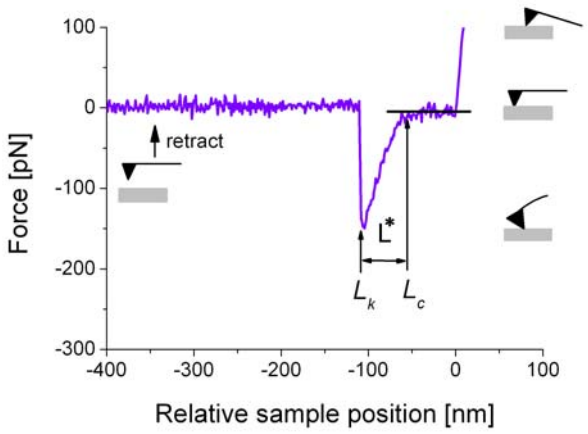


Figure 5.11 Example of the force curve recorded for the interaction occurring between antigen−antibody complex.

The value of the rupture length brings information about the mechanical resistance of the formed complex to the applied external force. In case of isolated molecules, the rupture length can be used as an estimate of the bond stiffness.

The distribution of the rupture length obtained for the interactions where ligand (monoclonal antibody against albumin, a–BSA) was immobilized on a surface of the AFM probe and the complementary receptor albumin molecules (BSA) were immobilized on a surface of mica showed only one peak, centered at 23.7 ± 5.3 nm (Figure 5.12). The bin size reflecting the experimental detection limits (i.e. distance between two subsequent z-steps) was of 3 nm.

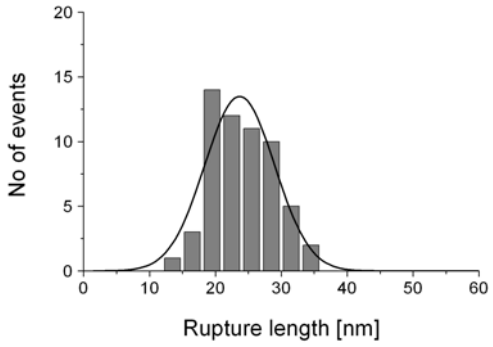


Figure 5.12. Histogram of the rupture length obtained for the interaction between albumin molecules and their antibody. The line denotes the Gauss function.

However, if the bond is formed with the receptor embedded in the cell membrane, the rupture length reflects the overall mechanical resistance of the whole system composed of the bond and the cell membrane, at the place of the receptor anchorage. Since most receptors present on a surface of living cells are linked with actin cytoskeleton, the mechanical resistance will be influenced by properties and structure of such linkage. The magnitude of the contribution depends on the force value that causes the membrane bending.

The unbinding experiment performed for receptors embedded in a plasma membrane results in curves having different characteristic shape. Figure 5.13 illustrates three most common scenarios of the ligand–receptor unbinding for receptors present on the cell membrane.

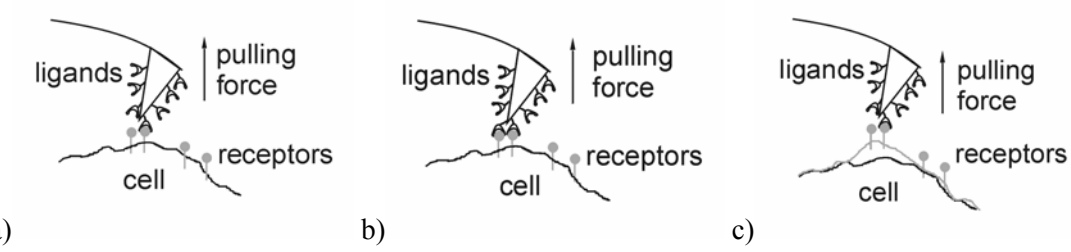


Figure 5.13. Three most common scenarios of the ligand–receptor unbinding that may occur for receptors present on a cell membrane: a) rupture of a single complex, b) simultaneous unbinding of two or more bonds of the same type, and c) unbinding events obtained for a given receptor embedded in cell membrane.

When only the rupture of a single complex occurs (Figure 5.13a), the resulting force curve contains the characteristic "jump" that can be parameterized by two quantities: the unbinding force $F$ and

the rupture length *L*. Each curve recorded for the same type of interaction delivers two histograms on which the unbinding force and rupture length are represented by relatively narrow distributions. However, the surface of the cell is very heterogeneous with a huge amount of distinct cell surface receptors and, therefore, their distribution and their number within the contact area cannot be controlled. Figure 5.13b presents the scenario when two (or more) bonds of the same type are simultaneously ruptured. The length histogram has only one peak at the most probable rupture length *L*, but in the force histogram, multiple maxima are expected (see for example Figure 5.13b). Each peak is centered at *F*, *2F, ..., nF* values. The two-abovementioned cases are also valid for experiments with the use of isolated proteins, where one protein is attached to the AFM probe and the other, complementary one, is immobilized on the substrate surface. The embedding of receptors in a plasma membrane can often influence the unbinding process by the induction of the membrane deformation, i.e. pulling off as it is presented in Figure 5.13c. The membrane deformation manifests in the broadening of the range of the rupture length but the unbinding force remains unchanged (unless any unrecognized non-specific interaction is present in the analyzed data). Thus, the unbinding events obtained for a given receptor embedded in the cell membrane produce the maximum in the force histogram and a broad distribution of the rupture lengths with or without distinguished peaks. In this case, the mean value of the rupture length will be shifted to higher values.

### *5.2.3. The bond stiffness*

The quantity, closely related to the rupture length, is a stiffness of the pulled complex, which can reveal either the stiffness of a single bond or a system with bond and membrane contributions. The AFM cantilever and the bond(s) can be imagined as the one-dimensional springs that are connected in series (Figure 5.14).

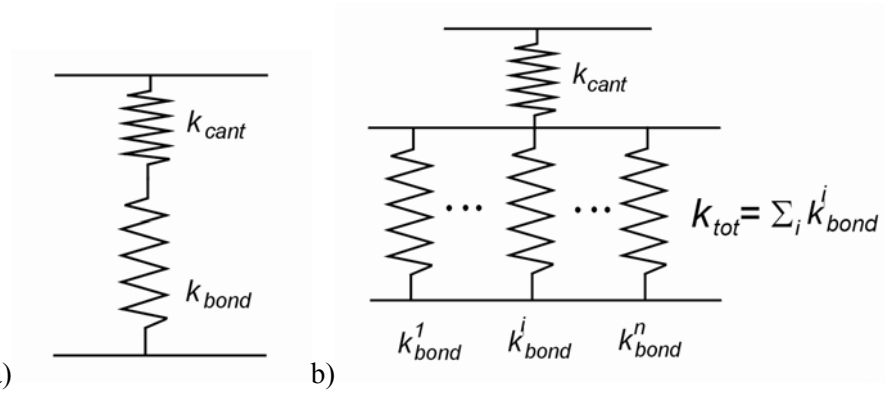


a) b)

Figure 5.14. a) A model of two springs linked series: an AFM cantilever spring constant $k_{cant}$ and bond stiffness $k_{bond}$. b) For multiple bonds formed within the contact area, the effective spring constant can be modeled as system of springs linked in series and in parallel.

The effective spring constant, $k_{syst}$, of two springs linked in series can be calculated using the following formula

$$\frac{1}{k_{syst}} = \frac{1}{k_{cant}} + \frac{1}{k_{bond}} \tag{5.8}$$

where $k_{cant}$ is the cantilever spring constant and $k_{bond}$ is the bond stiffness.

When within the contact area of the AFM tip and the investigated surface, $n$ bonds of the same type are formed, the resulting effective spring constant increases according to

$$\frac{1}{k_{syst}^{n}} = \frac{1}{k_{cant}} + \frac{1}{\sum_{i}^{n} k_{bond}^{i}} \tag{5.9}$$

The effective spring constant can be calculated directly from the equation if the spring constant of the cantilever and the spring of the bond are known. In practice, the effective spring constant is determined by fitting the line to the unbinding part of the force curve (as it is marked in Figure 5.15).

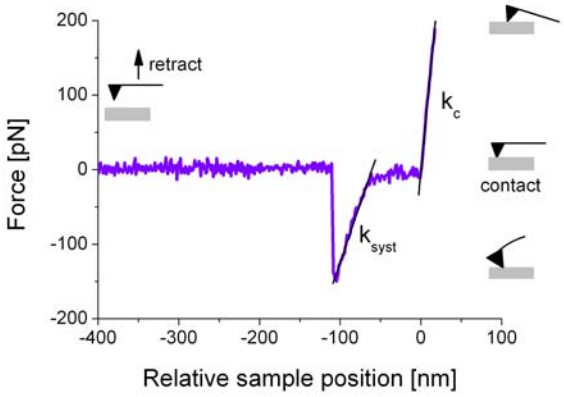


Figure 5.15. Example of the force curve recorded for the interaction occurring between antigen−antibody complex. $k_C$ is the cantilever spring constant; $k_{syst}$ is the system spring constant taking into account the cantilever spring constant and the bond stiffness.

Then, the effective spring constant can be roughly estimated by taking

$$k_{syst} = \frac{F}{L} \tag{5.10}$$

Basing on the experimental spring constant, the stiffness of the pulled system can be obtained using the following formula

$$k_{bond} = \frac{\frac{F}{L} \cdot k_{cant}}{k_{cant} - \frac{F}{L}} \tag{5.11}$$

The experimental error, $\delta k_{bond}$, can be estimated in the standard way as a maximum error

$$\Delta k_{bond} = \sqrt{\left|\frac{\frac{k_{cant}^2}{L}}{\left(k_{cant} - \frac{F}{L}\right)^2}\right|^2 \cdot \Delta F^2 + \left|\frac{\frac{-\left(k_{cant}^2\right)\cdot F}{L^2}}{\left(k_{cant} - \frac{F}{L}\right)^2}\right|^2 \cdot \Delta L^2} \tag{5.12}$$

### *5.2.4. The number of ruptured bonds*

Very often, during the measurements on the surface of living cells, force histograms show multiple maxima (like for example in Figure 5.10b) that correspond to the simultaneous rupture of subsequent complexes. To quantify this case, the area under each peak can be used as an indicator of the probability of simultaneous rupture of *n* bonds.

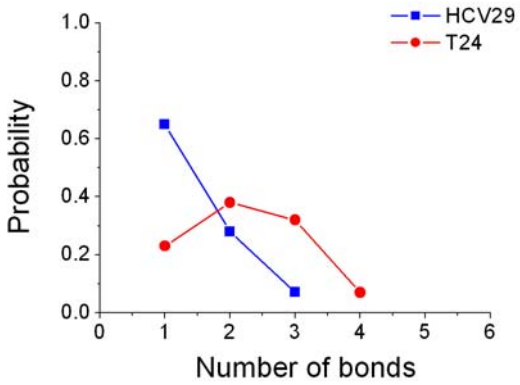


a)

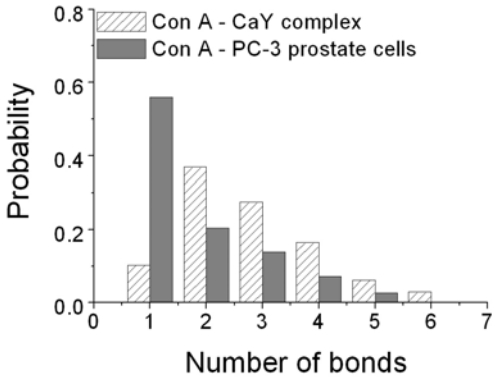


b)

Figure 5.16 Probability of the simultaneous rupture of *n* bonds obtained for a) N-cadherin−antibody complex in cancerous T24 and reference HCV29 cells, b) for the lectin concanavalin A (ConA*)* and glycans either attached to isolated protein (carboxypeptidase Y, CaY) or present in a plasma membrane of prostate cells (cell line: PC-3). The distributions were normalized to the total number of events *(Lekka et al. 2004)*.

The probability of the simultaneous rupture of *n*-bonds, obtained for the same interaction occurring between N-cadherin and its monoclonal antibody in cancerous T24 and reference HCV29 cells, is shown in Figure 5.16a. One can observe that the simultaneous rupture of 2−3 bonds was the most

probable for the cancerous cells (T24) as compared to the reference cells (HCV29) where only the rupture of a single bond was most prominent. When lectin was used as a probe for mannose bearing glycans, the simultaneous rupture was observed when these glycans were attached to the isolated protein where they were better accessible (Figure 5.16b). Such situation indicates larger number of active, isolated and single protein molecules on the investigated surface.

### *5.2.5. The unbinding probability*

Another quantity related to the number of molecule present on the surface is the unbinding probability $P_{unbinding}$ that is usually defined as a ratio between the number of curves with the unbinding events to the total number of the recorded force curves

$$P_{unbinding} = \frac{Number\ of\ \ curves\ showing\ unbinding\ events}{Total\ number\ \ of\ the\ recorded\ \ force\ curves} \tag{5.13}$$

Its value corresponds directly to the number of molecules present on a surface of living cells, which can vary depending on the studied complex or on the studied cell type (Table 5.1).

Table 5.1. The unbinding probability determined for non-malignant HCV29 and malignant T24 bladder cells *(Lekka et al. 2006)*.

| Cells | Lectin-glycan complex | Number of force curves | Number of unbinding events | Unbinding probability |
|---|---|---|---|---|
| HCV29 | ConA[21] − mannose | 3982 | 438 | 0.110 |
| HCV29 | SNA[22] − sialic acid | 4057 | 215 | 0.053 |
| T24 | ConA − mannose | 3983 | 111 | 0.028 |
| T24 | SNA − sialic acid | 4095 | 344 | 0.084 |

The way of the determination of the unbinding probability gives only the robust estimation of the number of receptors present on the investigated cells' surfaces. This parameter does not describe the receptor distribution over the cell surface. The same unbinding probability value can be obtained for receptors randomly distributed over a certain area as in case when receptors are grouped around one place in the same area.

[21] ConA – lectin from *Canavalia ensiformis,*
[22] SNA – lectin from *Sambucus nigra.*

# CHAPTER 6

# Cancerous changes studied by AFM

The chapter presents extensive studies and results of the studies of the expression of these molecules (or their glycan components) in living cells that are involved in oncogenic transformation. Thus, the adhesive interactions were studied between two types of complexes: i) N-cadherin and the monoclonal antibody against this cadherin type and ii) glycans (containing either mannose or *N*–acetylglucosamine or sialic acids residues) and the corresponding lectins. The AFM measurements were carried out with the aim to answer the question whether an individual molecule or its part displays different binding properties in normal and cancerous cells.

In this chapter, only studies performed on human bladder non-malignant (HCV29) and malignant (T4) cells were chosen from the broader research material. Measurements were carried out on living cells in culture conditions, at room temperature. The commonly used method of the AFM data analysis delivering the unbinding force value and probability values was extended by other parameters such as the rupture length and the effective spring constant of the studied complex. The implementation of these parameters enables the complete characterization of static and dynamic properties of the unbinding process of a single molecular complex.

Two types of molecules complexes are chosen since it is known that alterations in the expression and the function of cadherins and of distinct glycans can correlate with the progression to tumor malignancy *(Przybyło et al. 2002; Shariat et al. 2005)*.

## 6.1. Molecules on a cell surface

### *6.1.1. N-cadherin*

Cadherins (see *Chapter 2*) are transmembrane proteins having both extracellular and cytoplasmic domains (Figure 6.1). The extracellular domain consists of five cadherins repeats (called *ectodomains*), each of about 110 amino acids residues. Between two repeats, calcium ions are bound participating in the formation of calcium–dependent, homophilic bonds. The cytosolic domain of the cadherin is directly associated with β–catenin or/and plakoglobin (γ–catenin). These proteins are members of armadillo family, sharing a common motif called “armadillo repeat domain”. Both γ–catenin and plakoglobin are composed of 12 such repeats (40 to 42 amino acids residues) with unique amino- and carboxyl-terminal domains. They share 76% identity in the armadillo repeats, and thus, they are highly homologous and often interact with the same partners *(Fouquet et al. 1992; Ramburan et al. 2002)*. However, there is one exception: plakoglobin can

associate with both classical cadherins (e.g. E- or N-cadherin) and desmosomal cadherins while γ–catenin associates only with the members of the classical cadherin family. Both γ–catenin and plakoglobin bind to α–catenin, which links the cadherin/catenin complex to the actin cytoskeleton *(Nollet et al. 1999)*.

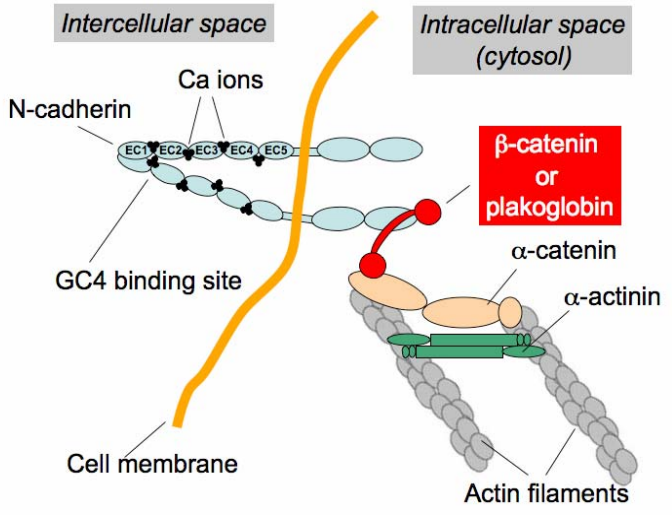


Figure 6.1. Illustration of the cadherin – catenin complex in cell membrane

In order to detect N-cadherin on a surface of living cells, the monoclonal antibody (see *section 4.3.2*) against the extracellular domain was applied (GC4 antibody, *Reiss et al. 2005*). The used antibody inhibits adherens junction formation and disrupts existing junctions in cultured cells. The binding site for the antibody is located between the two first, outermost ectodomains (denoted usually as EC1 and EC2, Figure 6.1). For simplicity, the studied complex composed of the antibody and N-cadherin is referred as ***the GC4-Ncadh complex***.

### *6.1.2. Glycans*

It is well known that tumorigenesis and metastasis are frequently associated with altered structure and expression of glycans (see *Chapter 2*) on cell surface *(Dali'olio 1996; Fukuda 1996; Ørntoft et al. 1998; Gorelik et al. 2001)*. A glycan, assembled from several single sugar units by removal of water during the linkage of simple sugars, forms its primary structure characterized by such linkages. Variety of types of a simple sugar defines a large number of distinct glycans' structures.

The studied bladder cells (HCV29 and T24) are characterized by distinct glycan pattern as it was already reported in studies of the degree of glycosylation of such surface molecules as integrins *(Lityńska et al. 2000)* and cadherins *(Przybyło et al. 2002)*. The high mannose type, N-acetylglucosamine β(1-6) branched triantenary and/or tetrantenary complex type glycans, as also sialic acid residues occupying the terminal positions in N-linked oligosaccharides, were found to be

expressed in different ways in both HCV29 and T24 cells. Therefore, these glycan types were chosen for the AFM measurements of the unbinding force.

They were probed using lectins, i.e. proteins that recognize them with very specific binding affinities, comparable with those observed for enzyme–substrate or antigen–antibody interactions *(Sharon et al. 2004)*. A single lectin molecule may contain two or more non-covalently associated subunits of the same or different type. Single subunits have a single carbohydrate-binding site and usually show lower affinity strength. The oligomeric nature of lectins generates multivalency that increases affinity towards their specific ligands. For simplicity reasons, the studied complexes composed of the given lectin and the corresponding glycan structures are called as ***lectin-glycan complexes***.

The lectins used in the presented studies recognized only the *N*-glycans attached to proteins *(Hsu et al. 1982; Shibuya et al. 1982; Bryce et al. 2001)*:

- *Concanavalin A (*ConA) is a lectin isolated from *Canavalia ensiformis*. It is composed of identical subunits of 237 amino acid residues ($M_r$ ~ 26.5 kDa, PDB entry 1DQ1). According to McKenzie *et al. (McKenzie et al. 1972),* at pH 4.5–5.6 ConA exists as a single dimer. Above pH 7 it is predominantly tetrameric having four identical binding sites. Concanavalin A sequentially binds a transition metal ion in the metal-binding site (S1) and a calcium ion in the metal-binding site (S2) to form its saccharide-binding site. ConA recognizes oligosaccharide structures containing glucose and mannose residues *(Baenzinger et al. 1979)*.
- *Leucoagglutinin (*PHA-L, $M_r$ ~ 114 kDa, PDB entry 1FAT) is one of isolectins obtained from *Phaseolus vulgaris*. Its conformation is pH dependent i.e. PHA-L exists as a dimer at pH 2.4 and as a tetramer at 7.4 *(Hamelryck et al. 1996)*. This lectin is specific for complex type N-linked glycans, in particular galactosylated triantenary and tetrantenary glycopeptides that have at least one of the α-linked mannose residues at two carbon positions[23] (C-2 and C-6) with linked *N*-acetylglucosamine residues.
- *SNA agglutinin* (SNA) is a lectin isolated from *Sambucus nigra* (elderberry bark). This lectin is also a tetrameric glycoprotein consisting of four disulfide-linked chains: two of about 36 kDa and two of about 38 kDa *(Shibuya et al. 1987)*. SNA lectin binds preferentially to sialic acids attached to terminal galactose. This lectin does not appear to bind sialic acid linked to *N*-acetylgalactosamine. Within SNA family, one can distinguish few different types of lectins. The most common ones are SNA-I, SNA-II, SNA-IV, and SNA-V. The lectin from *Sambucus nigra* used for the AFM experiments on living cells was a mixture of all types of SNA lectins. Therefore, it was used to detect the presence of a whole class of cell surface glycans composed of sialic acids residues.

[23] see Appendix 8

## 6.2 AFM studies of N-cadherin and of glycans interactions

In order to compare the given type of molecular interactions occurring for GC4−Ncadh and lectin−glycan complexes in both non-malignant (HCV29) and malignant (T24) cells, the AFM measurements were performed in well controlled experimental conditions.

The typical force curves recorded by AFM for the GC4-Ncadh (a) and lectin-glycan (b) complexes are presented in Figure 6.2 (only retraction parts are shown). All analyzed curves showed the typical non-linear elastic behavior, characteristic for the separation of two molecules. Before the rupture, both molecules were stretched. Such single unbinding events differed in terms of the unbinding force and the rupture length values.

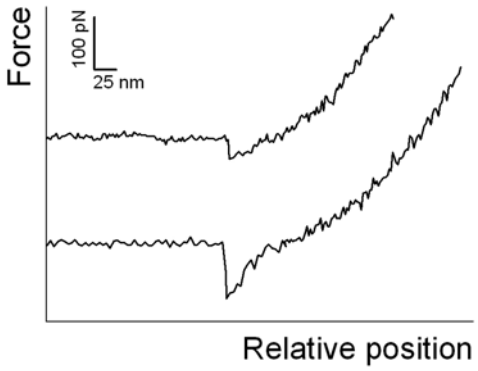


a)

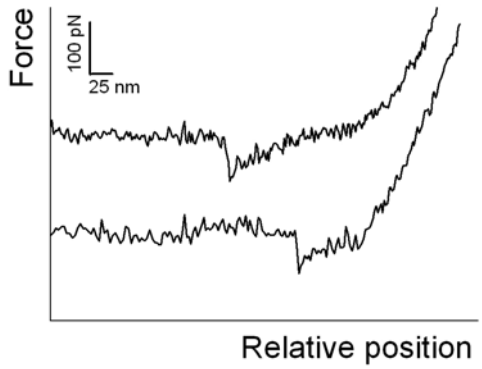


b)

Figure 6.2. Typical force curves recorded for the interaction between GC4-Ncadh (a) and lectin-glycan (b) complexes measured in T24 cells.

For the GC4−Ncadh complex studied in both cell types, the force value did not exceed 150 pN. The maximum force value of the measured lectin−glycan complexes did not exceed 400 pN except the case of the T24 cells surface probed with the PHA-L coated cantilever, when the observed maximum force was about of 800 pN.

### *6.2.1. Force histograms and unbinding force determination*

The force histograms of the interaction force measured in both cell types are presented in Figures 6.3 and 6.6, for GC4−Ncadh and lectin−glycan complexes, respectively. The observed peaks were fitted with the Gaussian function in order to determine the value of the most probable unbinding force. The half width at the half maximum denotes the standard deviation (SD).

*GC4−Ncadh complex*

The rupture of the GC4−Ncadh complex *(Lekka, unpublished data)* in the reference cells (HCV29) results in the histogram (Figure 6.3a) with four distinct peaks centered at 26.1 ± 7.1 (SD) pN, 56.9 ± 11.6 (SD) pN, 86.3 ± 6.3 (SD) pN, and 108.3 ± 8.8 (SD) pN, while in the cancerous T24 cells (Figure 6.3b), one dominant maximum was observed centered at 61.7 ± 14.6 (SD) pN and a small, second peak was visible at 112.2 ± 10.9 (SD) pN.

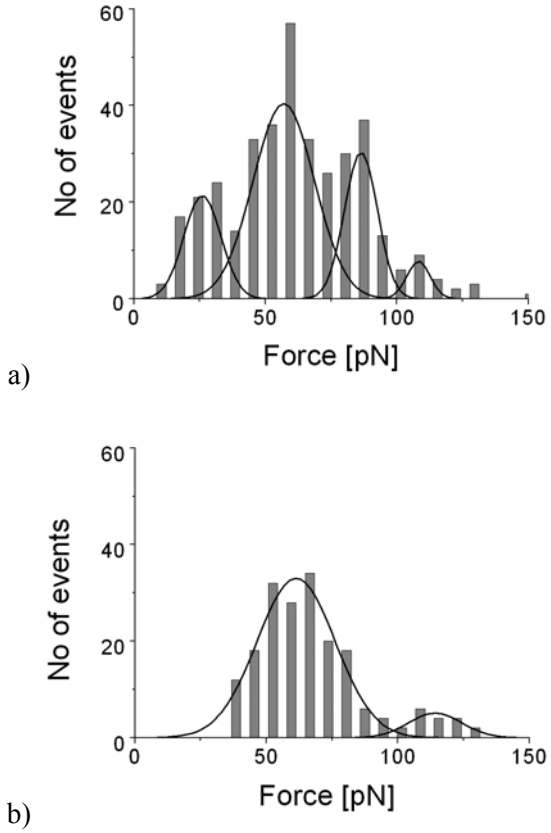


Figure 6.3. Force histogram of the GC4–Ncadh interaction measured in a) reference HCV29 and b) cancerous T24 cells. The bin size was 7 pN corresponding to the force detection limit in the experiment (the solid line denotes the fitted Gaussian functions).

The interaction force of a single GC4–Ncadh complex was expected to have the same value for both cell types (if the structure of the N-cadherin binding site was unchanged upon cancer transformation). However, the experimental results were clearly different. The unbinding force

studied for N-cadherins present in cancer cells (T24) was about 2.5 times higher than in case when cadherins were probed on a surface of the reference HCV29 cells (61.7 ± 14.6 (SD) pN versus 26.1 ± 7.1 (SD) pN). These results indicated an altered structure of the binding site of the cadherins, influencing the binding stability.

The presence of multiple peaks in force histograms can be translated into the relationship of the unbinding force determined for each consecutive peak and the number of bonds simultaneously ruptured (Figure 6.4).

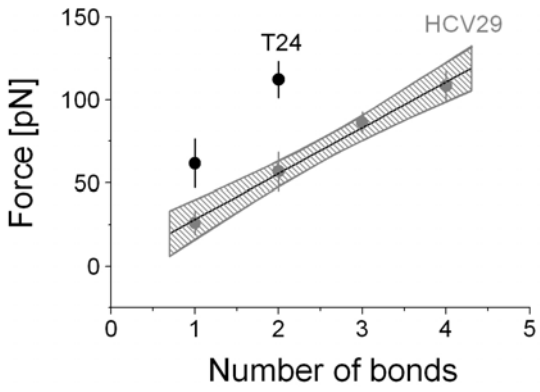


Figure 6.4. Unbinding force as a function of number of simultaneously ruptured bonds. Data points correspond to centers of Gaussians fitted to the corresponding peaks present in force histograms. The 95% confidence bands are marked as grey region.

The linear character is expected when the distance between subsequent maxima is equal, what indicates that only one type of interaction is present. Such relation indicates the specificity of the obtained unbinding events. The slope of the fitted line was 28.1 ± 3.5 pN (the error is the standard deviation of the slope) what corresponds well with the position of the first maximum in the histogram (26.1 ± 7.1 (SD) pN). Therefore, this value was attributed to the unbinding of a single bond. Such analysis was not possible for N-cadherins probed on the surface of T24 cancer cells since only two maxima were observed. Nevertheless, the equal distance between the first and the second peaks strongly suggests the discrete character of the observed unbinding what is characteristic for the specific molecular interactions (see *section 6.2.8* for the results of the AFM data verification).

So far there is no data reporting the different structure of N-cadherins in cancer and normal cells. Therefore, one may assume that the primary structure of N-cadherin in both non-malignant (HCV29) and malignant (T24) cells is the same. Consequently, the difference of the unbinding forces can be attributed to structural changes of oligosaccharide ligands caused by cancer progression, especially since the different glycosylation[24] pattern was already observed for these

[24] Glycosylation is the process or results of addition of oligosaccharide's chains (i.e. glycans) to proteins and/or to lipids.

cell lines *(Przybyło et al. 2002)*. As T24 cancer cells have ability to generate more complex glycans attached to cadherins than HCV29 cells, one should expect smaller unbinding force in T24 due to the presence of large amount of attached glycans generating a steric–originated repulsion, preventing cadherins from achieving distances necessary for the effective interaction. However, for the T24 cells, a larger unbinding force was observed in the experiment than for the HCV29 cells. This result might indicate the smaller amount of glycans present in the neighborhood of the antibody (GC4) binding site and thereby less prominent steric repulsion.

Apart from the determination of the unbinding force for the rupture of a single complex, the positions of the force peaks, plotted as a function of the number of broken bonds, can be compared with two models describing the mechanism of the unbinding "zipper-like" and "parallel-like" ones (Figure 6.6, see *Chapter 3*).

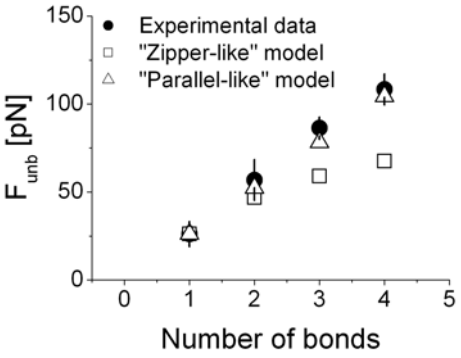


a)

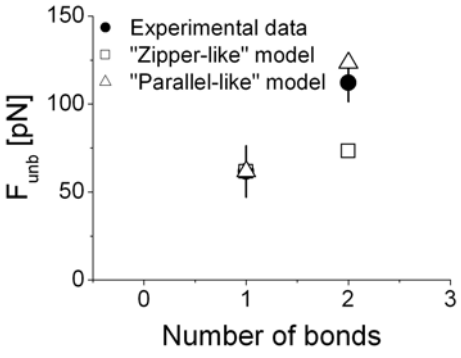


b)

Figure 6.6. The experimental data compared with two theoretical models describing the mechanism of the unbinding: "zipper-like" and "parallel-like" for GC4−Ncadh complex in a) HCV29 and b) T24 cells.

The general character of the unbinding of GC4−Ncadh complex in both cell types followed the "parallel-like" unbinding mechanism in which the applied external force is equally distributed to all single complexes ruptured at the same moment. These results showed also the cooperative character of the N-cadherin unbinding indicating the similarity to the interaction, recently reported for E-cadherin *(Tsukasaki et al. 2007)*. However, in HCV29 cells, such mechanism of the unbinding was strongly suggested only after the rupture of 3 or 4 single complexes. For 2

complexes, the "zipper-like" model could be applied also with relative high accuracy. In cancerous T24 cells, the simultaneous rupture of two single complexes showed disagreement with "zipper-like" model.

*Lectin − glycan complexes*

The force distributions obtained for the interactions between a given lectin type (ConA, PHA-L, and SNA) and the complex glycans present on a surface of the human bladder cells (HCV29 and T24) are presented in Figure 6.7 *(Lekka et al. 2006)*.

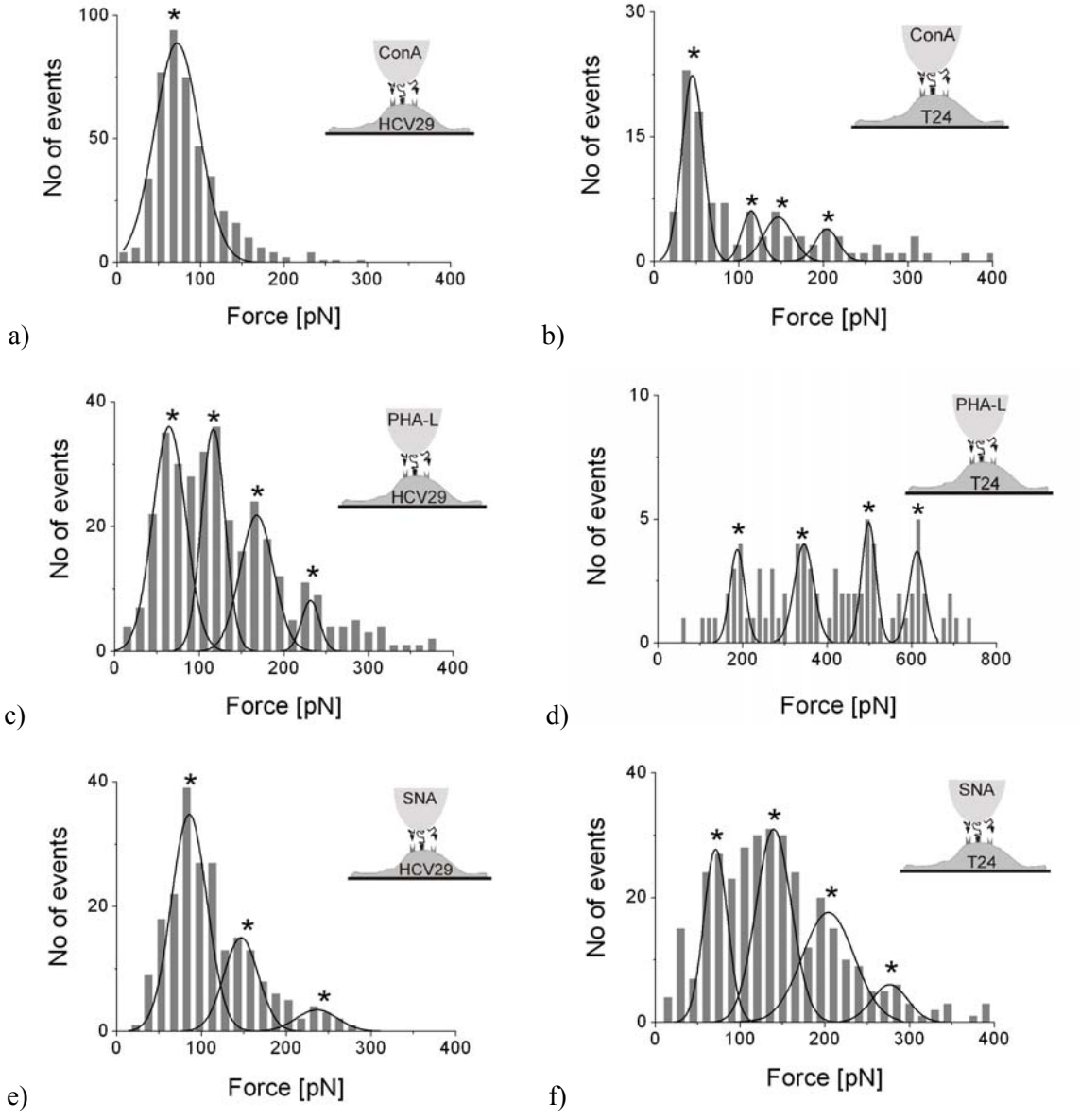


Figure 6.7. Force histograms obtained for the interaction between glycans composed of mannose, N-acetylglucosamine, and sialic acids and the corresponding lectin (ConA, PHA-L, and SNA), measured on a surface of reference HCV29 (a, c, e) and cancerous T24 (b, d, f) cells. The solid line is the Gaussian function; stars denote the most probably force for simultaneous unbinding of 1, 2, 3, and 4 bonds *(Lekka et al. 2006)*.

The histograms were created with the bin size of 15 pN (the minimum detected force, see section 4.2.4 in *Chapter 4*). Depending on a type of the measured system, the histograms were more or less wide, usually wider for cancer cells. Furthermore, most histograms showed more than one force peak. The only exception was when ConA–modified probe was scanned over the surface of HCV29 cells. The observed peaks (marked by stars in Figure 6.7) were attributed to the formation and simultaneous rupture of the subsequent bonds within the contact area of the AFM probe and cell surface since the unbinding probability was always below 30 %, independent of the studied case (this indicates that only few bonds could be created within the contact area (*Tees et al. 2001*).
When the surface of the reference HCV29 cells was probed using the AFM cantilever modified with concanavalin A, only one peak was observed. This suggests that within the contact area (~0.3 $\mu m^2$), only a single complex composed of ConA and mannose residue was ruptured. In contrast to reference cells, cancer cells showed four peaks, suggesting that up to four mannose bearing ligands could interact with ConA. The most unexpected result was obtained when the surface of T24 and HVC29 cells was probed with the AFM cantilever coated with PHA-L. The number of unbinding events was much larger for the reference cells than for the T24 cells. However, for cancerous cells, four maxima corresponding to the rupture of the consecutive bonds were still observed. In force histograms obtained for glycans detected by lectin from *Sambucus nigra* (SNA), 3 and 4 peaks were observed for reference and cancerous cells, respectively.
By fitting the Gauss function, the values of the unbinding force for each histogram were determined (Table 6.1). The error is a standard deviation calculated as a half of the width taken at the half maximum.

Table 6.1. The position of the peaks determined for a single lectin-glycan complexes: (i) ConA − mannose, (ii) PHA-L − *N*-acetylglucosamine, and (iii) SNA − sialic acid.

| Lectin – glycan complex | ConA− mannose | PHA-L− *N*-acetylglucosamine | SNA − sialic acid |
|---|---|---|---|
| **HCV29 (reference) cells** | | | |
| Peak No 1 | 72 ± 18 pN | 64 ± 19 pN | 80 ± 22 pN |
| Peak No 2 | | 116 ± 14 pN | 152 ± 20 pN |
| Peak No 3 | | 168 ± 18 pN | 243 ± 15 pN |
| Peak No 4 | | 232 ± 10 pN | |
| **T24 (cancerous) cells** | | | |
| Peak No 1 | 49 ± 15 pN | 201 ± 23 pN | 73 ± 28 pN |
| Peak No 2 | 115 ± 12 pN | 337 ± 20 pN | 143 ± 22 pN |
| Peak No 3 | 147 ± 17 pN | 501 ± 18 pN | 212 ± 17 pN |
| Peak No 4 | 201 ± 15 pN | 626 ± 25 pN | 281 ± 22 pN |

Analogously to the GC4-Ncadh complex, the unbinding force was plotted versus the number of simultaneously ruptured bonds (Figure 6.8).

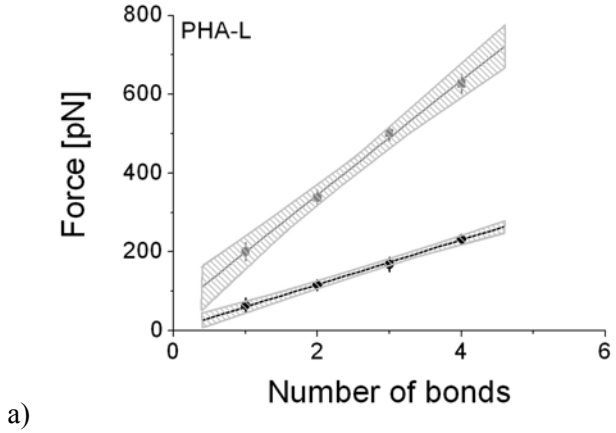


a)

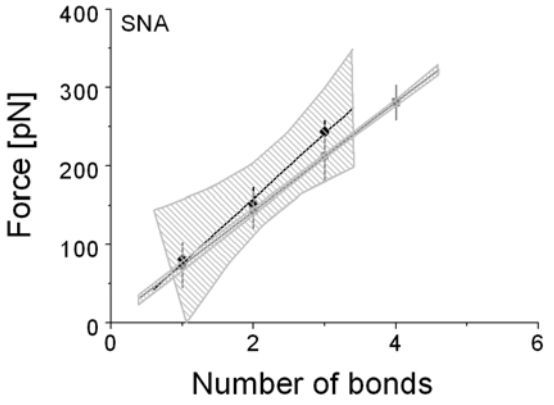


b)

Figure 6.8. Linear regression fitted to the unbinding force as a function of the number of bonds simultaneously ruptured for HCV29 (grey dots) and T24 (black diamonds) cells, probed with two types of lectins: PHA-L (a), SNA (b). Data points correspond to centers of Gaussians fitted to each single maximum from Figure 6.7, while error bars represent their standard deviations *(Lekka et al. 2006)*.

The correlation factors for all studied cases ranged from 0.998 to 0.999. For each curve, confidence bands were calculated (grey region). The true regression line fits within these bands with certainty of 95 %. From such a plot, the exact value of the unbinding forces for a given individual lectin–glycan complex was determined from the slope of the fitted line (Table 6.2). The obtained unbinding force of a single complex overlapped within the experimental error with the values determined on the basis of the unbinding force histogram. Only in case of AFM cantilevers modified with PHA-L and its oligosaccharide ligand present on a surface of T24 cells, the values of the unbinding force obtained from the linear regression was significantly smaller than the value obtained from the histogram. This can be explained by the presence of the non–specific forces that compete with the specific ones. These non–specific forces can e.g. arise due to the procedure of the

cantilever modification (PHA-L was directly attached to the surface of AFM probe without any spacer). The advantage of using the linear regression is that errors are smaller and the obtained value is only slightly influenced by other non–specific forces. Moreover, the linear character can be used as an additional way of data verification, confirming the specificity of the studied interaction.

Table 6.2. The unbinding force of single pairs: (i) *N*-acetylglucosamine–PHA-L, (ii) mannose–ConA and (iii) sialic acid–SNA. Its value was determined in two approaches: (1) by linear regression where the force value and its error correspond to the slope and the standard deviation of the slope, and (2) from the first force peak present in force histograms where the error is a half width of the peak at the maximum and it denotes standard deviation *(Lekka et al. 2006)*.

| Cell lines | Lectin − glycan complex | *F* [pN] (from linear regression) | *F* [pN] (from force histogram) |
|---|---|---|---|
| HCV29 | ConA − mannose | – | 72 ± 18 |
| | PHA-L − *N*-acetylglucosamine | 57 ± 6 | 64 ± 19 |
| | SNA − sialic acid | 83 ± 13 | 80 ± 22 |
| T24 | ConA − mannose | 51 ± 11 | 49 ± 15 |
| | PHA-L − *N*-acetylglucosamine | 145 ± 10 | 201 ± 23 |
| | SNA − sialic acid | 69 ± 11 | 73 ± 28 |

The steric organization of the plasma membrane oligosaccharides at the cell's or molecule's surface has a great significance, as they can be accessible for the lectin. Therefore, multiple peaks observed in the unbinding force histograms can be attributed either to the number of lectin's binding sites that are involved in oligosaccharide recognition process or to the number of ligands present on a cell surface in a form of groups, composed of few closely located single oligosaccharide chains, involved in the adhesive interaction with the lectin. The analysis of force histograms showed that such "clustering" of cell surface glycans was the most pronounced for PHA-L and SNA lectins. ConA measurements performed on the surface of reference cells indicated only one bond formed between ConA and its mannose ligands on cell surface. In addition, taking into account the number of unbinding events, the clusters of glycans were more obvious for reference cells.

The mechanism of the multiple unbinding of a single SNA− sialic acid complex was recognized from the comparison with theoretical models (Figure 6.9, *Lekka, unpublished data*). The good agreement of the unbinding force values with the "parallel-like" model indicated the cooperative mechanism of unbinding was visible already for the simultaneous rupture of two single complexes.

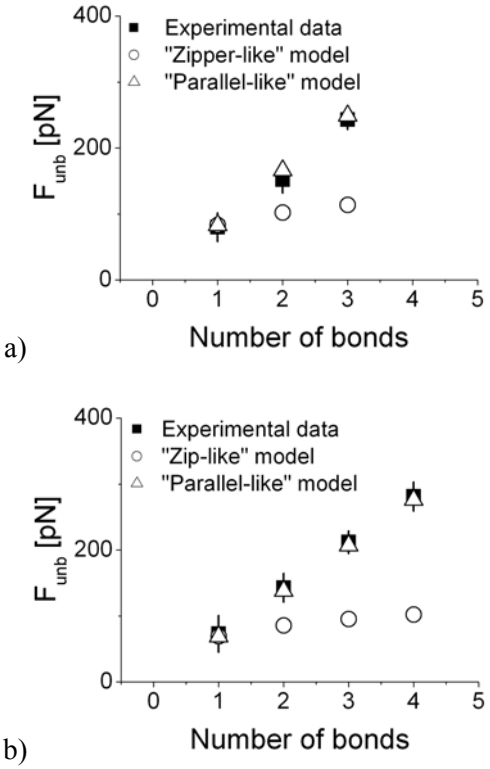


Figure 6.9. The experimental data compared with two theoretical models describing the mechanism of the unbinding: “zipper-like” and “paralell−like” models for SNA-sialic acid complex in a) HCV29 and b) T24 cells.

Similar comparisons were obtained for mannose−type glycans studied on cancerous cell surface and for *N*-acetylglucosamine−type one in both cell types. The results strongly indicated that all studied lectin-glycan complexes interacted in a cooperative way, following the “parallel-like” model.

### *6.2.2. Bell model parameters*

The Bell model gave a theoretical framework for understanding how the force affects the dissociation pathway of the molecular complex *(Bell 1978)*. Later on, it was shown that the unbinding force depended on the loading rate value *(Evans et al. 1997)*. This parameter, bearing the information about how the external force changes in time, should be chosen carefully and kept constant. The loading rate applied during the rupture of the GC4-Ncadh complex varied from 2500 to 5000 pN/s and from 3600 to 6000 pN/s, for the HCV29 and T24 cells, respectively. The corresponding unbinding forces were of $25.3 \pm 8.2$ pN and $27.9 \pm 7.5$ pN for HCV29, and of $59.7 \pm 13.0$ pN and $64.1 \pm 10.6$ pN for T24. Similar dependency on the loading rate was observed for lectin-glycan complexes where the loading rates were in the range of 800 pN/s − 2500 pN/s. Such weak dependence of the interaction forces on the loading rate justifies direct comparison of interactions in both cell types measured within the chosen loading rate range. It is generally known

that the force distorts the energy landscape of the complex by lowering the energy barrier and consequently increasing exponentially the dissociate rate (see Equation (3.9) in the *Chapter 3*). Under conditions of the constant loading rate and the known value of the unbinding force, the probability density function for the unbinding of a single complex is a function of two parameters: the position of the energy barrier $x_b$, and the dissociation rate constant $k_0$ describing the kinetics of the complex dissociation.

*GC4−Ncadh complex*

Figures 6.10a&b present the probability density function (solid lines, Equation 5.2) fitted to each peak present in the force histogram obtained of the GC4–Ncadh complex measured for the HCV29 and T24 cells, respectively (see section 6.2).

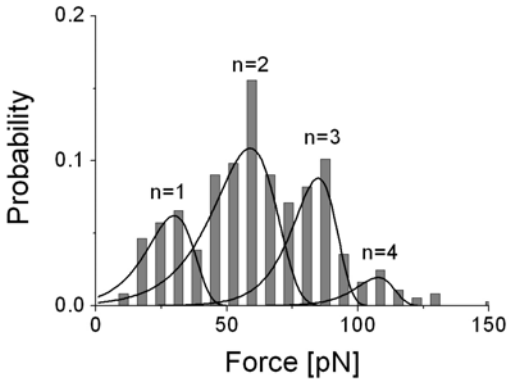


a)

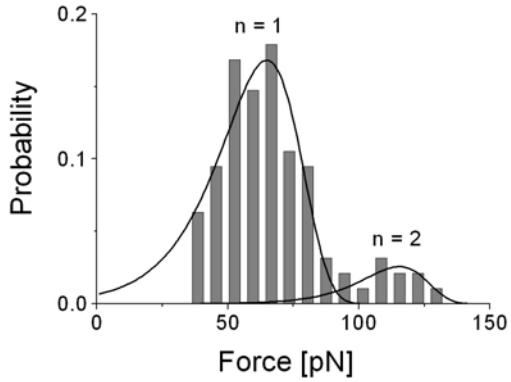


b)

Figure 6.10. Force histogram (same as in Figure 6.4) of the single GC4–Ncadh complexes measured in a) reference HCV29 and b) cancerous T24 cells. Peaks (*n* denotes the number of bonds simultaneously ruptured) were fitted with the probability density function given by the Equation (5.2).

All fits were performed under the assumption that unbinding, independently of the number of single complexes involved, proceeds through a single energy barrier. In the other words, the simultaneous rupture of *n* single complexes is modeled as a rupture of a single composite complex with the energy landscape defined by the convolution of those originating from all single GC4-

Ncadh complexes involved. Thus, from the fits, the positions of the energy barriers $x_b$ were calculated according to the Equation (5.3). The dissociation rate constants $k_0$ were determined following the Equation (5.4), at the loading rate value given by the product of the retraction velocity (1500 nm/s) and the system spring constant of either 2.93 mN/m or 1.66 mN/m for the HCV29 and T24 cells, respectively. The corresponding loading rate values were ~ 2490 pN/s and ~ 4395 pN/s. The obtained quantities were plotted as a function of the number of bonds simultaneously ruptured (Figures 6.11).

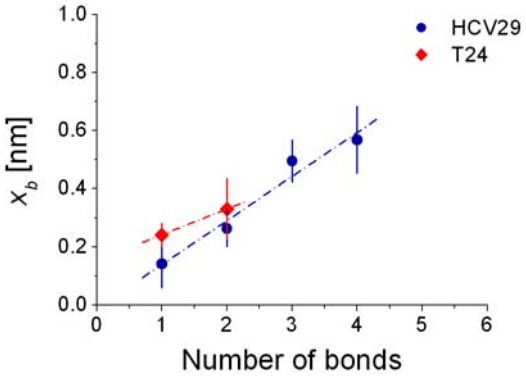


a)

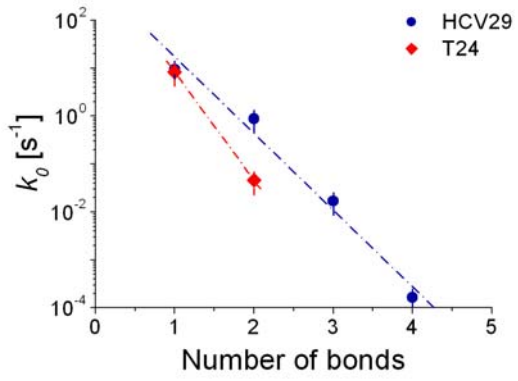


b)

Figure 6.11. The relation between the position of the energy barrier $x_b$ and the dissociation rate constant $k_0$ on the number of ruptured bonds obtained for GC4−Ncadh complex probed on the surface of HCV29 and T24 cells. The dash-dot lines denote the assumed linear dependence.

The results indicated clearly that the values for both Bell's model parameters scale with the number of bonds ruptured at the same time, but the character of scaling was different – the position of the energy barrier increased linearly (dash-dot lines in Figure 6.11a), while the dissociation rate decreased exponentially (dash-dot lines in Figure 6.11b). The barrier, closest to the energy minimum ($x_{b1} = 0.14 \pm 0.08$ (MaxEr[25]) nm), was observed during the unbinding of a single GC4−Ncadh complex in reference cells. The rupture of the same complex performed in cancerous cells shifts it to the distance almost two times larger ($x_{b1}$ = 0.24 ± 0.03 (MaxEr) nm). In spite of

[25] MaxE is the maximum error calculated according to Equations (5.5) and (5.6) for $x_b$ and $k_0$, respectively.

rather large experimental error, the results suggest higher $x_{b2}$ value for cancerous cells. Since the position $x_b$ determines the width of the energy barrier, the observed increase of its value denotes the widening of the barrier as the number of simultaneously ruptured bonds. An exponential decrease of the dissociation rate constant with the number of bonds was found to decrease faster for cancerous cells.

*Lectin − glycan complexes*

Analogously, like in case of N-cadherins, the probability density function was fitted to force histograms obtained for lectin-glycan complexes studied in the HCV29 and T24 cells (in example SNA − sialic acid complex in Figure 6.12).

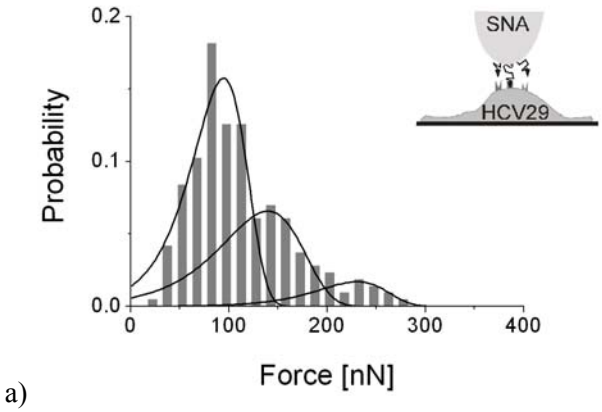


a)

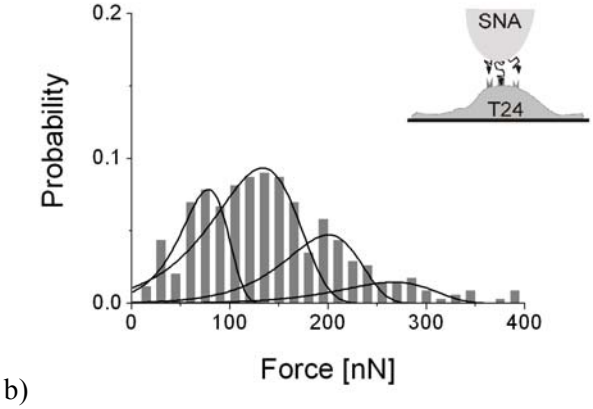


b)

Figure 6.12. Force histograms obtained for the interaction between sialic acids glycans and lectin *Sambucus nigra* probed on a surface of reference HCV29 (a) and cancerous T24 (b) cells. The lines denote the probability distribution (Equation (5.2)). Peaks correspond to simultaneous rupture of 1, 2, 3, and 4 bonds.

The dependence of the energy barrier position on the number of simultaneously ruptured bonds had different character than that observed for the GC4−Ncadh complex. Independently of the cell type, $x_b$ decreased slightly (Figure 6.13a). In the HCV29 (reference) cells, the position remained almost constant, independently of the number of ruptured bonds and of the probing lectin (ConA or SNA).

Its almost constant value (of ~ 0.15 nm, for $n = 1$) signified also a similar width of the barrier in the energy landscapes, corresponding to the unbinding of each type of the studied single lectin−glycan complex (i.e. ConA−mannose; SNA−sialic acid).

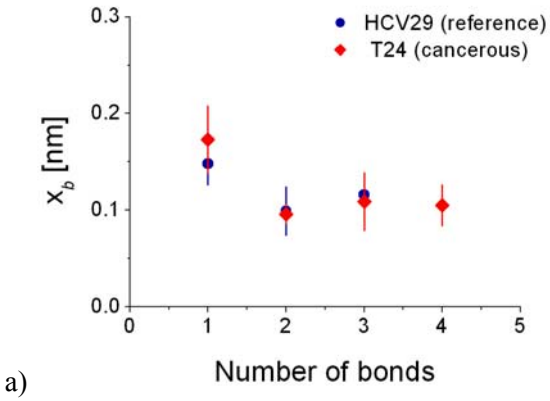


a)

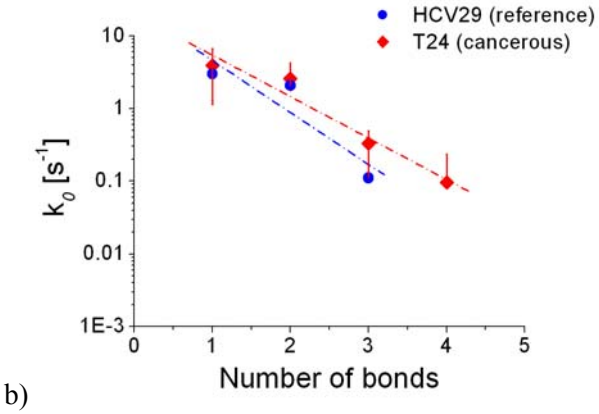


b)

Figure 6.13. The dependence of the energy barrier position (a) and the dissociation rate constant (b) on the number of ruptured bonds obtained for SNA−sialic acid complexes in reference HCV29 (blue) and cancerous T24 (red) cells.

The simultaneous rupture of a few bonds ($n = 2, 3, 4$) showed smaller values (of about 0.03 nm for $n = 3$), pointing to the weak modification of the energy barrier widths. In cancerous cells, the position of the energy barrier was the largest for the case when only one bond was ruptured for both types of complexes[26]: 0.26 ± 0.03 (MaxEr) nm for ConA−mannose and 0.17 ± 0.04 (MaxEr) nm for SNA−sialic acid ones. These values are larger than those obtained for reference, non-malignant cells for the same type of the lectin−glycan complex.

The simultaneous rupture of a few SNA−sialic acids complexes results in the large drop of the $x_b$ value to ~0.07 nm, what indicates the larger modification in the interacting potential. The observed differences indirectly denote alterations in the structure of the glycan binding sites interacting with

[26] The position of the energy barrier and the dissociation rate constant of PHA-L−*N*-acetylglucosamine complex were not determined for due to not sufficient statistics in the force histogram.

the probing lectin what was already detected as various unbinding force values. However, the position of the energy barrier brings the information about the dissociation of the single molecular complex and, therefore, its distinct values indicate different kinetics of the unbinding process.

The loading rate of lectin−glycan complexes used for the $k_0$ determination was 2500 pN/s. The dissociation rate constant for ConA − mannose complex was found to be higher in cancerous cells (7.64 ± 4.96 (MaxEr) $s^{-1}$) than in reference ones (4.89 ± 2.59 (MaxEr) $s^{-1}$). In case of SNA − sialic acid complex, the dissociation rate was strongly dependent on the number of bonds simultaneously ruptured (Figure 6.13b). It decreased exponentially similarly as observed for the GC4−Ncadh complex.

### *6.2.3. Energy landscape reconstruction*

The single–molecule studies enable to characterize the intermolecular potential of a single ligand–receptor complex. Without the external force, the dissociation of a complex is governed by its activation energy. By applying an external force, the potential is modified by tilting it and lowering the energy barrier. Such action alters the kinetics of the system. The extent of this change depends on the nature of the intermolecular potential of the dissociating complex *(Evans et al. 1997)*.

The simultaneous rupture of *n*-bonds (i.e. *n* single complexes) can be modeled as a failure of a bond (complex) requiring the unbinding force being *n* times higher than the force needed to break a single bond. The other assumption is that the unbinding of this new bond proceeds through single energy barrier. In such way, the shape of the energy landscape(s) was reconstructed basing on Bell model parameters obtained by fitting the probability density function to the corresponding force histogram. The obtained dissociation rate constants for the interaction of the single complex indicated also the modification of the energy landscape induced by the simultaneous unbinding of the consecutive bonds. For example, the calculated difference between the energy heights (for the simultaneous rupture of one and two single GC4−Ncadh complexes in HCV29 cells) is the following

$$\Delta G_{n=1} - \Delta G_{n=2} = k_B T \cdot \ln\left(\frac{k_{02} = 0.885}{k_{01} = 9.53}\right) = -2.4 \cdot k_B T \qquad (6.1)$$

Thus, the height of the energy barrier describing the simultaneous rupture of two single GC4-Ncadh complexes is higher by about $2.4 \cdot k_B T$ with respect to the unbinding of a single bond.

*GC4−Ncadh complex*

The reconstructed intermolecular potentials of the GC4–Ncadh complex probed in the HCV29 and T24 cells are presented in Figure 6.14a&b (all proportions are preserved).

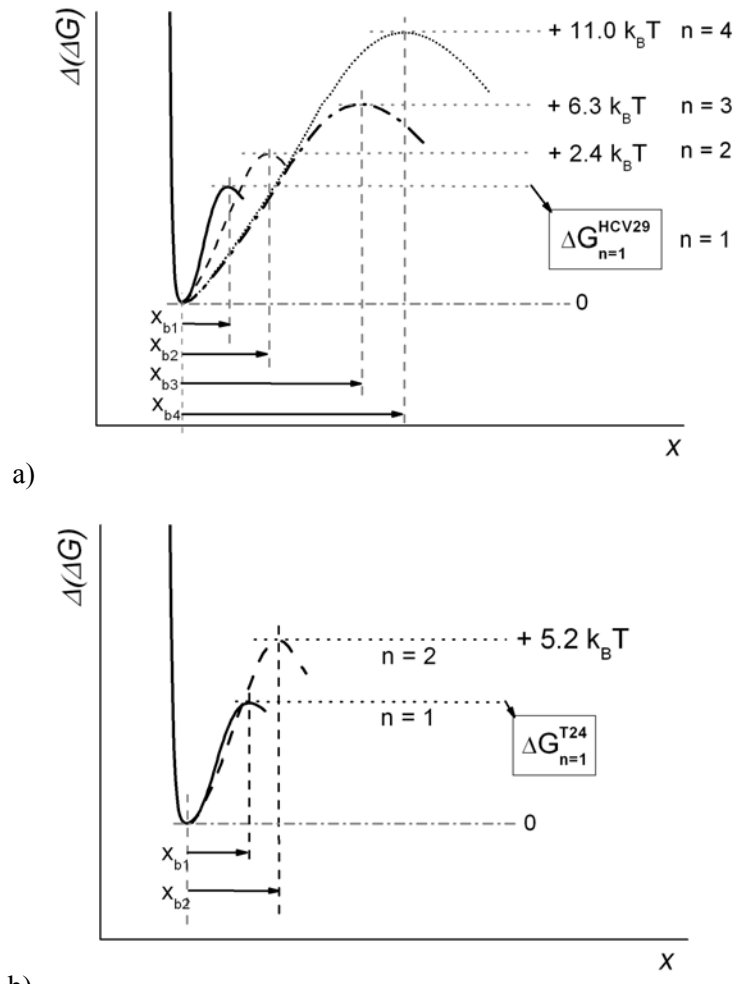


Figure 6.14. a) The reconstructed intermolecular potentials of the single GC4–Ncadh complexes probed in non-malignant HCV29 cells. b) The energy landscape of GC4–Ncadh complex in malignant T24 cells ($x_{b1}$, $x_{b2}$, $x_{b3}$, and $x_{b4}$ are the positions of the energy barriers).

Alongside with the number of simultaneously ruptured bonds, the height of the energy barrier becomes larger in both cell types. Its increase was estimated from the Equation (3.21) by comparing the corresponding dissociation rate constants $k_{0i}$. Since, from AFM measurements, it is not possible to determine the absolute height of the energy barrier, the extent of the increase was calculated with reference to the height of the energy barrier obtained for the single GC4–Ncadh complex measured either in the HCV29 cells ($\Delta G_{n=1}^{HCV29}$) or in the cancerous T24 ones ($\Delta G_{n=1}^{T24}$). For the reference cells, the height of the energy barrier augmented by about $2.4 \cdot k_B T$, $6.3 \cdot k_B T$ and $11.0 \cdot k_B T$ for the simultaneous rupture of 2, 3, and 4 bonds, respectively, while for the cancerous ones the energy barrier height was by $5.2 \cdot k_B T$ higher with respect to $\Delta G_{n=1}^{T24}$.

By applying the same Equation (3.21), it is possible to compare the height of the energy barrier for the rupture of the same number of bonds. The results showed that the energy barrier of the single GC4–Ncadh complex in the malignant cells (T24) was minimally higher (of about $0.13 \cdot k_B T$) in

comparison with the same complex studied in the non-malignant cells (HCV29). When two bonds were simultaneously ruptured, the corresponding difference barrier height was larger ($0.98 \cdot k_B T$).

The other characteristic feature observed in the reconstructed energy landscapes was the widening of the barrier as the number of simultaneously ruptured complexes increased. That was more pronounced for the simultaneous unbinding of 3 or 4 single complexes in HCV29 cells, where the obtained barrier widths were 1.0 ± 0.1 (MaxEr) nm and 1.1 ± 0.1 (MaxEr) nm, respectively. It reached the smallest value of 0.28 ± 0.16 (MaxEr) nm during the unbinding of a single GC4−Ncadh complex.

The unbinding of 1 or 2 single complexes in cancerous cells showed the 0.1 nm difference in the barrier width. However, when the rupture was compared with the unbinding of the same complex type in reference cells, distinct properties of the energy landscape were revealed. The unbinding of a single complex proceeded through a barrier almost 2 times higher (0.28 ± 0.16 (MaxEr) nm versus 0.48 ± 0.06 (MaxEr) nm). The simultaneous rupture of two single GC4−Ncadh complexes showed smaller $x_{b2}$ value (0.52 ± 0.12 (MaxEr) nm) in HCV29 cells as compared to cancerous one (0.66 ± 0.20 (MaxEr) nm).

*Lectin − glycan complexes*

The intermolecular potentials of the cell surface glycans probed with two lectins ConA and SNA in the HCV29 and T24 cells were also reconstructed analogously as for the GC4-Ncadh complex. In the cancerous cells (Figure 6.15), the energy barrier height, corresponding to rupture of a single complex ($n = 1$) was slightly higher of $0.45 \cdot k_B T$ and significantly wider than in the reference cells (the width increased from 0.32 ± 0.05 (MaxEr) nm to 0.52 ± 0.07 (MaxEr) nm).

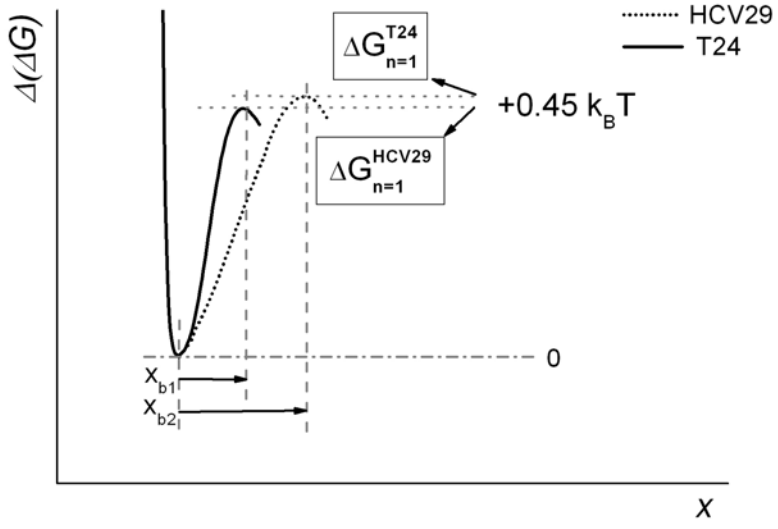


Figure 6.15. Energy landscapes for the mannose type glycans probed by lectin ConA in HCV29 and T24 cells.

The complete comparison between the reference and cancerous cells was performed for the most important glycan type – the one composed of sialic acids residues. The overexpression of this glycan type is a characteristic feature of the malignant transformation *(Albuquerque et al. 2004)*. The results of the reconstruction are presented in Figure 6.16 a&b.

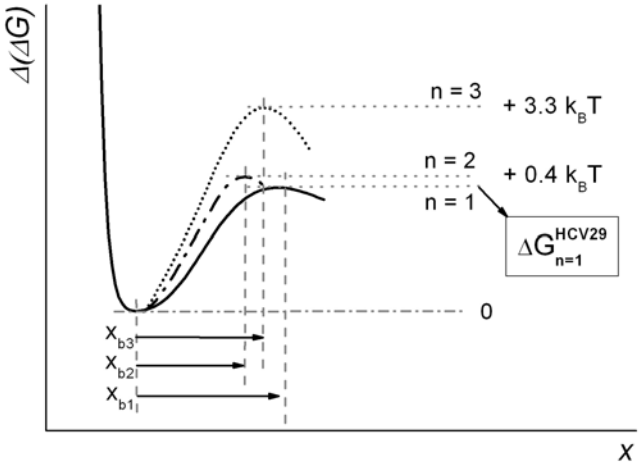


a)

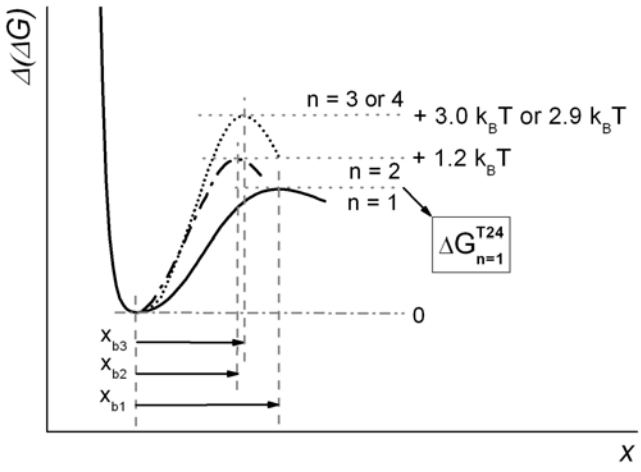


b)

Figure 6.16. The reconstructed intermolecular potentials of the interaction between sialic acids type glycans and lectin from *Sambucus nigra* (SNA) probed in non-malignant HCV29 (a) and malignant T24 (b) cells.

The energy landscapes of the interaction involving glycans containing sialic acids residues probed in both cell types were similar. The rupture of a single complex ($n$ = 1), resulted in the lower energy barrier height of $0.27 \cdot k_B T$ but the width larger of about 17% than in case of reference cells. For the rupture of 2, 3, and 4 complexes, the height of the energy barrier in cancerous cells decreased with respect to that for reference one but the width of the barrier remained constant.

### *6.2.4. Lifetime of the studied complexes*

The lifetimes calculated from the Equation (3.3) for the rupture of the single GC4−Ncadh complex were similar in both reference HCV29 and cancerous T24 cells: 0.11 ± 0.05 (MaxEr) s

and 0.12 ± 0.06 (MaxEr) s, correspondingly. However, the large discrepancy in the unbinding forces, i.e. 26.1 ± 7.1 (SD) pN (HCV29 cells) and 61.7 ± 14.6 (SD) pN (T24 ones), indicates the altered stability of the formed complex − an easier unbinding require less of force. The lifetime in function of the number of simultaneously ruptured bonds increases with the latter quantity (Figure 6.17). For the simultaneous rupture of two GC4−Ncadh complexes, the lifetime of the complex in the cancerous cells is 20 times larger (21.8 ± 10.9 (MaxEr) s) when compared with the reference cells (1.1 ± 0.6 (MaxEr) s). In that case the energy barrier height differs only by about 0.98·$k_BT$).

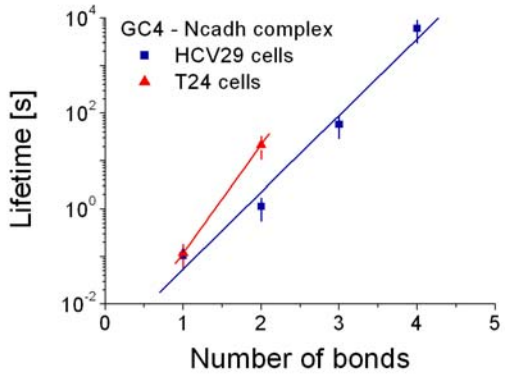


Figure 6.17. The bond lifetimes of single GC4–Ncadh complex for bladder cells.

The lifetimes of lectin−glycan complexes are much different from the lifetime for the GC4-Ncadh complex. When mannose type complex was studied, the lifetimes of the single ConA−mannose pair were comparable within the experimental error (0.21 ± 0.11 (MaxEr) s for the HCV29 cells and 0.13 ± 0.09 (MaxEr) s for the T24 cells) with slight tendency of the formation of more stable complexes in reference cells involving the mannose type glycans. The complexes involving the interaction with sialic acid residues showed similar raising relation for both HCv29 and T24 cells with the number of simultaneously ruptured single complexes (Figure 6.18).

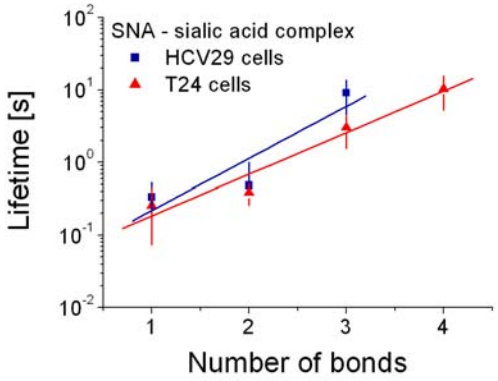


Figure 6.18. The bond lifetimes of single SNA–sialic acid complex.

Initially, for both cell types, the lifetimes for the rupture of one and two complexes were slightly larger for the reference HCV29 cells. Their values were: 0.34 ± 0.19 (MaxEr) s for $n = 1$ and 0.49 ± 0.32 (MaxEr) s for $n = 2$. The corresponding lifetimes determined for cancerous cells were

0.26 ± 0.18 (MaxEr) s and 0.39 ± 0.12 (MaxEr) s for $n = 1$ and $n = 2$, respectively. Larger increase was observed for the rupture of 3 complexes in the same time. The lifetime for non-malignant cells was three time larger (9.09 ± 4.45 s) than for cancerous cells (3.03 ± 1.46 (MaxEr) s).

### *6.2.5. Kinetic profiles*

The kinetic profile is a dependence of the dissociation rate on the external force applied to the bond. Such relation determines how long a bond or a complex will last under the changing force. It is analytically described by the Equation (3.9). Based on the determined $x_b$ and $k_0$ parameters, the kinetic profiles were plotted for all studied complexes. The slope of the kinetic profile is largely determined by the width of the energy barrier. Its larger values result in a steeper slope in the profile.

*GC4−Ncadh complex*

In order to characterize the differences in the kinetics of Ncadh−GC4 complex in non-malignant HCV29 and malignant T24 cells, the direct comparison of the dissociation kinetics was performed only for cases where one or simultaneous rupture of two complexes occurred.

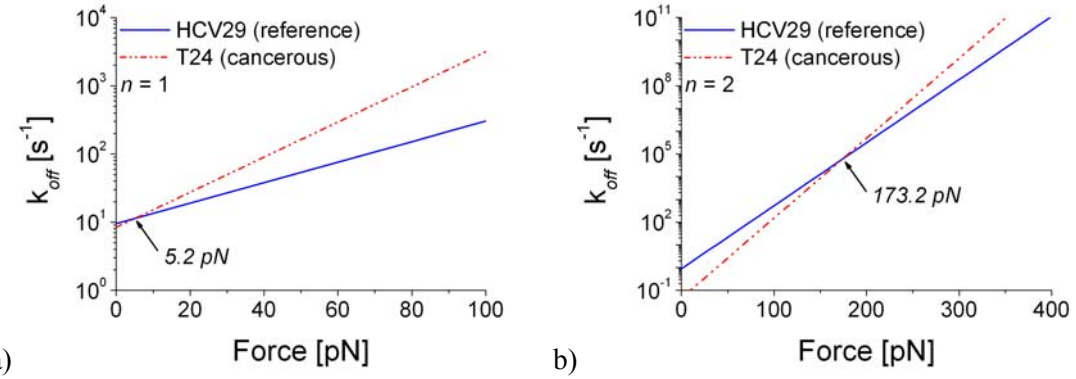


Figure 6.19. The comparison of kinetic profiles of the dissociation of the GC4–Ncadh complex probed on the surface of non-malignant HCV29 cells, plotted for 1 and 2 simultaneously ruptured complexes.

The rupture of a single Ncadh−GC4 complex, in case of very small unbinding forces (Figure 4.19a) from $F = 0$ to $F = 5.2$ pN (comparable with thermal noise fluctuations), the mutual relation between the corresponding dissociation rate is the following

$$k_{off}(\text{HCV29};\, n = 1) > k_{off}(\text{T24};\, n = 1)$$

what means that rupture of the GC4−Ncadh complex occurs easier in reference cells (Figure 6.19a). Above the 5.2 pN, the relation is opposite

$$k_{off}(\text{HCV29};\, n = 1) < k_{off}(\text{T24};\, n = 1)$$

and the unbinding proceeds easier in cancerous cells.

The kinetic profile delivered for the simultaneous unbinding of two complexes (Figure 6.19b) showed the shift of the pint of intersection towards larger force values (173.2 pN) where the relation

$$k_{off}(\text{HCV29};\, n = 2) > k_{off}(\text{T24};\, n = 2)$$

turns into

$$k_{off}(\text{HCV29};\, n = 2) < k_{off}(\text{T24};\, n = 2)$$

indicating the transition from slower to faster dissociation of complexes in cancerous cells.

*Lectin − glycan complexes*

Analogously, the kinetic profiles delivered for the lectin–glycans complexes were studied in both cell types. The corresponding relations for ConA − mannose and SNA − sialic acid complexes are presented in Figures 6.20 & 6.21, respectively.

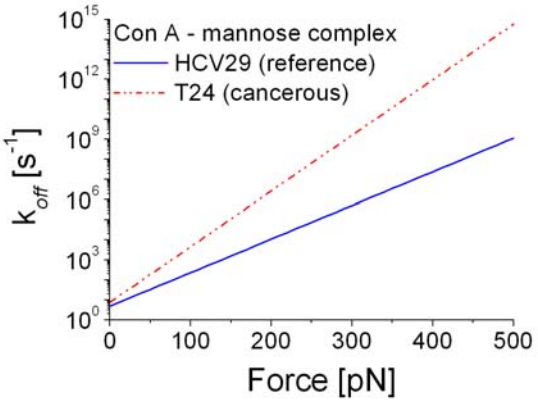


Figure 6.20. The kinetic profiles of a single ConA − mannose complex probed in HCV29 (blue line) and T24 (red line) cells.

Alongside the whole force range, from 0 to 500 pN, the same relation between dissociation rate constant of a single ConA − mannose complex was observed

$$k_{off}(\text{HCV29};\, n = 1) < k_{off}(\text{T24};\, n = 1).$$

The kinetic profiles obtained for the SNA − sialic acid complex are observed to behave differently (Figure 6.21). For $n = 1$, the relation between dissociation rate constants in HCV29 and T24 cells is given by

$$k_{off}(\text{HCV29};\, n = 1) < k_{off}(\text{T24};\, n = 1)$$

in the whole force range, from 0 to 800 pN.

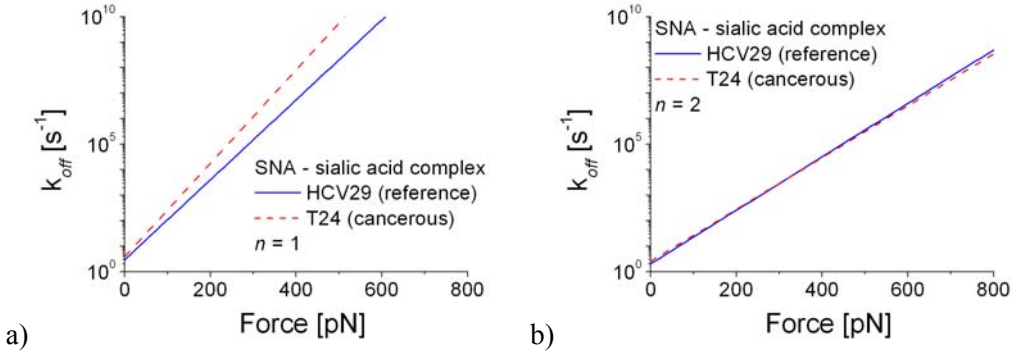


Figure 6.21. The kinetic profiles for sialic acids-type glycans probed by SNA in both HCV29 (blue line) and T24 (red line) cells. The corresponding number of simultaneously ruptured single complexes was: (a) $n$ = 1, (b) $n$ = 2.

The unbinding of two single complexes in the same time results in the change of the relation sign from

$$k_{off}(\text{HCV29};\, n = 2) < k_{off}(\text{T24};\, n = 2)$$

to

$$k_{off}(\text{HCV29};\, n = 2) > k_{off}(\text{T24};\, n = 2)$$

at the transition point of 309 pN. Similar behavior, as for $n = 2$, was observed for the simultaneous breaking of 3 complexes but the point of intersection shifts to at a much higher force (F = 646 pN).

### *6.2.6. Unbinding length and bond stiffness*

If a bond between the antibody and the antigen is formed, the AFM probe withdrawal generates bending of the cell membrane. The moment when tip detaches from the cell surface (i.e. the interacting molecules unbind) corresponds to the most probable unbinding force and reveals the mechanical resistance of the whole molecular complex for stretching. For cell surface molecules embedded in the cell membrane, the rupture length reflects the overall mechanical resistance of the complex at the molecule anchorage place. Thus, such a rupture will bring the information about the strength of the molecule attachment to cell membrane and it can be influenced by proteins linking it to the actin cytoskeleton. The magnitude of the contribution depends on the force that causes the membrane bending.

The application of the pulling force can result in a formation of membrane tethers (i.e. cylindrical membrane tubes) what was reported in many papers *(Hochmuth et al. 2002; Girdhar et al. 2004)*. For example, during the rolling of human neutrophils on the endothelium, tethers are likely extracted from the neutrophil (*Girdhar et al. 2004)*. Tether extraction reduces the force imposed on the adhesive bond between the neutrophil and endothelium, thereby facilitating the rolling. Studies of the tether formation are usually carried out using micropipette aspiration *(Hochmuth 2000)* or using magnetic tweezers *(Hosu et al. 2007)*. Also, AFM can be applied. Sun and coworkers *(Sun et*

*al. 2005)* used this technique to extract tethers formed by nonspecific interactions between the AFM probe and the cell surface (three different cell types were measured: Chinese hamster ovary cells, a malignant human brain tumor cell line, and human endothelial cells. The presence of a tether was identified by an abrupt drop in the force value and long separation distance in the recorded force curves. The average force required to form a single tether was around 30 pN (measured for the cantilever retraction speed of 3 μm/s), irrespective of the cell types used and also independent of the chemical nature of the attachment to the AFM probe. This value is comparable with the interaction force obtained for measurements of molecular complex with low affinity. The only feature distinguishing the membrane tethers from the specific unbinding is a very large unbinding distance in the range of hundreds of nanometers to a few micrometers. In the abovementioned work, the average distance at which a single tether ruptured was 2.7 μm *(Sun et al. 2005)*.

### *GC4-Ncadh complex*

The antibody, attached to the AFM tip and bound to N-cadherin, creates the relatively strong connection. The force applied to the probe stretches the single cadherin and, if the interaction between antibody and cadherin is sufficiently strong, it causes the membrane bending which is transported inside the cell by the cadherin connection with actin cytoskeleton. Figure 6.22 presents the illustration of the bending of cell membrane at the point where N-cadherin is anchored. The whole system can be represented by a simple model of elastic springs linked in series, where each from the contributing molecules is characterized by the spring constant.

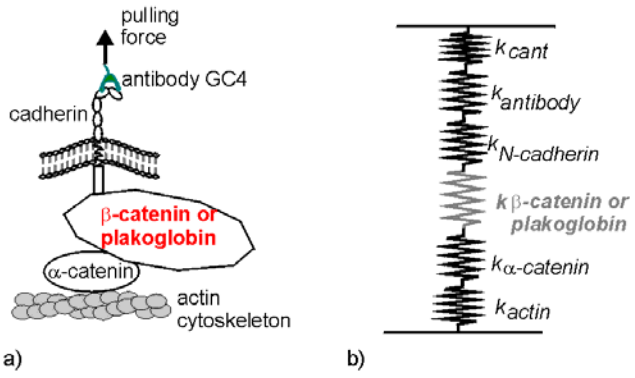


Figure 6.22. a) Bending of cell membrane at the anchoring point of a single N-cadherin molecule pulled off by the AFM probe. b) Simple model representing mechanical properties of the pulled cadherin−catenin complex.

Taking into account the proteins involved in the N-cadherin linkage to the actin cytoskeleton (though β-catenin or plakoglobin) in a cell membrane, the unbinding events included in the first peak present in the force histograms were analyzed in respect of the rupture length values. All unbinding events (87 cases) included in the first force peak (26.1 ± 7.1 pN in Figure 6.4a) obtained

for HCV29 cells, were used to create the distribution of the length at which the bond rupture occurred.

The histogram showed two clearly distinguishable maxima that were fitted with Gauss functions to determine the centre of the distributions (Figure 6.23a). Their positions were 15.1 ± 4.0 nm and 30.2 ± 5.5 nm. Next, analogously, the rupture length histogram (Figure 6.23b) was formed for cancerous T24 cells from 174 unbinding events recorded within the first peak in the unbinding force histogram ($F$ = 61.7 ± 14.6 pN). Again, two maxima, centered at 27.2 ± 7.4 nm and 49.8 ± 7.1 nm, were visible. Such small rupture length values exclude the tether formation during the unbinding of the single GC4−Ncadh complex *(Sun et al. 2005)*.

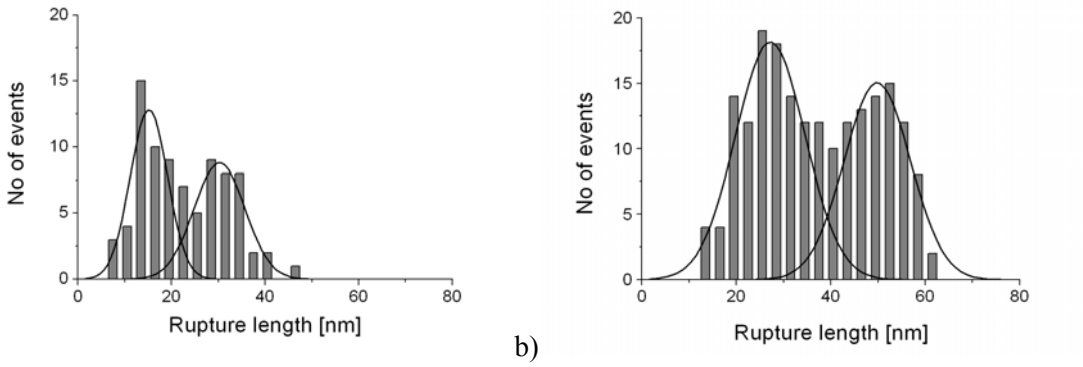


a) b)

Figure 6.23 Rupture length histograms of the GC4–Ncadh complex obtained for a) reference HCV29, and b) cancerous T24 cells. The bin size was ~ 3 nm equal to the distance between subsequent z-steps (only events from the first force peak were analyzed). To each peak the Gaussian function was fitted.

The presence of the two rupture lengths for the known unbinding force value enabled the estimation of the overall stiffness of the N-cadherin anchorage complex in cell membrane. The two stiffness values were calculated from the ratio of the unbinding force to the corresponding rupture length. Their values were: 1.66 ± 0.82 and 0.77 ± 0.31 mN/m. Like in case of reference cells, the overall stiffness of the N-cadherin anchorage in cell membrane of cancerous cells was estimated. In the latter case, two times larger values were obtained, i.e. 2.93 ± 1.04 and 1.41 ± 0.46 mN/m (Figure 6.24).

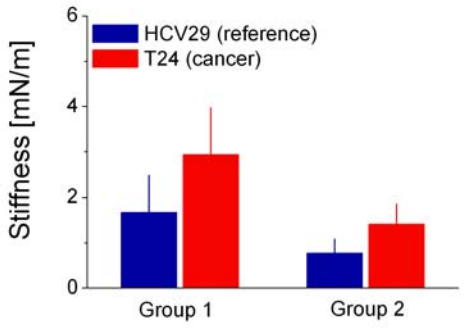


Figure 6.24. The stiffness of the GC4−Ncah complex in reference and cancerous cells.

The groups of stiffness for the GC4−Ncadh complex indicate different mechanical linkage of N-cadherin to actin cytoskeleton. This can be explained taking into account the structure responsible for the linking of cadherin to actin cytoskeleton. It has been already reported that cadherin connection to actin cytoskeleton involves the presence of two proteins, either γ–catenin or plakoglobin *(see section 6.1*), interacting with the same partners i.e. the cytosolic end of N-cadherin. In the work of Giroldi *et al. (Giroldi et al. 1999),* the expression of cadherin-catenin complexes has been analyzed in 17 human bladder-cancer cell lines. Among these lines, the malignant T24 cells were also studied. The obtained results showed the lower expression of E-cadherin to the advantage of N-cadherin. The lack of E-cadherin was correlated with changes in the catenin complex having tendency to deplete plakoglobin. However, in T24 cells a small amount of this catenin was still observed. Therefore, the two rupture lengths and thereby, two stiffness values indicate the presence of two groups of N-cadherins, either those connected through γ–catenin or plakoglobin (see Figure 6.1).

A separate question arises whether it is possible to identify which stiffness value is related to a particular type of connection with the actin cytoskeleton. It is natural to postulate that stronger connection (i.e. larger rupture length since it indicates stronger complex anchorage in a plasma membrane) will designate the more favorable interactions. Taking into account that γ–catenin interacts only with classical cadherins (*Ramburan et al. 2002*), we may deduce that the formation of the cadherin–cytoskeleton linkage will manifest in a lower stiffness (second pairs of stiffness values for HCV29 and T24 cells, group II in Figure 6.23). Since the plakoglobin can also associate less favorable with cadherins (*Nollet et al. 1999; Giroldi et al. 1999*), it seems to be clear that the other pair of stiffness values (group I in Figure 6.23) will be attributed to the weaker strength of the linkage.

These two types of cadherin linkages to the actin cytoskeleton were present in both non-malignant and malignant cells but their mechanical properties were different. The stiffness was larger in case of cancerous cells for both linkage types ($2.93 \pm 1.04$ versus $1.67 \pm 0.82$ mN/m and $1.41 \pm 0.46$ versus $0.77 \pm 0.31$ mN/m for the T24 and HCV29 cells, respectively), strongly indicating the other possible source of alterations in the single GC4-Ncadh complex – cancerous transformation, manifesting in stiffening of the molecular linkage.

### *Lectin−glycan complexes*

Lectins attached to the AFM tip recognize different glycans that are covalently attached either to proteins (called glycoproteins) or to lipids (called glycolipids). Despite the specific character of the interaction, for these complex types, AFM alone is unable to distinguish between the target attachments on a cell surface. Such distinction is possible by using a given type of lectins as it has been performed for the studied presented here i.e. the chosen lectins recognized *N*-glycans attached

to proteins *(Hsu et al. 1982; Shibuya et al. 1982; Bryce et al. 2001)*. However, it should be pointed out that the *N*-glycans constitute a large class of different structural chains. Thus, the applied pulling force stretches different types of glycans. If the interaction between a lectin and a single glycan structure is sufficiently strong, it can cause the membrane bending which maybe transported inside the cell if the glycoprotein is linked with the actin cytoskeleton (Figure 6.24).

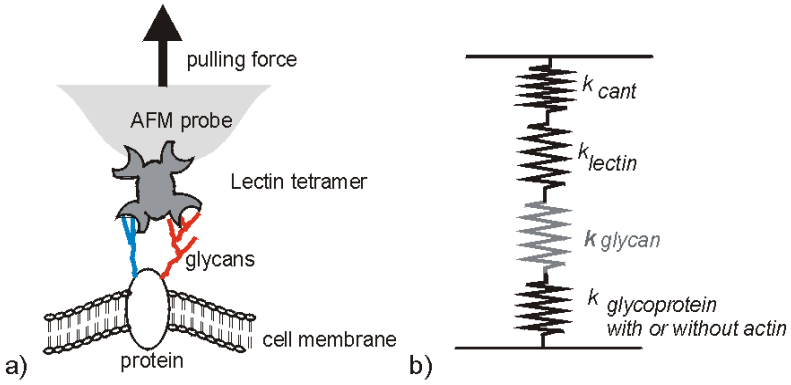


Figure 6.24. a) Bending of the cell membrane realized by pulled the lectin−glycan complex. b) Simple mechanistic model of the pulled lectin−glycan complex anchored in a plasma membrane.

Similarly to the analysis performed for the GC4−Ncadh complex, the first force peaks in the force histograms (Figure 6.6) were analyzed. The resulting distributions of the rupture length, at which the two studied lectin − glycan complexes unbind are presented in Figure 6.25a−d.

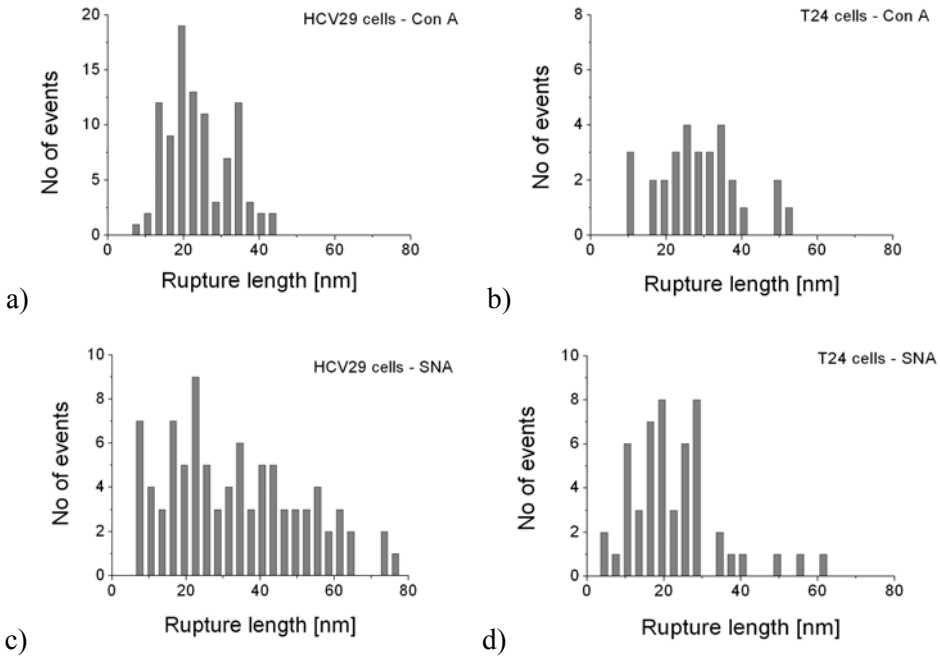


Figure 6.25 Rupture length histograms of ConA – mannose complex for (a) reference HCV29 (the total number of events *N* = 100) and (b) cancerous T24 (*N* = 30) cells, and of SNA – sialic acid complex for (c) reference HCV29 (*N* = 100) and (d) cancerous T24 (*N* = 51) cells. The bin size was ~ 3 nm equal to the distance between subsequent z-steps.

Contrary to the GC4−Ncadh case, histograms do not show any regularity. In general, the range of the rupture distance does not reach 100 nm. However, sometimes larger rupture distances (from 150 − 700 nm) were observed independently of the studied lectin − glycan complex (not shown in Figure 6.25). They were more frequent in HCV29 cells than in T24 cells. The rupture length in this range indicates the tethering of cell membrane that has been already shown to be in the force range of tens of piconewtons *(Sun et al. 2005)*.

To quantify the rupture length for the studied lectin − glycan complexes, the corresponding mean values and their standard deviations were calculated (Table 6.3).

Table 6.3. The mean value of the rupture length (*L*) and its standard deviation (*SD*) calculated for ConA − mannose and SNA − sialic acid complexes studied in HCV29 and T24 cells.

| Cell lines | Lectin − glycan complex | $L \pm SD$ [nm] | Full *L* range [nm] | System spring constant [mN/m] |
|---|---|---|---|---|
| HCV29 | ConA − mannose | 23.9 ± 8.3 | 6.4 − 43.4 | 1.7 − 11.3 |
| | SNA − sialic acid | 32.5 ± 18.2 | 7.6 − 76.2 | 0.6 − 6.4 |
| T24 | ConA − mannose | 28.3 ± 11.1 | 9.2 − 51.9 | 1.5 − 8.7 |
| | SNA − sialic acid | 22.6 ± 11.7 | 4.9 − 62.2 | 1.2 − 14.9 |

The broad range of the rupture length denotes also the wide range of the spring constant of the system composed of two springs i.e. cantilever and the studied complex. This is not surprising for the lectin − glycans complexes since the glycans can be attached either to proteins or lipids.

### *6.2.7 Number of ruptured bonds*

The area under each peak present in a force histogram is related to the probability of simultaneous rupture of a given number of single complexes.

*GC4-Ncadh complex*

The results of the rupture of the GC4-Ncadh complex showed that in case of reference cells the simultaneous unbinding of two single complexes was dominant (probability of ~0.6, Figure 6.26).

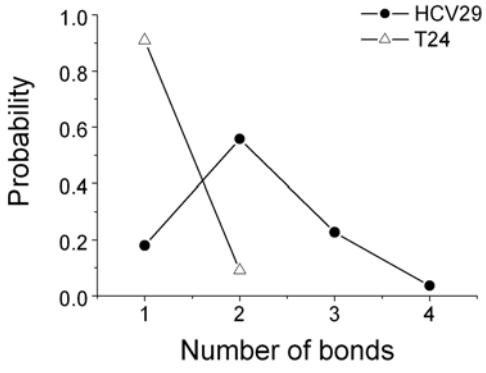


Figure 6.26. Frequency occurrence related to the probability of the unbinding of *n*-bonds for reference, non-malignant HCV29 and cancerous T24 cells.

The probability of the unbinding of 1 or 3 bonds was around 0.2. The simultaneous unbinding of 4 bonds was still probable at the very low level of about 0.02. For cancerous cells, the unbinding of a single pair of molecules was dominant (0.91), however, a small fraction (0.09) of simultaneous rupture of two bonds was also observed.

*Lectin− glycan complexes*

For cell surface glycans, the simultaneous unbinding of two or more ConA molecules was less probable than the unbinding of one bond (Figure 6.27 a&b).

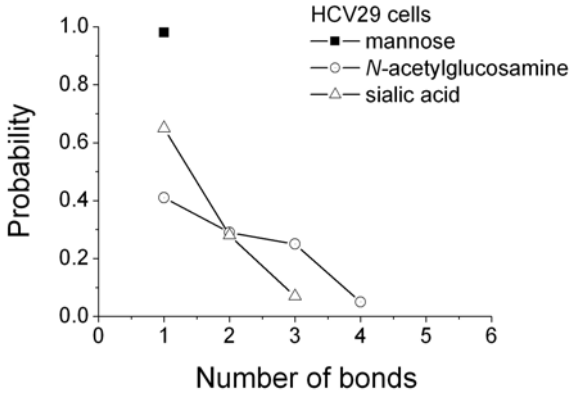


a)

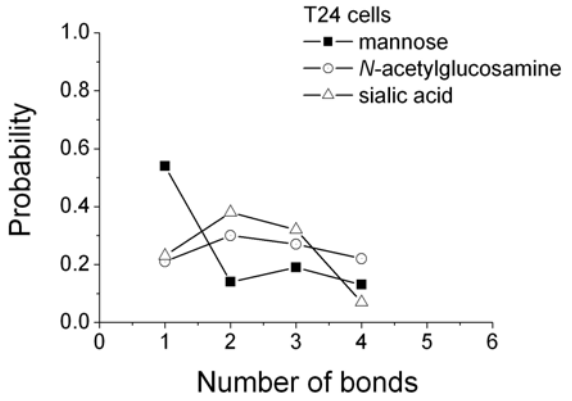


b)

Figure 6.27. Probability of the unbinding of *n*-bonds for reference non-malignant HCV29 (a) and cancerous T24 (b) cells probed in search of three glycan types composed of mannose, or *N*-acetylglucosamine, or sialic acids units.

The similar effect was observed for the lectin from *Sambucus nigra*, where 3 and 4 peaks were detected for reference and cancer cells, respectively. The most unexpected result was obtained when the surface of cancerous T24 and reference HVC29 cells was probed with the AFM cantilever coated with PHA-L. The number of unbinding events was larger for reference cells and, similarly to other lectins, the probability of breaking bonds was the same for one or two bonds formation. For cancer cells, the force histogram showed four maxima corresponding to the rupture

of the consecutive bonds. Their almost equal area indicated that *N*–acetylglucosamine residues of α(1,6) branched glycans were more accessible for PHA-L than that present in reference cells.

### *6.2.8. Unbinding probability*

The unbinding probability is often used to prove the specificity of the interaction (see *section 5.2.5*). To assure this, cells are incubated with the freely dissolved molecules of the same type as those attached to the AFM probe. In this manner, freely dissolved molecules bind to some of the N-cadherin binding sites, thereby competing with antibody molecules attached to the AFM probe. As a consequence, the number of recorded curves showing the unbinding events decreases.

For the GC4−Ncadh complex, the unbinding probability dropped from 0.040 to 0.026 and from 0.078 to 0.046 for HCV29 and T24 cells, respectively, after blocking the N-cadherins on the cell surface. The specificity of the lectin−glycan interactions was determined in the same manner. The results showed the decrease of the number of the unbinding events *(Lekka et al. 2006)*.

On the other hand, the unbinding probability correlates with the number of binding sites present on a surface and participating in the binding process. This is true for the homogeneous (or at least random) distribution of specific binding sites. If, like in our case, the studied molecule has only one type of binding site, the unbinding probability is proportional to the number of single complexes. It describes in a quantitative way the expression of cell surface molecules. The values determined by AFM were in the agreement with indirect (but rather qualitative) results obtained using standard biochemical methods *(Przybyło et al.2002; Marquez et al. 2004)*.

The unbinding probability determined for GC4-Ncadh complex in HCV29 and T24 cells was smaller for reference cells (0.046) than in cancerous cells (0.078). The lower unbinding probability value indicates a smaller number of binding sites for the antibody recognizing N-cadherins on a surface of HCV29 cells, which has been qualitatively observed by Laidler et al. *(Laidler et al. 2000)*.

The higher content of sialic acid residues (0.05 versus 0.08 for HCV29 and T24 cells, respectively) has been reported as a consequence of an increased sialylation of cancer cells *(Marquez et al. 2004)*. Larger expression of mannose bearing ligands (0.11) in HCV29 cells in comparison with the value obtained for T24 cancer cells (0.03) showed much higher amount of the high–mannose type glycans on their surface what was previously reported *(Przybyło et al. 2002)* for the same cell line. The specific interaction with PHA-L lectin indicated the presence of triantenary or tetrantenary structures (*N*-acetylglucosamine α(1,6)−branched) of complex type glycans. The decrease of the unbinding probability of PHA-L (from 0.08 to 0.02) suggested the loss of such structures in T24 cancer cells.

### *6.2.9. Summary*

The main aim of the studies presented in this monograph was to measure and quantitatively describe the adhesive properties of cancerous cells using atomic force microscopy. The studies have been focused on two types of molecular complexes: i) N-cadherin and its monoclonal antibody (GC4) and, ii) surface glycans (bearing either mannose or sialic acids units) and the corresponding lectin probe (ConA or SNA). The choice of these complexes was advocated by their potential use as indicators for cancerous cells. The level of the expression of molecules, determined by AFM, is limited only to molecules present in a plasma membrane and it can be directly related to the classical way of the molecule expression determination through the unbinding probability value: a parameter describing the number of molecules on cell surface. The obtained results are in good agreement with indirect (rather qualitative) results which have been already reported pointing out an increased expression of N-cadherin and sialic acids glycans in cancerous cells *(Giroldi et al. 1999; Marquez et al. 2004)*. Also, the higher content of mannose type glycans in non-malignant transitional epithelial cells of the ureter (cell line: HCV29) is consistent with the results presented in the work by Przybyło *et al. (Przybyło et al. 2006)*.

The analysis of the interaction between a given pair of single molecules performed by AFM allows determination of sets of parameters that more precisely and in a quantitative way describe the expression of molecules on a cell surface. These parameters can be divided into three classes correspondingly describing:

- the static properties of a single molecular complex where its strength of interaction and stiffness of the studied complex can be obtained,
- dynamic properties, on the basis of which the kinetic properties of the unbinding process can be delivered. They are described by two parameters: dissociation rate constant and the position of the energy barrier in the energy potential.
- properties of adhesion clusters, where the inter-relation between single complexes can be characterized, in particular the mechanism of the unbinding can be obtained.

The quantitative description of the molecule expression by means of AFM for two types of molecular complexes, i.e. GC4-Ncadh and lectin−glycan ones, studied in the context of cancerous transformation, is summarized below.

***GC4−Ncadh complex***

- *static properties*

The interaction occurring between N-cadherin and its monoclonal antibody (GC4) forms more stable complexes in cancerous (T24) cells when compared to non-malignant (HCV29) ones:

visualized by the unbinding force values of 26 pN and of 61 pN measured for HCV29 and T24 cells, respectively. This difference is attributed to the changes of the antibody binding site, what may reveal the alterations in both the primary N-cadherin structure and/or different glycan pattern in the neighborhood of the binding site.

The mechanical properties of the N-cadherin anchorage in a plasma membrane, i.e. cadherin−catenin complex, shows two types of the complexes with the participation of either α-catenin or plakoglobin. These two types of complexes are present in both reference HCV29 and cancerous T24 cells but they are stiffer in cancerous cells than in non-malignant ones indicating changes induced by oncogenic transformation.

- *dynamic properties*

The GC4−Ncadh complex dissociates differently depending on cell type studied. The reconstructed energy potential for cancerous cells has almost two times larger barrier than that obtained for the energy landscape of reference cells. The calculated height of the corresponding barriers (the difference was of $0.13 \cdot k_B T$, defined by the dissociation rate constants) is similar. This indicates faintly slower way of the GC4−Ncadh complex dissociation in cancerous cells.

The lifetime of a single GC4−Ncadh complex, determined from the dissociation rate constant, has similar values what means that, independently of the minimal difference in the energy heights, passing over the energy barrier is only slightly burden by the oncogenic transformation.

The calculated kinetic profiles show differences in the complex dissociation induced by the applied external force. The point of intersection, at $F$ = 10 pN, indicates the moment when the faster dissociation of GC4-Ncadh complexes in reference cells become slower than in cancerous cells.

- *properties of adhesion clusters formed from GC4−Ncadh complexes*

By keeping the constant contact area between the AFM probe and cell surface, the presence of more than one, single GC4−Ncadh complexes is observed mainly for HCV29 cells (i.e. simultaneous unbinding of multiple single complexes). In case of cancerous cells, the rupture of only one complex is most probable, however, some fraction of double complexes is also detected.

The mechanism of unbinding of GC4−Ncadh complexes in both cell types followed the "parallel-like" unbinding mechanism. These results showed the cooperative character of the N-cadherin unbinding indicating the similarity to the interaction for E-cadherin.

The dynamic properties of the adhesion clusters show that the width of the energy barrier scales linearly, showing an increase of its height with the number of simultaneously ruptured complexes. Oppositely, the dissociation rate constant decreases what might indicate slower dissociation. When the external force is applied to induce the complex unbinding, the point of intersection is observed

(c.f. Figure 6.19b), indicating the moment when the dissociation of the GC4−Ncadh complex starts to be faster in cancerous cells than in non-malignant cells.

***Lectin−glycan complexes***

- *static properties*

The unbinding force for two types of single lectin−glycan complexes (SNA−sialic acids and ConA−mannose type) showes close values independently on the studied cells (cancerous or reference ones), pointing out only slight changes in the structure of lectin−binding site in the studied sialic acids and mannose type glycans. However, the observed slightly larger force values indicates formation of more stable complexes for reference HCV29 cells.

The studies of mechanical properties of lectin-glycan complexes show the broad range of the stiffness values independently of the studied cells, with no characteristic values. This may reflect either the structural variety of glycan chains alone and/or distinct glycoproteins serving as an anchorage point for *N*-linked glycans.

- *dynamic properties*

The dissociation of both lectin−glycan complexes varies with the complex type in cancerous T24 cells. The reconstructed energy potential for the ConA−mannose complex is slightly higher (by about $0.45 \cdot k_B T$) and has significantly wider energy barrier in cancerous cells when compared with the energy landscape determined for non-malignant HCV26 cells. This indicates slower dissociation of ConA−mannose type complexes in cancerous cells. Analogously, the energy potential for SNA−sialic acid complex is reconstructed. In cancerous cells, it has larger width of the energy barrier but, oppositely as for ConA−mannose complexes, its height is smaller (by about $0.27 \cdot k_B T$) when compared with that calculated for reference cells.

The lifetime, determined on the basis of dissociation rate constant, for both types of lectin−glycans complexes type is larger in reference cells then in cancerous ones independently on the complex type, indicating easier unbinding of these complexes in cancerous cells.

The application of an external force inducing the complex to unbind causes faster dissociation in cancerous cells independently of the studied lectin−glycan complex.

- *properties of adhesion clusters formed from lectin−glycan complexes*

The clusters composed of lectin−glycan complexes are observed in both cancerous and reference cells for SNA−sialic acid complexes. The clusters made of ConA−mannose type glycans are observed only in cancerous cells.

The mechanism of the unbinding follows “parallel-like” model showing the cooperativity of the interaction in both types of lectin−glycan complexes.

The dynamic properties of the clusters formed from lectin−glycan complexes do not show any increase of the width of the energy barrier i.e. it remains almost constant independently on the number of ruptured complexes. The height of the energy barrier increases with the number of involved complexes in the smaller range of energy than for the GC4−Ncadh complex. The dissociation rate constant decreases slowly than in case of the GC4-Ncadh complex showing slight tendency for speeding up the unbinding as the number of complexes increases.

When the external force is applied to induce the unbinding of these complexes, the dissociation proceeds similarly in both reference and cancerous cells.

# CHAPTER 7

# Conclusions

Despite the fact that AFM has become a method that is widely applied to study of biology-related aspects *(Stroh et al. 2004; Puntheeranurak et al. 2006; Johnson et al. 2007)*, its advantages over standard biochemical methods are still not fully recognized. Some of them are obvious, like for example the fact that proteins are immobilized using a fairly uncomplicated protocol or that there is no need to use fluorescently labeled probes (with the exception of very specific cases). Apart from a high resolution enabling measurements of a single molecule, the great and most important advantage of AFM lies in the quantitative character of the method. By using fluorescent-based methods, the detection of proteins can be performed relatively easy for the single molecule, but gathering quantitative information about their number (related to the molecule density) and about the strength of the interaction is rather more difficult. The use of immunodetection of blotted proteins shows the formed complexes as a band of a given molecular mass. Consequently, those experiments deliver only qualitative information.

The main aim of the studies presented in this monograph was to measure and quantitatively describe the adhesive properties of cancerous cells. This was accomplished using the novel experimental approach − atomic force microscopy. The studies have been focused on two types of molecular complexes: i) N-cadherin and its monoclonal antibody (GC4) and, ii) surface glycans (bearing either mannose or sialic acids units) and the corresponding lectin probe (ConA or SNA). The choice of these complexes was advocated by their potential use as indicators for cancerous cells. The level of the expression of molecules, determined by AFM, is limited only to molecules present in a plasma membrane and it can be directly related to the classical way of the molecule expression determination through the unbinding probability value: a parameter describing the number of molecules on cell surface. The obtained results were in the good agreement with indirect (but rather qualitative) results which have been already reported pointing out an increased expression of N-cadherin and sialic acids glycans in cancerous cells *(Giroldi et al. 1999; Marquez et al. 2004)*. Also, the higher content of mannose type glycans in non-malignant transitional epithelial cells of the ureter (cell line: HCV29) was consistent with the results presented in the work by Przybyło *et al. (Przybyło et al. 2006)*.

The qualitative and quantitative description of the expression of molecules on a cell surface studied by AFM is possible only after the analysis of a large number of force curves showing (or not) a characteristic unbinding event. The observed events may origin not only from the specific interaction between molecules but also from non–specific, attractive forces, always present

between charged surfaces in electrolyte solution *(Lekka et al. 2004)*. The common procedure in studies of molecular interactions with the use of antibodies involves attaching a particular type of protein to the AFM probing tip. Thus, the recorded interaction can be limited to this particular type. However, still remains a difficulty to distinguish the specific force from the non-specific one. In addition, during the AFM experiment, different types of curves are usually obtained, corresponding to either specific or non-specific intermolecular interactions which involve the formation of weak (tens of picoNewtons) non–covalent bonds. Therefore, the data interpretation becomes rather difficult due to high complexity of the system. Fortunately, the determined unbinding probability is not the only criterion defining the interaction type. Curves matching the specific interaction have their own distinctive features such as unbinding force, rupture length or effective spring constant. These parameters are often essential to quantitatively describe properties of a given molecule type in plasma membrane of living cells.

The analysis of the interaction between a given pair of single molecules performed by AFM allows determination of sets of parameters that more precisely and in a quantitative way describe the expression of molecules on a cell surface. These parameters can be divided into three classes correspondingly describing:

- the static properties of a single molecular complex where its strength of interaction and stiffness of the studied complex can be obtained,
- dynamic properties, on the basis of which the kinetic properties of the unbinding process can be delivered,
- properties of adhesion clusters, where the inter-relation between single complexes can be characterized, in particular the mechanism of the unbinding can be obtained.

The presented characterization of the interaction force between single molecules demonstrates that atomic force microscopy can be used as a complementary or even alternative technique to study the expression of molecules on cell surface. Such measurements are not limited to a typical interactions occurring, for example, in antigen−antibody complex but also it is possible to study the interactions between parts of molecules. However, certain level of the specificity of the interaction between the investigated molecules should exist.

So far, the criteria used to detect cancer cells have mainly relied on a biological description, which is achieved on a morphological basis usually complemented by a variety of techniques including genetic, chemical, biochemical, and immunological methods. When cancer is suspected, usually specimens from tissues biopsy are examined under the microscope and, based on the characteristics of the individual cells and the patterns they form, a specific diagnosis is made. This process has not changed fundamentally for decades, even though it is widely accepted that

biological and molecular properties of tumor cells may be much more predictive of the tumor aggressiveness and the patient response to treatment.

The results presented in this monograph point to a novel approach to identify cancer−related changes in a quantitative way what can be used for describing and confirming the pathological state of a single cell. Ideally, such way of the identification of cancer at the level of individual cells may increase the efficiency of early cancer detection. However, in order to apply AFM in such area, a further development of the technique towards an accurate cancer diagnostics tool is still necessary. There is a need to answer the crucial questions:

– whether the obtained set of parameters may be a general or specific indicator for cancer,

– whether they can be used as a marker for early diagnostic of cancer,

– which of them are most suitable to be employed in the cost-effective, easy to use clinical technique, as an additional indicator in case when a common detection method is not working.

# ACKNOWLEDGEMENTS

There are many people who in different way helped me in my research. Therefore, I would like to take this moment to express my deep gratitude to all of them. In particular, I would like to mention:

**Zbigniew Stachura** (IFJ PAN), who was always ready to answer questions, to give invaluable advices, and to discuss strange results. His continuous support enabled to start and organize the biological activity of the AFM laboratory; **Andrzej Z. Hrynkiewicz**, the supervisor of my PhD thesis initiating research I am involved in, **Piotr Laidler** (CM UJ) for teaching me how to understand biological phenomena, for his help during the realization of my biological experiments, and, first of all, for showing me the importance of my studies; **Andrzej Kulik** (IPMC EPFL, Lausanne) for his advices enabling the development of our AFM system into a tool which can be successfully applied in biophysics; **Jan Styczeń** (IFJ PAN) for his support and for encouraging me in my studies over many years during his heading of the former Department of Nuclear Spectroscopy.

I am also very grateful to **Dorota Gil**, **Joanna Dulińska,** and **Maryla Łabędź** (CM UJ) who shared with me the knowledge how to work with biological material. In particular, I am very grateful to **Maryla Łabędź** for her help with cell culturing. I would like to acknowledge also **Joanna Wiltowska** (IFJ PAN) for her invaluable help with managing the AFM laboratory, especially during the time when I was writing this monograph.

In recent years I was working with several PhD students, helping them with their AFM measurements. In particular, I appreciate a lot all questions I had to answer during discussions with **Joanna Gryboś, Kateryna Lebed, Grażyna Pyka-Fościak**, and **Ida Dulińska.**

During my research, the collaborations with two scientific groups broadened significantly my experience and knowledge. Therefore, I would like to thank to **Andrzej Budkowski**, **Jakub Rysz,** and **Joanna Raczkowska** from the Institute of Physics UJ and **Laszlo Forró** from the Institute of Physics of Complex Matter, Lausanne, together with all members of his group (especially **Andrzej Sienkiewicz**, and **Sylvia Jeney**) for the fruitful time spent on common research and many discussions concerning distinct scientific problems.

I would like also to acknowledge to **Wojciech Zając** (IFJ PAN) for his great help in solving many statistical issues, vital for interpretation of my data.

I would like to say „thank you“ to all my colleagues from the former Department of Nuclear Spectroscopy and the present Department of Applied Spectroscopy.

Finally, I would like to thank my whole Family supporting me all the time, especially to my husband **Janusz** whose mildly sarcastic insight on life made the time always fun.

# PUBLICATIONS

*Book chapters relevant to the monograph:*

1. M.Lekka, P.Laidler – "Mikroskop sił atomowych (AFM)" ang. „Atomic force microscopy (AFM)" *Chapter in „Na pograniczu chemii i biologii"* tom XII, eds. Jan Barciszewski, Henryk Koroniak, Wydawnictwo Naukowe Uniwersytetu Adama Mickiewicza, Poznań, 2005, ISBN 83-232-1624-X, 569–592.
2. M.Lekka, A.J.Kulik – "Quantitative nanomechanical measurements in biology" – *Chapter 7 in "Applied Scanning Probe Methods II"*, eds. B.Bhushan, H.Fuchs, Springer, Berlin Heidelberg New York, 2006, ISBN-10 3-540-26242-3, 205–239.
3. K.Lebed, M.Lekka, A.Dąbrowska, A.J.Kulik, J.Lekki, Z.Stachura, – „Combined atomic force microscopy and microcontact printing techniques" – *Chapter 8 in „Progress in Condensed Matter Research"*, eds. M.P. Dass, 2006, ISBN 1-60021-022-8, 345–366.
4. M.Lekka, P.Laidler, A.J.Kulik – "Direct detection of ligand–protein interaction using AFM" – *Chapter 16 in "Applied Scanning Probe Methods VI"*, eds. B.Bhushan, S.Kawata, Springer, Berlin Heidelberg New York, 2007, ISBN-10 3-540-37318-7, 165–203.

*Publications relevant to the monograph:*

1. K.Lebed, A.J. Kulik, L.Forró, M.Lekka – „Study the kinetics of lectin carbohydrate interaction using atomic force microscopy and quartz crystal microbalance methods" – *Acta Physica Polonica A* 111 (2) (2007) 273-287.
2. M.Lekka, P.Laidler, M.Łabędź, A.J.Kulik, J.Lekki, W.Zając, Z.Stachura – "Specific detection of glycans on a plasma membrane of living cells using atomic force microscopy" – *Chemistry & Biology,* 13 (5) (2006) 505–512.
3. K.Lebed, A.J. Kulik, L.Forro, M.Lekka – "Lectin–carbohydrate affinity measured using quartz crystal microbalance", *J. Coll. Interf. Sci.*, 299 (1) (2006) 41-48.
4. M.Lekka, A.J.Kulik, S.Jeney, J.Raczkowska, J.Lekki, A.Budkowski, L.Forro – Friction force microscopy as an alternative tool for probing molecular interactions – *J. Chem. Phys.,* 123(1) (2005) 014702:1-7.
5. K.Lebed, G.Pyka–Fosciak, J.Raczkowska, M.Lekka, J.Styczeń – "Binding interaction of concanavalin A and carboxypeptidase Y studied using AFM", *J. Phys.: Condens Matter.*, 17 (18) (2005) S1447-S1458.
6. P.Laidler, J.Dulińska, M.Lekka, J.Lekki – "Expression of prostate specific membrane antigen in androgen–independent prostate cancer cell line PC–3", *Archives of Biochemistry and Biophysics,* 435(1) (2005) 1–14.
7. M.Lekka, P.Laidler, J.Dulińska, M.Łabędź, G.Pyka – "Probing molecular interaction between concanavalin A and mannose ligands by means of SFM", *European Biophysics Journal,* 33(7) (2004) 664–650.
8. J.Gryboś, G.Pyka–Fościak, K.Lebed, M.Lekka, J.Lekki, Z.Stachura, J.Styczeń –"Study of adhesion interaction using scanning force microscopy", *Acta Physica Polonica A*, 105 (2004) 501– 510.
9. M.Lekka, J.Gryboś, J.Lekki, Z.Stachura, J.Styczeń – „Single–bond force measured by means of SFM", *Acta Physica Polonica A* 102 (3) 2002 p.403–412.

## ***Other publications:***

book chapters (excluding the above mentioned positions) – 2,
peer-reviewed papers (excluding the above mentioned positions) – 34,
other papers – 6,
invited talks – 8,
other conference contributions (both oral and posters) – 79.

# REFERENCES


Afrin R., T.Yamada, A.Ikai − "Analysis of force curves obtained on the live cell membrane using chemically modified AFM probes", *Ultramicroscopy,* 100 (2004) 187−195.

de Albuquerque Garcia Redondo P., C.V.Nakamura, W.de Souza, J.A.Morgado–Diaz, − "Differential expression of sialic acid and N-acetylgalactosamine residues on the cell surface of intestinal epithelial cells according to normal or metastatic potential", *J.Histochem. Cytochem.* 52 (2004) 629−640.

Allen S., J.Davies, M.C.Davies, A.C.Dawkes, C.J.Roberts, A.J.B.Tendler, P.M.Williams − "The influence of epitope availability on atomic-force microscope studies of antigen-antibody interactions", *Biochem. J.,* 341 (1999) 173−178.

Allsbrook, W.C., W.W. Simms – "Histochemistry of the prostate", *Human Pathol.* 23 (1992) 297–305.

Alcaraz J., L.Buscemi, M.Puig de Morales, J.Colchero, A.Baro, D.Navajas – "Correction of microrheological measurements of soft samples with atomic force microscopy for the hydrodynamic drag on the cantilever", *Langmuir*, 18 (2002) 3578–3588.

Arenas M.I., E.Romo, M.Roynuela, B.Fraile, R.Paniagua – "E-, N-, P-cadherin and alpha-, beta-, and gamma-catenin protein expression in normal, hyperplastic and carcinomatous human prostate", *Histochem. J.* 32 (2000) 659–667.

Baenzinger, J.U. D.Fiete – "Structural determinants of concanavalin A specificity for oligosaccharides", *J. Biol.Chem.,* 254 (1979) 2400–2407.

Bausch A.R., W.Möller, E.Sackmann – "Measurements of local viscoelasticity and forces in living cells by magnetic tweezers", *Biophys. J.,* 76 (1999) 573–579.

Brakebusch C., R.Fässler – "β1 integrin function *in vivo*: adhesion, migration and more", *Cancer Metastasis Rev.,* 24 (2005) 403–411.

Bell G.I. – "Models for the specific adhesion of cells to cells ", *Science* 200 (1978) 618–627.

Ben–Ze'ev A. – "Cytoskeletal and adhesion proteins as tumor suppressors", *Curr. Opin. Cell Biol.,* 9 (1997) 99–108.

Binnig G., C.F.Quate, Ch.Gerber – "Atomic force microscopy", *Phys. Rev. Lett.*, 56 (1986) 930–933.

Bhushan B., S.Kawata (eds.) − *"*Applied Scanning Probe Methods VI*"*, (2007) Springer, Berlin Heidelberg New York.

Bongrand P. – "Ligand-receptor interactions", *Rep. Prog. Phys.,* 62 (1999) 921–968.

Bryce R.A., I.H.Hiller, J.H.Naismith − "Carbohydrate-protein recognition: molecular dynamics simulations and free energy analysis of oligosaccharide binding to concanavalin A", *Biophys. J.,* 81 (2001) 1373−1388.

Butt H.J., B.Cappella, M.Kappl – "Force measurements with the atomic force microscope: Technique, interpretation and applications", *Surf. Sci. Rep.,* 59 (2005) 1–152.

Cappella B., G.Dietler – "Force-distance curves by atomic force microscopy", *Surf. Sci. Rep*, 34 (1999) 1–104.

Carlier M.F., D.Pantaloni, – "Control of actin assembly dynamics in cell motility", *J.Biol.Chem.,* 282 (2007) 23005–23009.

Catalona, W.J., J.P.Richie, F.R.Ahmann, M.A.Hudson, P.T.Scardino, R.C.Flanigan, J.B.deKernion, T.L.Ratliff, L.R.Kavoussi, B.L.Dalkin, W.B.Waters, M.T.MacFarlane, P.C.Southwick – "Comparison of digital rectal examination and serum prostate specific antigen in the early detection of prostate cancer: results of a multicenter clinical trial of 6,630 men", *J.Urol.*, 151 (1994) 1283−1290.

Christofori G. − "New signals from the invasive front", *Nature,* 441 (2006) 444−450.

Chtcheglova L.A., G.Dietler − "Force spectroscopy of polyclonal and monoclonal anti-bovine serum albumin antibodies − BSA complexes", *Acta Phys. Pol.,* 104 (2003) 321−326.

Cocco S., R.Monasson, J.F.Marko − "Force and kinetics barriers to initiation of DNA unzipping", *Phys. Rev. E.*, 65 (2001) 041907-1−6.

Conacci-Sorrell M., J.Zhurinsky, A.Ben-Ze'ev − "The cadherin-catenin adhesion system in signaling and cancer", *J. Clin. Invest.*, 109 (2002) 978−991.

Dali'olio F. − "Protein glycosylation in cancer biology: an overview", *Clin. Mol. Pathol.,* 49 (1996) 126−135.

Damjanov I. − "*Pathology for the health-related professions*", W.B.Saumders Company, Philadelphia, 1996.

Davies D.R., E.A.Padlan − "Antibody-antigen complexes", *Annu. Rev. Biochem.,* 59 (1990) 439−473.

Delamarche E., H.A.Biebuyck, H.Schmid, B.Michel − "Stability of molded polydimethyl-siloxane microstructures" *Adv. Mater.,* 9 (1997) 741−746.

Dembo M., D.C.Torney, K.Saxman, D.Hammer − „The reaction-limited kinetics of membrane-to-surface adhesion and detachment", *Proc. Royal Soc. London Biol. Sci.,* 234 (1988) 55−83.

Drury J.L., M.Dembo − "Hydrodynamics of micropipette aspiration", *Biophys. J.,* 76 (1999) 110−128.

Dubowchik G.M., M.A.Walker − "Receptor−mediated and enzyme−dependent targeting of cytotoxic anticancer drugs", *Pharm. & Therap.,* 83 (1999) 67−123.

Evans E., K.Ritchie − "Dynamic strength of molecular adhesion bonds", *Biophys. J.,* 72 (1997) 1541−1555.

Evans E. − "Energy landscape of biomolecular adhesion and receptor anchoring at interfaces explored with dynamic force spectroscopy", *Faraday Discuss.,* 111 (1998) 1−16.

Evans E. − "Looking inside molecular bonds at biological interfaces with dynamic force spectroscopy", *Biophysical Chemistry* 82 (1999) 83−97.

Evans E. − "Probing the relation between force−lifetime−and chemistry in single molecular bonds", *Annu. Rev. Biophys. Biomol. Struct.,* 30 (2001) 105−128.

Evans E., A.Leung, D.Hammer, S.Simon − "Chemically distinct transition states govern rapid dissociation of single L-selectin bonds under force", *Proc. Natl. Acad. Sci.,* 98 (2001) 3784−3789.

Farina K.L., J.B.Wyckoff, J.Rivera, H.Lee, J.E.Segall, J.S.Condeelis, J.G.Jones − "Cell motility of tumor cells visualized in living intact primary tumors using green fluorescent protein", *Cancer Res.*, 58 (1998) 2528−2532.

Florin E.L., V.T.Moy, H.E.Gaub − "Adhesion forces between individual ligand-receptor pairs", *Science*, 264 (1994) 415−417.

Fouquet B., R.Zimbelmann, W.W.Franke − "Identification of plakoglobin in oocytes and early embryos of Xenopus laevis: maternal expression of a gene encoding a junctional plaque protein", *Differentiation*, 51 (1992) 187−194.

Fritz J., A.G.Katopodis, F.Kolbinger, D.Anselmetti − "Force-mediated kinetics of single P-selectin/ligand complexes observed by atomic force microscopy", *Proc. Natl. Acad. Sci. USA,* 95 (1998) 12283−12288.

Fukuda F. − "Possible roles of tumor−associated carbohydrate antigens", *Cancer Res.,* 56 (1996) 2237−2244.

Geiger B., A.Bershadsky, R.Pankov, K.M.Yamada − "Transmembrane extracellular matrix-cytoskeleton crosstalk" *Nature Rev. Mol. Cell Biol.*, 2 (2001) 793−805.

Girdhar G., J.Y.Shao − "Membrane tether extraction from human umbilical vein endothelial cells and its implication in leukocyte rolling", *Biophys. J.,* 87 (2004) 3561−3568.

Giroldi L.A., P.P.Bringuier, T.Shimazui, K.Jansen, J.A.Schalken − "Changes in cadherin−catenin complexes in the progression of human bladder carcinoma", *Int. J. Cancer*, 82 (1999) 70−76.

Gittes F., Ch.Schmidt − "Thermal noise limitations on micromechanical experiments", *Eur. Biophys. J.,* 27 (1998) 75−81.

Goffin J.M., P.Pittet, G.Csucs, J.W.Lussi, J.J.Meister, B.Hinz – "Focal adhesion size controls tension–dependent recruitment of α-smooth muscle actin to stress fibers", *J. Cell. Biol.,* 172 (2006) 259–268.

Goldmann W.H., R.M.Ezzel – "Viscoelasticity in wild-type and vinculin deficient (5.51) mouse F9 embryonic carcinoma cells examined by atomic force microscopy and rheology", *Exp. Cell Res.*, 226 (1996) 234–237.

Goochee C.F., M.J.Gramer, D.C.Andersen, J.B.Bahr, J.R.Rasmussen − "The oligosaccharides of glycoproteins: bioprocess factors affecting oligosaccharide structure and their effect on glycoprotein properties", *Biotechnology,* 9 (1991) 1347–1355.

Gorelik E., U.Galili, A.Raz − "On the role of cell surface carbohydrates and their binding proteins (lectins) in tumor metastasis", *Cancer Metas. Rev.,* 20 (2001) 245−277.

Grandbois M., W.Dettmann, M.Benoit, H.E.Gaub – "Affinity imaging of red blood cells using an atomic force microscope", *J. Histochem. Cytochem*., 48 (2000) 719–724.

Green Ch.P., H.Lioe, P.Mulvaney, J.E.Sader − "Normal and torsional spring constants of atomic force microscope cantilevers", *Rev. Sci. Instrum.,* 75 (2004) 1988−1996.

Grubmüller H., B.Heymann, P.Tavan – "Ligand binding: Molecular mechanics calculations of the streptavidin-biotin rupture force", *Science*, 271 (1996) 997–999.

Gryboś J. – "Badanie sił molekularnych w układach biologicznych z użyciem mikroskopii sił atomowych ", PhD thesis, IFJ PAN, 2005.

Gryboś J., G.Pyka–Fościak, K.Lebed, M.Lekka, J.Lekki, Z.Stachura, J.Styczeń –"Study of adhesion interaction using scanning force microscopy", *Acta Physica Polonica A*, 105 (2004) 501– 510

Guck J., S.Schinkinger, B.Lincoln, F.Wottawah, S.Ebert, M.Romeyke, D.lenz, H.M.Erickson, R.Ananthakrishnan, D.Mitchell, J.Käs, S.Ulvick, C.Bilby – "Optical deformability as an inherent cell marker for testing malignant transformation and metastatic competence", *Biophys. J.,* 88 (2005) 3689–3689.

Hamelryck T.W., M.H.Dao–Thi, F. Poortmans, M.J. Chrispeelsi, L.Wyns, R.Loris – "The crystallographic structure of phytohemagglutinin-L". *J. Biol. Chem.,* 271 (1996) 20479–20485.

Han T., J.M.Williams, T.P.Beebe − "Chemical bonds studied with functionalized atomic force microscopy tips", *Anal. Chim. Acta,* 307 (1995) 365−376.

Hanahan D., R.A.Weinberg – „The hallmarks of cancer", *Cell*, 100 (2000) 57–70.

Hänggi P., P.Talkner, M.Borkovec – "Reaction-rate theory: fifty years after Kramers", *Rev. Mod. Phys.,* 62 (1990) 251–341.

Hazan R.B., G.R.Philips, R.F.Qiao, L.Norton, S.A.Aaronson – "Exogenous expression of N-cadherins in breast cancer cells indices cell migration, invasion, and metastasis", *J. Cell Biol.,* 148 (2000) 779–790.

Helm C.A, W.Knoll, J.N.Israelachvili − "Measurements of ligand-receptor interactions", *Proc. Natl. Acad. Sci. USA,* 88 (1991) 8169−8173.

Hinterdorfer P., W.Baumgartner, H.J.Gruber, K.Schilcher, H.Schindler – "Detection and localization of individual antibody-antigen recognition events by atomic force microscopy", *Proc. Natl. Acad. Sci. USA,* 93 (1996) 3477–3481.

Hinterdorfer P., Y. Dufrene − "Detection and localization of single molecular recognition events using atomic force microscopy", *Nature*, 3 (2006) 347−355.

Hochmuth R.M. – "Micropipette aspiration of living cells", *J.Biomech.*, 33 (2000) 15–22.

Hochmuth R.M., W.D.Marcus − "Membrane tethers formed from blood cells with available area and determination of their adhesion energy ", *Biophys. J.*, 82 (2002) 2964−2969.

Homola J. – "Present and future of surface plasmon resonance biosensors", *Anal. Bioanal. Chem.* 377 (2003) 528–539.

Horwitz A.F. – "Integrins and health", *Sci. Am.,* 276 (1997) 86-75.

Hosu B.G., M.Sun, F.Marga, M.Grandbois, G.Forgacs − "Eukaryotic membrane tethers revisited using magnetic tweezers", *Phys. Biol.,* 4 (2007) 67−78.

Hsu S., L. Raine − "Discovery of a high affinity of *Phaseolus vulgaris* agglutinin (PHA) with gastrin-secreting cells", *Am. J. Clin. Pathol.,* 77 (1982) 396−400.

Hummer G., A.Szabo – "Free energy reconstruction from non-equilibrium single-molecule pulling experiments", *Proc. Natl. Acad. Sci. USA*, 98 (2001) 3658–3661.

Ikai A. – "Nano-mechanics of proteins with possible applications", *Superlattices and Microstructures,* 31 (2002) 43−62.

Ikai A, R.Afrin − "Toward mechanical manipulations of cell membranes and membrane proteins using an atomic force microscope", *Cell Biochem. Biophys.,* 39 (2003) 257−277.

Ikai A. − "Nanomechanics of protein-based biostructures", *Jpn. J. Appl. Phys.,* 1 (2004) 7365−7375.

Israelaschivili J.N. – *"Intermolecular and surface forces"*, Academic Press, San Diego, 1992.

Izrailev S., S.Stepaniants, M.Balsera, Y.Oono, K.Schulten – "Molecular dynamics study of unbinding of the avidin-biotin complex", *Biophys. J.,* 72 (1997) 1568−1581.

Janoviak H., J.Struckmeier, D.J.Muller – "Hydrodynamic effects in fats AFM single-molecule force measurements", *Eur. Biophys. J.,* 34 (2005) 91–96.

Jaschke M., H.J.Butt – "Height calibration of optical lever atomic force microscopes by simple laser interferometry", *Rev. Sci. Instrum.* 66 (1995) 1258–1259.

Jelesarov I., H.R.Bosshard − "Isothermal titration calorimetry and differential scanning calorimetry as complementary tools to investigate the energetics of biomolecular recognition", *J. Mol. Recognit.,* 12 (1999) 3−18.

Johnson C.P., H.Y.Tang, C.Carag, D.W.Speicher, D.E.Disher − "Forced unfolding of proteins within cells", *Science,* 317 (2007) 663−666.

Kannagi R., M.Izawa, T.Koike, K.Miyazaki, N.Kimura – „Carbohydrate-mediated cell adhesion in cancer metastasis and angiogenesis", *Cancer Sci.*, 95 (2004) 377−384.

Kellermayer M.S. – "Visualizing and manipulating individual protein molecules", *Physiol. Meas.,* 26 (2005) R119–R153.

Kienberger F., G.Kada, H.Mueller, P.Hinterdorfer − "Single molecule studies of antibody−antigen interaction strength versus intra-molecular antigen stability", *J. Mol. Biol.*, 347 (2005) 597−606.

Koleske D.D., G.U.Lee, B.I.Gans, K.P.Lee, D.P.DiLella, K.J.Wahl, W.R.Barger, L.J.Whitman, R.J.Colton − "Design and calibration of a scanning force microscope for friction, adhesion, and contact potential studies", *Rev. Sci. Instrum.,* 66 (1995) 4566−4574.

Kramers H.A. – "Brownian motion in a field of force and the diffusion model of chemical reactions", *Physica* VII(4) (1940) 284–304.

Kundu T., J.P.Lee, C.Blasé, J.Bereiter-Hahn – "Acoustic microscope lens modeling and its application in determining biological cell properties from single- and multi-layered cell models", *J. Acoust. Soc. Am.,* 120 (2006) 1646–1654.

Laidler P., J.Dulińska, M.Lekka, J.Lekki – "Expression of prostate specific membrane antigen in androgen–independent prostate cancer cell line PC–3", *Arch. Biochem. Biophys.,* 435(1) (2005) 1–14.

Laidler P., D.Gil, A.Pituch-Noworolska, D.Ciołczyk, D.Książek, M.Przybyło, A.Lityńska − "Expression of $\beta_1$−integrins and N−cadherin in bladder and melanoma cell lines", *Acta Biochim. Pol.*, 47 (2000) 1159−1170.

Landau L.D., E.M.Lifshtz − *"Fluid Mecchanics"*, Pergamon Press, Oxford, 1987.

Lebed K., A.J. Kulik, L.Forro, M.Lekka – "Lectin–carbohydrate affinity measured using quartz crystal microbalance", *J. Coll. Interface Sci.*, 299 (2006) 41−48.

Lebed K., A.Dąbrowska, G.Sharma, J.Lekki, Z.Stachura, M.Lekka – "Force spectroscopy of mannose-binding to patterned concanavalin A and lentil lectin"– *Proccedings of the VIII Linz Winter Workshop*

*„Advances in Single Molecule Research for Biology and Nanoscience”*, eds. P.Hinterdorfer, G.Schutz, P.Pohl, 2006, Linz, ISBN 3-85499-163-0, pages: 84–86.

Leckband D.E., T.L.Kuhl, H.K.Wang, W.Mueller, J.Herron, H.Ringsdorf − “Force probe measurements of antibody-antigen interactions”, *Methods,* 20 (2000) 329−340.

Leckband D.E., J.Israelachvili – “Intermolecular forces in biology“, *Quar. Rev. Biophys.,* 34 (2001) 105−267.

Leckband D.E., A.Prakasam − „Mechanism and Dynamics of Cadherin Adhesion”, *Annu. Rev. Biomed.Eng.*, 8 (2006) 259−287.

Lekenkari P.P, M.A.Horton − “Single integrin molecule adhesion forces in intact cells measured by atomic force microscopy”, *Biochem. Biophys. Res. Comm.,* 259 (1999) 645−650.

Lekka M. – “Biologiczne zastosowania skaningowego mikroskopu sił.“, PhD thesis, IFJ PAN, 1998.

Lekka M., J.Gryboś, J.Lekki, Z.Stachura, J.Styczeń – “Single–bond force measured by means of SFM”, *Acta Physica Polonica A* 102 (2002) 403–412.

Lekka M., P.Laidler, D.Gil, J.Lekki, Z.Stachura, A.Z.Hrynkiewicz – “Elasticity of normal and cancerous human bladder cells studied by scanning force microscopy”, *Eur. Biophys. J.,* 28 (4), 1999a, 312-316.

Lekka M., J.Lekki, M.Marszałek, P.Golonka, Z.Stachura, B.Cleff, A.Z.Hrynkiewicz – “Local elastic properties of cells studied by SFM”, *Appl. Surf. Sci.,* 141 (3-4), 1999b 345–349.

Lekka M., P.Laidler, J.Ignacak, M.Łabędź, J.Lekki, H.Struszczyk, Z.Stachura, and A.Z.Hrynkiewicz – “The effect of chitosan on stiffness and glycolytic activity of human bladder cells”, *Biochim. Biophys. Acta (Molecular Cell Research),* 1540 (2) (2001) 127–136.

Lekka M., P.Laidler, J.Dulińska, M.Łabędź, G.Pyka – “Probing molecular interaction between concanavalin A and mannose ligands by means of SFM”, *Eur. Biophys. J.,* 33(7) (2004) 664–650.

Lekka M., A.J.Kulik, S.Jeney, J.Raczkowska, J.Lekki, A.Budkowski, L.Forro – “Friction force microscopy as an alternative tool for probing molecular interactions“, *J. Chem. Phys.,* 123(1) (2005) 014702:1-7.

Lekka M., P.Laidler, M.Łabędź, A.J.Kulik, J.Lekki, W.Zając, Z.Stachura – “Specific detection of glycans on a plasma membrane of living cells using atomic force microscopy” – *Chemistry & Biology,* 13 (5) (2006) 505–512.

Lekka M., “Quantitative description of cancer alterations of single living cells by AFM” – *Proceedings of the International Conference on Emerging Mechanical Technology “Macro to Nano”*, eds. R.K.Mittal, N.N.Scharma, 2007, India, ISBN 81-904262-8-1, pages 4–9.

Li F., S.D.Redick, H.P.Ericksom, V.T.Moy − “Force measurements of the $\alpha_5\beta_2$ integrin-fibronectin interaction”, *Biophys. J.,* 84 (2003) 1252−1262.

Lindblom A., A.Liljegren − “Tumour markers in malignancies”, *BMJ,* 320 (2000) 424−427.

Lipowsky R., E.Sackmann (eds) − “Structure and dynamics of membranes”, (1995) Elsevier, Amsterdam.

Lityńska A., Przybyło M., Książek D., Laidler P., − ”Differences of $\alpha_3\beta_1$ integrin glycans from different human bladder cell lines”, *Acta Biochimica Polonica,* 47 (2000) 427−434.

Lodish H., A.Berk, P.Matsudaira, C.A.Kaiser, M.Krieger, M.P.Scott, S.L.Zipursky, J.Darnell (eds) – “Molecular Cell Biology”, 5th ed, (2004) WH Freeman and Company, New York.

Mareel M., A.Leroy − “Clinical, Cellular, and Molecular Aspects of Cancer Invasion”, *Physiol. Rev.,* 83 (2003) 337−376.

Marquez M., S.Nilson, L.Lennartsson, Z.Liu, T.Tammela., M.Rai Tanen, A.R.Holmberg − “Charge−dependent targeting results in six tumor cell lines”, *Anticancer Res.,* 24 (2004) 1347−1351.

McKenzie G., W.Sawyer, L.Nicol – “The molecular weight and stability of Concanavalin A“, *Biochim. Biophys. Acta*, 263 (1972) 283–293.

Mechref Y., M.V.Novotny – “Structural investigations of glycoconjugates at high sensitivity“, *Chem. Rev.,* 102 (2002) 321–369

Merkel R., P.Nassoy, A.Leung, K.Ritchie, E.Evans – "Energy landscapes of receptor-ligand bonds explored with dynamic force spectroscopy", *Nature,* 397 (1999) 50–53.

Nelson D.L., M.M.Cox − "*Lehringer principles of biochemistry*", Worth Publishers, New York third edition, (2003).

Neuert G., C.Albrecht, E.Pamir, H.E.Gaub − "Dynamic force spectroscopy of the digoxigenin−antibody complex", *FEBS Lett.,* 580 (2006) 505−509.

Neumaister J..M., W.A.Ducker – "Lateral, normal, and longitudal spring constants of atomic force microscopy cantilevers", *Rev. Sci. Instrum.*, 65 (1994) 2527−2531.

Nishizaka T., R.Seo, H.Tadakuma, K.Kinosita, S.Ishiwata − "Characterization of single actomyosin rigor bonds: load dependence of lifetime and mechanical properties", *Biophys. J.,*79 (2000) 962−974.

Nollet F., G.Berx, F.vanRoy – "The role of the E-cadherin/catenin adhesion complex in the development and progression of cancer", *Mol. Cell Biol. Res. Comm.,* 2 (1999) 77−85.

Oesterhelt, F., D.Oesterhelt, M.Pfeiffer, A.Engel, H.E.Gaub, D.J.Muller − "Unfolding pathways of individual bacteriorhodopsins", *Science*, 288 (2000) 143–146.

Orsello C.E., D.A.Lauffenburger, D.A.Hammer − "Molecular properties in cell adhesion: a physical and engineering perspective", *Trends Biotechnol.,* 19 (2001) 310−316.

Ørntoft T.F., H.Wolf , − "Molecular alternation in bladder cancer", *Urol. Res.* 26 (1998) 223−233.

Pashley R.M., − "Hydration forces between mica surfaces in aqueous electrolyte solutions", *J.Coll. Interface Sci.,* 80 (1981) 153−162.

Park S., D.Koch, R.Cardenas, J.Käs, C.K.Shih – "Cell Motility and Local Viscoelasticity of Fibroblasts", *Biophys. J.,* 89 (2005) 4330–4342.

PDB – Protein Data Bank; www.pdb.org (entry ***1FAT***).

Pereira R. − "Atomic force microscopy as a novel pharmacological tool", *Biochem. Pharm.,* 62 (2001) 975−983.

Pierres A., A.M.Benoliel, P.Bongrand, P.A. van der Merwe – "Determination of the lifetime and force dependence of interactions of single bonds between surface–attached CD2 and CD48 adhesion molecules", *Proc. Natl. Acad. Sci.*, 93 (1996) 15114–15118.

Plow E.F., T.A.Haas, L.Zhang, J.Loftus, J.W.Smith − "Ligand binding to integrins", *J. Biol. Chem.*, 275 (2000) 21785−21788.

Przybyło M., D.Hoja-Łukowicz, A.Lityńska, P.Laidler – "Different glycosylation of cadherins from human bladder non-malignant and cancer cell lines", *Can. Cell Int.,* 2 (2002) 6−10.

Przybyło M., A.Lityńska, E.Pocheć − "Different adhesion and migration properties of human HCV29 non-malignant urothelial and T24 bladder cancer cells: role of glycosylation", *Biochimie,* 87 (2005) 133−142.

Puntheeranurak T., L.Wildling, H.J.Grüber, R.K.H.Kinne, P.Hinterdorfer − "Ligands on the string: single-molecule AFM studies on the interaction of antibodies and substrates with the $Na^+$-glucose co-transporter SGLT1 in living cells", *J. Cell Sci.* 119 (2006) 2960−2967.

Ramburan A., D.Govender – "Cadherins and catenins in pathology", *Curr. Diagn. Pathol.,* 8 (2002) 305−317.

Radmacher M.– "Measuring the elastic properties of biological samples with the atomic force microscope", *IEEE Med. Eng. Biol.,* 16 (1997) 47–57.

Reiss K., T.Maretzky, A.Ludwig, T.Tousseyn, B.deStrooper, D.Hartmann, P.Saftig – "ADAM10 cleavage of N-cadherin and regulation of cell-cell adhesion and β-catenin nuclear signaling", *EMBO J.,* 24 (2005) 742−752.

Sader J.E., I.Larson, P.Mulvaney, L.R.White – "Method for the calibration of atomic force microscope cantilevers", *Rev. Sci. Instrum.* 66 (1995) 3789–3798.

Seifert U. − "Rupture of multiple parallel bonds under dynamic loading", *Phys. Rev. Lett.,* 84 (2000) 2750−2754.

Sharon N., H.Lis – "History of lectins: from hemagglutinins to biological recognition molecules", *Glycobiology,* 14 (2004), 53R–62R.

Shariat S.F., K.Matsumoto, R.Casella, W.Jian, S.P.Lerner – "Urinary levels of soluble E-cadherin in the detection of transitional cel carcinoma of the urinary bladder", *Eur. Urology,,* 48 (2005) 69−76.

Shibuya N., I.J.Goldstein, W.F.Broekkaert, M.Nsimba-Lubaki, B.Peeters, W.J.Peumans – "The elderberry (*Sambucus nigra L.*) bark lectin recognizes the Neu5Ac(α2–6)Gal/GalNAc sequence", *J. |Biol. Chem..,* 262 (1987) 1596–1601.

Simon A., M.C.Durrieu − "Strategies and results of atomic force microscopy in the study of cellular adhesion", *Micron*, 37 (2006) 1−13.

Sleep J., D.Wilson, R.Simmons, W.Gratzer – "Elasticity of the red cell membrane and its relation to hemolytic disorders: and optical tweezers study", *Biophys. J.,* 77 (1999) 3085–3095.

Smith S.B., L.Finzi, C.Bustamante – "Direct mechanical measurements of the elasticity of single DNA molecules by using magnetic beads", *Science*, 258 (1992) 1122–1126.

Sneddon I.N. − "The relation between load and penetration in the axisymmetric Boussinesq problem for a punch of arbitrary profile", *Int. J. Engng. Sci.,* 3 (1965) 47−57.

Sokolov I. – "Atomic force microscopy in cancer cell research" in *Cancer Nanotechnology,* H.S.Nalwa, T.Webster (eds.), American Scientific Publishers, 2007, New York, ISBN: 1-58883-071-3, *pages*: 1–17.

Staveley – Staveley Sensors; www.staveleyndt.com or www.olympusndt.com.

Stroh C., H.Wang, R.Bash, B.Ashcroft, J.Nelson, H.Grüber, D.Lohr, S.M.Lindsay, P.Hinterdorfer − "Single-molecule recognition imaging microscopy", *Proc. Natl. Acad. Sci.,* 101 (2004) 12503−12507.

Strunz T., K.Oroszlan, R.Schaefer, H.J.Gunterodt − "Dynamic force spectroscopy of single DNA molecules", *Proc. Natl. Acad. Sci. USA*, 96 (1999) 11277−11282.

Sulchek T.A, R.W.Friddle, K.Langry, E.Y.Lau, H.Albrecht, T.V.Ratto, S.J.DeNardo, M.E.Colvin, A.Noy −"Dynamic force spectroscopy od parallel individual mucin1−antibody bonds", *Proc. Natl. Acad. Sci. USA*, 102 (2005) 16638−16643.

Sun M., J.S.Graham, B.Hegedüs, F.Marga, Y.Zhang, G.Forgacs, M.Grandbois − "Multiple membrane tethers probed by atomic force microscopy", *Biophys. J*, 89 (2005) 1–10.

Sung S., C.Hsieh, D.Wu, L.Chung, P.Johnstone – „Tumor microenvironment promotes cancer progression, metastasis and therapeutic resistance", *Curr. Probl. Cancer*, 31 (2007) 36–100.

Taubenberger A., D.A.Cisneros, J.Friedrichs, P.H.Puech, D.J.Muller, C.M.Franz − "Revealing early steps of $\alpha_2\beta_1$ integrin-mediated adhesion to collagen type I by using single-cell force spectroscopy ", *Mol. Cell Biol.,* 18 (2007) 1634−1644.

Tees D.F., R.E.Waugh, D.A.Hammer – "A microcantilever device to assess the effect of force on the lifetime of selectin-carbohydrate bonds", *Biophys. J.,* 80 (2001) 668–682.

Tees D.F., K.C.Chang, S.D.Rodgers, D.A.Hammer − "Simulation of cell adhesion to bioreactive surfaces in shear: the effect of cell size", *Ind. Eng. Chem. Res.,* 41 (2002) 486−493.

Tsukasaki Y., K.Kitamura, K.Shimizu, A.H.Iwane, Y.Takai, T.Yanagida − "Role of multiple bonds between the single cell adhesion molecules, nectin and cadherin, revealed by high sensitive force measurements", *J. Mol. Biol.,* 367 (2007) 996−1006.

Weisel J.W., H.Shumanz, R.I.Litvinov – "Protein-protein unbinding induced by force: single-molecule studies", *Curr. Opin. Struct. Biol.,* 13 (2003) 227–235.

Weisenhorn A.L., M.Khorsandi, S.Kasas, V.Gotzos, H.J.Butt – "Deformation and height anomaly of soft surfaces studied with an AFM", *Nanotechnology,* 4 (1993)106–113.

Williams P.M. – "Analytical descriptions of dynamic force spectroscopy: behavior of multiple connections", *Anal. Chim. Acta,* 479 (2003) 107–115.

Wojciechowicz D.C., P.Y.Park, R.V.Datta, P.B.Paty, − "CEA is the major PHA-L-reactive glycoprotein in colon carcinoma cell lines and tumors: relationship between K-ras activation and beta1-6 branching of N-linked carbohydrate on CEA", *Biochem. Biophys. Res. Commun.* 273 (2000) 147–153.

Wojcikiewicz E.P., X.Zhang, V.T.Moy – "Force and compliance measurements on living cells using atomic force microscopy (AFM)", *Biol. Proced. Online*, 6 (2004) 1–9.

Varki A. − "Selectin ligands", *Proc.Natl. Acad. Sci.,* 91 (1994) 7390−7397.

Veeco – Veeco GmbH; www.veeco.com

Yamazaki D., S.Kurisu, T.Takenawa − "regulation of cancer motility through actin reorganization", *Cancer Sci.,* 96 (2007) 379−386.

Yersin A., H.Hirling, S. Kasas, C.Roduit, K.Kulangara, G.Dietler, F.Lafont, S.Catsicas, P.Steiner − "Elastic properties of the cell surface and trafficking of single AMPA receptors in living hippocampal neurons", *Biophys. J.,* 92 (2007) 4482−4489.

Zahalak G.I., S.P.Ma – "Muscle activation and contaction: constitutive relations based directly on cross-bridge kinetics" *J. Biomech. Eng.*, 112 (1999) 52–62.

Zhang X., S.E.Craig, H.Kirby, M.J.Humphries, V.T.Moy − "Molecular basis for the dynamic strength of the integrin $\alpha_4\beta_1$/VCAM-1 interaction", *Biophys. J.,* 87 (2004) 3470−3478.

Zhang X., D.F.Bogorin, V.T.Moy – "Molecular basis of the dynamic strength of the sialyl Lewis X – selectin interaction", – *ChemPhysChem*, 5 (2004) 175–182.

Zlatanova J., K.vanHolde − "Single-molecule biology: what is it and how does it work?", *Mol. Cell,* 24 (2006) 317−2329.

# FIGURE CAPTIONS

Figure 1.1. Illustration of an integrin (i.e. a cell surface adhesion receptor) anchorage in cell membrane and its linkage with actin filaments

Figure 1.2. Binding between proteins. The complementary shape of the binding sites (a) together with the non-covalent interactions results in a strong adhesion. Lack of complementarity (b) leads to a less stable complex [adapted from *(Lodish et al. 2004)*].

Figure 1.3. Surface topography (left) and friction force (right) images recorded at the same lateral loading rate of $1.4 \times 10^9$ pN/s, measured for (a) ConA−CaY and (b) ConA−BSA molecular complex measured in a buffer solution *(Lekka et al. 2005)*. Lack of contrast in friction force images, observed for ConA−BSA, confirms the specificity of the ConA−CaY interaction (a).

Figure 1.4. The distributions of sialic acids residues on the surface of (a) non-malignant HCV29 and (b) malignant T24 bladder cells. The central part of a cell (~20 μm diameter) was probed, each spot has the same size of ~1 μm. Black color denotes no adhesion events.

Figure 1.5. The correlation between the decrease of Young's modulus with the increase of malignancy of melanoma cells *(Lekka et al. 2007)*

Figure 2.1. Fluid mosaic model of a plasma membrane (Image was adopted from *Nelson et al. 2005*).

Figure 3.1. Scheme of an energy landscape of the unbinding process of two interacting molecules as a function of the reaction coordinate $x$. For the molecule composed of only two atoms the reaction coordinate is the distance between these two interacting atoms.

Figure 3.2. Thermal length-scale ($L_{th}$) as a function of a protein mass with marked three examples of proteins (stars): albumin from bovine serum (BSA), concanavalin A (ConA), and fibronectin (FN).

Figure 3.3. Schematic representation of an energy landscape of two interacting molecules (i.e. ligand-receptor complex, black line). The applied external force $F$ (as it is in the case of measurements by means of atomic force microscopy) lowers the height of the energy barrier, resulting in easier bond disruption (dashed line). The transition state is characterized by a barrier height $E_b$ and its distance from the bound state $x_b$ (termed also *an energy barrier position*).

Figure 3.4. Probability distributions as a function of an unbinding force calculated for different loading rates (from 100 pN/s to $10^6$ pN/s).

Figure 3.5.a) The dependence of the most probable unbinding force on the logarithm of the loading rate measured for the interaction between the albumin (BSA) and its antibody (aBSA) *(Grybos 2005)*. b) The single line corresponds to the energy landscape with only one energy barrier characterized by two parameters: its height $E_b$ and position $x_b$.

Figure 3.6. a) The force versus loading rate dependence measured for BSA−EDTA complex showing two segments of linear dependencies *(Gryboś et al. 2004)*. b) The corresponding energy landscape possessing two energy barriers (outer and inner ones), each represented as a line in Figure 3.6 a).

Figure 3.7. Schematic representation of the consecutive unbinding of $N$-bonds – the "zipper-like" model.

Figure 3.8. Factor $G$ (Equation (3.26)) as a function of the number of simultaneously broken bonds calculated for $x_b = 1$ nm and $x_b = 0.1$ nm in the "zipper-like" model ($k_BT = 4.1$ pN·nm)

Figure 3.9. Scheme of the simultaneous rupture of cooperative $N$-bonds – the "parallel–like" model.

Figure 4.1. Basic elements of an atomic force microscope (AFM).

Figure 4.2. Silicon nitride cantilevers: a) three types of cantilevers (C, D, and E) with the corresponding spring constants of 0.01 N/m, 0.03 N/m and 0.1 N/m. b) The image of the four-sided pyramidal AFM tip with the radius of curvature of 50 nm.

Figure 4.3. An ideal *force curve* between the end of the AFM tip and the hard surface. Arrows indicate direction of movement of the AFM cantilever *(*adapted from *Lekka 1998)*

Figure 4.4. An ideal *force curve* characteristic for the interaction between a single pair of ligand and receptor molecules. Similarly as in Figure 4.3, red line denotes approach and the black one – retract.

Figure 4.5. Multiple bonds unbinding showing cooperative (a) and independent (b) adhesion.

Figure 4.6. The tip–sample distance in AFM. $D$ is the actual tip-sample distance, $Z$ is the distance between the sample and the cantilever "rest" position. The difference between them takes into account the cantilever deflection $d_C$ and depth of the sample deformation $d_S$.

Figure 4.7. a) & c) Cantilever fluctuations around the base line measured in PBS buffer for two randomly chosen cantilevers, both with the nominal spring constant value of 0.01 N/m, functionalized with the antibody against prostate specific membrane antigen. b) & d) The corresponding histograms of the cantilever fluctuations. FWHM defines the range of fluctuations.

Figure 4.8. a) Schematic representation of the method proposed by Jaschke and Butt applied for the piezoelectric scanner calibration at each location (black dots) on a mirror surface. b) Reflected beam intensity as a function of the voltage applied to the scanner recorded in both direction of scanner movement: to and from the mirror and the distance ($\Delta s$) is between two subsequent interference maxima.

Figure 4.9. Dependence of the scanner nonlinearity coefficients on a relative position of the sample surface with respect to the scanner centre (EBL#2 from Staveley Sensors (see Appendix 2). a) & c) scan size of 2.5 μm. b) & d) 30 μm.

Figure 4.10. Typical force curve recorded on a glass surface with the cantilever $k = 0.01$ N/m (only approach part is shown). The *PSDcal* coefficient was determined as a slope of the fitted line (range marked by arrows).

Figure 4.11. The distribution of the *PSDcal* coefficients determined for the three different cantilever types. Cantilevers of type C, D, E were used for the measurements presented in this monograph. $N_T$ is the total number of cantilevers analyzed.

Figure 4.12. Resonant frequency measured for the thermally excited cantilever. The obtained resonant frequency is 5.8 kHz what corresponds to the calculated cantilever spring constant of 0.007 N/m

Figure 4.13 Relation between the scanner elongation and time (scanner type EBL#2). Arrows indicate the temporary speed

Figure 4.14. Force histograms before (a) and after (b) the determination of the exact value of the retraction velocity. The same set of data is shown on both histograms.

Figure 4.15. Two ways of the AFM probe surface modification: a) direct method where the desired ligand is attached through crosslinking agents as glutaraldehyde (GL), and b) indirect one where ligands are attached through a polymeric spacer.

Figure 4.16 a) HCV29 cells on glass coverslip prepared for AFM measurement. b) The Young's modulus value of WM35 melanoma cells determined for cells growing on a glass and poly-L-lysine coated surfaces in culture

Figure 4.17 a) The idea of the inhibition of binding sites on cell surface. b) The distributions of the unbinding events before (black columns) and after (grey columns) the inhibition of the interaction between the prostate specific membrane antigen (PSMA) and its monoclonal antibody (anti-PSMA).

Figure 5.1. The retraction part of the force curve with no unbinding event.

Figure 5.2. The retraction part of the force curve showing the non-specific adhesion.

Figure 5.3a&b. Retraction curves recorded during the separation of the functionalized AFM tip from the cell membrane. Two distinct shapes of the unbinding events can be observed.

Figure 5.5. The retraction part of the force curves recorded on a surface of living HCV29 bladder cells probed with cantilever functionalized with monoclonal antibody against N-cadherin. Curves demonstrate the single unbinding events occurring between N-cadherin and its monoclonal antibody.

Figure 5.6. Example of the force curve recorded for the interaction occurring between the antigen−antibody complex.

Figure 5.7. The pull-off (a) and single−bond (b) forces as a function of $CaCl_2$ concentration measured between the bare silicon nitride cantilever and two surfaces: the mica and the glass covered by poly-L-lysine. Grey lines denote the average values (185 ± 33 pN and 35 ± 8 pN, respectively).

Figure 5.8. Force histograms showing a) only one peak attributed to the specific interaction between mannose-type glycans present on the surface of prostate (PC-3) cells probed with AFM tip functionalized with lectin ConA, b) multiple peaks observed in the interaction occurring between the same glycan type present on the surface of melanoma cells (WM35) probed with ConA. The solid line is a Gaussian fit used for determination of the unbinding force.

Figure 5.9. The probability distribution *p(F)* of the unbinding force obtained for the interaction between concanavalin A and carbohydrate moiety of carboxypeptidase Y. Measurement were performed in Tris-buffered saline (supplemented with Ca and Mg ions that are crucial for lectin recognition). The solid line is the theoretical fit of the Equation (5.2) to the experimental data.

Figure 5.10. Linear regression (a) fitted to the unbinding force as a function of the number of succeeding peaks observed in the histogram (b) obtained for melanoma WM35 cells probed with lectin ConA. Data points correspond to centers of Gaussians fitted to each single peak present in force histogram while error bars represent their standard deviations. The 95% confidence bands are marked as grey lines.

Figure 5.11 Example of the force curve recorded for the interaction occurring between antigen−antibody complex.

Figure 5.12. Histogram of the rupture length obtained for the interaction between albumin molecules and their antibody. The line denotes the Gauss function.

Figure 5.13. Three most common scenarios of the ligand–receptor unbinding that may occur for receptors present on a cell membrane: a) rupture of a single complex, b) simultaneous unbinding of two or more bonds of the same type, and c) unbinding events obtained for a given receptor embedded in cell membrane.

Figure 5.14. a) A model of two springs linked series: an AFM cantilever spring constant $k_{cant}$ and bond stiffness $k_{bond}$. b) For multiple bonds formed within the contact area, the effective spring constant can be modeled as system of springs linked in series and in parallel.

Figure 5.15. Example of the force curve recorded for the interaction occurring between antigen−antibody complex. $k_C$ is the cantilever spring constant; $k_{syst}$ is the system spring constant taking into account the cantilever spring constant and the bond stiffness.

Figure 5.16 Probability of the simultaneous rupture of *n* bonds obtained for a) N-cadherin−antibody complex in cancerous T24 and reference HCV29 cells, b) for the lectin concanavalin A (ConA*)* and glycans either attached to isolated protein (carboxypeptidase Y, CaY) or present in a plasma membrane of prostate cells (cell line: PC-3). The distributions were normalized to the total number of events *(Lekka et al. 2004)*.

Figure 6.1. Illustration of the cadherin – catenin complex in cell membrane

Figure 6.2. Typical force curves recorded for the interaction between GC4-Ncadh (a) and lectin-glycan (b) complexes measured in T24 cells.

Figure 6.3. Force histogram of the GC4–Ncadh interaction measured in a) reference HCV29 and b) cancerous T24 cells. The bin size was 7 pN corresponding to the force detection limit in the experiment (the solid line denotes the fitted Gaussian functions).

Figure 6.4. Unbinding force as a function of number of simultaneously ruptured bonds. Data points correspond to centers of Gaussians fitted to the corresponding peaks present in force histograms. The 95% confidence bands are marked as grey region.

Figure 6.6. The experimental data compared with two theoretical models describing the mechanism of the unbinding: “zipper-like” and “parallel-like” for GC4−Ncadh complex in a) HCV29 and b) T24 cells.

Figure 6.7. Force histograms obtained for the interaction between glycans composed of mannose, N-acetylglucosamine, and sialic acids and the corresponding lectin (ConA, PHA-L, and SNA), measured on a surface of reference HCV29 (a, c, e) and cancerous T24 (b, d, f) cells. The solid line is the Gaussian function; stars denote the most probably force for simultaneous unbinding of 1, 2, 3, and 4 bonds *(Lekka et al. 2006)*.

Figure 6.8. Linear regression fitted to the unbinding force as a function of the number of bonds simultaneously ruptured for HCV29 (grey dots) and T24 (black diamonds) cells, probed with two types of lectins: PHA-L (a), SNA(b). Data points correspond to centers of Gaussians fitted to each single maximum from Figure 6.7, while error bars represent their standard deviations *(Lekka et al. 2006)*.

Figure 6.9. The experimental data compared with two theoretical models describing the mechanism of the unbinding: “zipper-like” and “paralell−like” models for SNA-sialic acid complex in a) HCV29 and b) T24 cells.

Figure 6.10. Force histogram (same as in Figure 6.4) of the single GC4–Ncadh complexes measured in a) reference HCV29 and b) cancerous T24 cells. Peaks (*n* denotes the number of bonds simultaneously ruptured) were fitted with the probability density function given by the Equation (5.2).

Figure 6.11. The relation between the position of the energy barrier $x_b$ and the dissociation rate constant $k_0$ on the number of ruptured bonds obtained for GC4−Ncadh complex probed on the surface of HCV29 and T24 cells. The dash-dot lines denote the assumed linear dependence.

Figure 6.12. Force histograms obtained for the interaction between sialic acids glycans and lectin *Sambucus nigra* probed on a surface of reference HCV29 (a) and cancerous T24 (b) cells. The lines denote the probability distribution (Equation (5.2)). Peaks correspond to simultaneous rupture of 1, 2, 3, and 4 bonds.

Figure 6.13. The dependence of the energy barrier position (a) and the dissociation rate constant (b) on the number of ruptured bonds obtained for SNA−sialic acid complexes in reference HCV29 (blue) and cancerous T24 (red) cells.

Figure 6.14. a) The reconstructed intermolecular potentials of the single GC4–Ncadh complexes probed in non-malignant HCV29 cells. b) The energy landscape of GC4–Ncadh complex in malignant T24 cells. ($x_{b1}$, $x_{b2}$, $x_{b3}$, and $x_{b4}$ are the positions of the energy barriers)

Figure 6.15. Energy landscapes for the mannose type glycans probed by lectin ConA in HCV29 (blue curve) and T24 (red curve) cells.

Figure 6.16. The reconstructed intermolecular potentials of the interaction between sialic acids type glycans and lectin from *Sambucus nigra* (SNA) probed in non-malignant HCV29 (a) and malignant T24 (b) cells.

Figure 6.17. The bond lifetimes of single GC4–Ncadh complex for bladder cells.

Figure 6.18. The bond lifetimes of single SNA− sialic acid complex.

Figure 6.19. The comparison of kinetic profiles of the dissociation of the GC4–Ncadh complex probed on the surface of non-malignant HCV29 cells, plotted for 1 and 2 simultaneously ruptured complexes.

Figure 6.20. The kinetic profiles of a single ConA − mannose complex probed in HCV29 (blue line) and T24 (red line) cells.

Figure 6.21. The kinetic profiles for sialic acids-type glycans probed by SNA in both HCV29 (blue line) and T24 (red line) cells. The corresponding number of simultaneously ruptured single complexes was: (a) $n = 1$, (b) $n = 2$.

Figure 6.22. a) Bending of cell membrane at the anchoring point of a single N-cadherin molecule pulled off by the AFM probe. b) Simple model representing mechanical properties of the pulled cadherin−catenin complex.

Figure 6.23 Rupture length histograms of the GC4–Ncadh complex obtained for a) reference HCV29, and b) cancerous T24 cells. The bin size was ~ 3 nm equal to the distance between subsequent z-steps (only events from the first force peak were analyzed). To each peak the Gaussian function was fitted.

Figure 6.24. The stiffness of the GC4−Ncah complex in reference and cancerous cells.

Figure 6.24. a) Bending of the cell membrane realized by pulled the lectin−glycan complex. b) Simple mechanistic model of the pulled lectin−glycan complex anchored in a plasma membrane.

Figure 6.25 Rupture length histograms of ConA – mannose complex for (a) reference HCV29 (the total number of events $N$ = 100) and (b) cancerous T24 ($N$ = 30) cells, and of SNA – sialic acid complex for (c) reference HCV29 ($N$ = 100) and (d) cancerous T24 ($N$ = 51) cells. The bin size was ~ 3 nm equal to the distance between subsequent z-steps.

Figure 6.26. Frequency occurrence related to the probability of the unbinding of *n*-bonds for reference, non-malignant HCV29 and cancerous T24 cells.

Figure 6.27. Probability of the unbinding of n-bonds for reference non-malignant HCV29 (a) and cancerous T24 (b) cells probed in search of three glycan types composed of mannose, or N-acetylglucosamine, or sialic acids units.

Figure 1.1.app. The structure of α-helix (image was taken from *Biotutorials*)

Figure 1.2.app. The β-sheet structure (image was taken from *Biotutorials*).

Figure 3.1.app. The triangular AFM cantilever with marked triangular plate (I) and two prismatic beams (II).

Figure 4.1.app The distribution of the resonant frequencies measured for two types of cantilevers with nominal spring constants of 0.01 N/m and 0.03 N/m coming from the same wafer and used later on for the AFM measurements. $N_T$ is the number of measured cantilevers.

Figure 5.1.app Adhesion force versus loading force obtained for: i) typical antigen−antibody interaction on example of PAP-aPAP (wine squares) and ii) lectin (ConA) −carbohydrate recognition on prostate cells PC-3 (cyan dots).

Figure 7.1.app. The hydrodynamic drag forces acting on AFM cantilever during a) approach and b) retreat.

Figure 7.2.app. The idea of the AFM measurement of hydrodynamic force, $F_{drag}$.

Figure 7.3.app. Distributions of the hydrodynamic force measured in PBS buffer, at the cantilever velocity of 2.4 μm/s (b) and 7.7 μm/s (c).

Figure 8.1.app α and β anomers of glucose.

# TABLES

Table 4.1. Force detection limit of cantilevers typically used for various biological applications, estimated for the room temperature of 23°C.

Table 5.1. The unbinding probability determined for non-malignant HCV29 and malignant T24 bladder cells *(Lekka et al. 2006)*.

Table 6.1. The position of the peaks determined for a single lectin-glycan complexes: (i) ConA − mannose, (ii) PHA-L − *N*-acetylglucosamine, and (iii) SNA − sialic acid.

Table 6.2. The unbinding force of single pairs: (i) *N*-acetylglucosamine–PHA-L, (ii) mannose–ConA and (iii) sialic acid–SNA. Its value was determined in two approaches: (1) by linear regression where the force value and its error correspond to the slope and the standard deviation of the slope, and (2) from the first force peak present in force histograms where the error is a half width of the peak at the maximum and it denotes standard deviation *(Lekka et al. 2006)*.

Table 6.3. The mean value of the rupture length (*L*) and its standard deviation (*SD*) calculated for ConA − mannose and SNA − sialic acid complexes studied in HCV29 and T24 cells.

Table App.1.1 List of amino acids and their abbreviations:

Table 2.1.app. Geometrical parameters of the silicon nitride cantilevers used in measurements of biological samples *(Veeco)*.

Table 2.2.app. Material properties of the piezoelectric scanner type EBL #2 *(Stavely)*

# APPENDICES

## Appendix 1.

### Protein structure organization

Generally, proteins are built up from the chain composed of amino acids are organized in a certain sequence (Table App.1.1). There are four ways of the protein chains organization: primary, secondary, tertiary and quaternary structures.

Table App.1.1 List of amino acids and their abbreviations:

| Amino acids (hydrophobic) | Three letter code | Single letter code |
|---|---|---|
| glycine | Gly | G |
| alanine | Ala | A |
| valine | Val | V |
| leucine | Leu | L |
| isoleucine | Ile | I |
| methionine | Met | M |
| phenylalanine | Phe | F |
| tryptophan | Trp | W |
| proline | Pro | P |
| Amino acids (hydrophilic) | Three letter code | Single letter code |
| serine | Ser | S |
| threonine | Thr | T |
| cysteine | Cys | C |
| tyrosine | Tyr | Y |
| asparagine | Asn | N |
| glutamine | Gln | Q |
| Amino acids (negative & hydrophylic | Three letter code | Single letter code |
| aspartic acid | Asp | D |
| glutamic acid | Glu | E |
| Amino acids (positive & hydrophilic) | Three letter code | Single letter code |
| lysine | Lys | K |
| arginine | Arg | R |
| histidine | His | H |

*Protein primary structure* is referred to the linearly ordered amino acids that are linked through the peptide bond. The resulting feature is that one end of the protein chain is N-terminated, what means that this end bears the residue with free amino group, and the other C-terminated containing free carboxyl group. The ordered array of amino acids in a protein confers regular conformational forms upon that protein. These conformations constitute the ***secondary structures of a protein***. In general proteins fold into two broad classes of structure termed, globular proteins or fibrous proteins.

Globular proteins are compactly folded and coiled, whereas, fibrous proteins are more filamentous or elongated. It is the partial double-bond character of the peptide bond that defines the conformations a polypeptide chain may assume. Within a single protein different regions of the polypeptide chain may assume different conformations determined by the primary sequence of the amino acids.

The *α–helix* is a common secondary structure encountered in proteins of the globular class. The formation of the *α–helix* is spontaneous. It is stabilized by H-bonding between amide nitrogens and carbonyl carbons of peptide bonds spaced four residues apart. This orientation of H-bonding produces a helical coiling of the peptide backbone such that the R-groups lie on the exterior of the helix and perpendicular to its axis. Not all amino acids favor the formation of the *α–helix* due to steric constraints of the R-groups. Amino acids such as alanine (A), aspartic acid (D), glutamic acid (E), isoleucine (I), leucine (L), and (methionine) M favor the formation of *α–helices*, whereas, glycine (G) and praline (P) favor disruption of the helix. The disruption of the helix is important as it introduces additional folding of the polypeptide backbone to allow the formation of globular proteins.

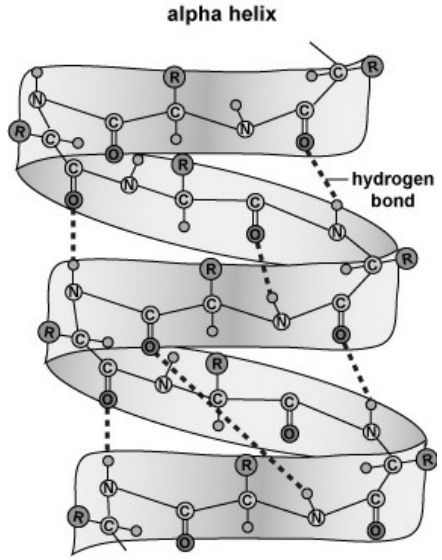


Figure 1.1.app. The structure of α-helix (image was taken from *Biotutorials*).

Whereas an *α–helix* is composed of a single linear array of helically disposed amino acids, *β–sheets* are composed of 2 or more different regions of stretches of at least 5-10 amino acids. The folding and alignment of stretches of the polypeptide backbone aside one another to form *β–sheets* is stabilized by H-bonding between amide nitrogens and carbonyl carbons. However, the H-bonding residues are present in adjacently opposed stretches of the polypeptide backbone as opposed to a linearly contiguous region of the backbone in the *α–helix*. *β–sheets* are said to be pleated. This is due to positioning of the α–carbons of the peptide bond, which alternates above and below the plane of the sheet. *β–sheets* are either parallel or antiparallel. In parallel sheets adjacent peptide chains proceed in the same direction (i.e. the direction of N-terminal to C-terminal

ends is the same), whereas, in antiparallel sheets adjacent chains are aligned in opposite directions.

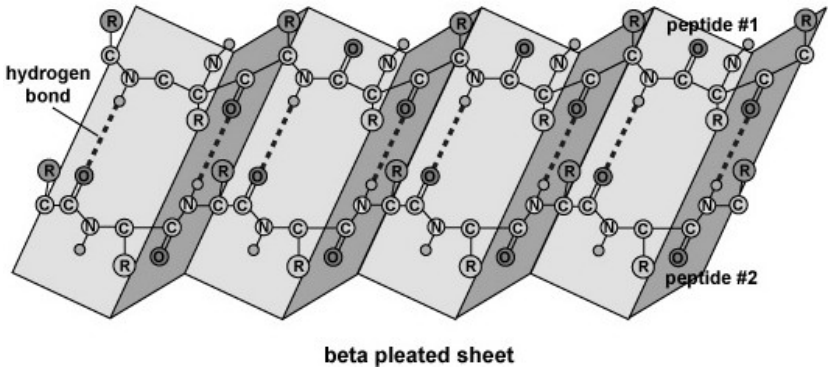


Figure 1.2.app. The β-sheet structure (image was taken from *Biotutorials*).

The *tertiary structure* describes the three-dimensional organization of the polypeptide chain of a given protein. Several forces such as hydrogen bonding, hydrophobic and electrostatic interactions, and van der Waals forces govern the interactions between different protein fragments.

Many proteins such for example hemoglobin contain two or more different polypeptide chains ordered in the tertiary structures. Such organized chains are held in association by the same non-covalent forces that stabilize the tertiary structures of proteins. Proteins with multiple polypeptide chains are termed oligomeric proteins. The structure formed by monomer-monomer interaction in an oligomeric protein is known as ***quaternary structure***. Oligomeric proteins can be composed of multiple identical polypeptide chains or multiple distinct polypeptide chains. Proteins with identical subunits are termed homo-oligomers. Proteins containing several distinct polypeptide chains are termed hetero-oligomers.

**References:**

Lodish H., A.Berk, P.Matsudaira, C.A.Kaiser, M.Krieger, M.P.Scott, S.L.Zipursky, J.Darnell (eds) – "Molecular Cell Biology", 5th ed, (2004) WH Freeman and Company, New York.

Biotutorials: *http://student.ccbcmd.edu/~gkaiser/biotutorials/proteins/protein.html*.

# Appendix 2.

## Cantilever and piezoelectric scanner properties

### *Silicon nitride cantilever (Veeco)*

Table 2.1.app. Geometrical parameters of the silicon nitride cantilevers used in measurements of biological samples *(Veeco)*.

| **Probe type** | **MLCT** | **AUHW** | | | |
|---|---|---|---|---|---|
| Cantilever type | A | C | D | E | F |
| Normal spring constant [N/m] | 0.05 | 0.01 | 0.03 | 0.1 | 0.5 |
| Length [μm] | 180 | 320 | 220 | 140 | 85 |
| Width [μm] | 18 | 22 | 22 | 18 | 18 |
| Thickness [a)] [μm] | 0.6 | 0.6 | 0.6 | 0.6 | 0.6 |
| **Probe type** | **DNP** | | | | |
| Cantilever type | A | B | C | D | |
| Spring constant [N/m] | 0.58 | 0.12 | 0.32 | 0.06 | |
| Length [μm] | 115 | 196 | 115 | 196 | |
| Width [μm] | 25 | 41 | 17 | 23 | |
| Thickness [a)] [μm] | 0.6 | 0.6 | 0.6 | 0.6 | |

[a)] According to manufacture's data, thickness varies from 0.5 to 0.7 μm

### *Piezoelectric scanner type EBL#2 (Staveley Sensors)*

A piezoelectric tube is composed of lead zirconate titanate. It has a shape of a tube with the length of 1.25", the diameter of 0.25" and a wall thickness of 0.02".

Table 2.2.app. Material properties of the piezoelectric scanner type EBL #2 *(Stavely)*

| **Piezoelectric scanner** | |
|---|---|
| Type | EBL #2 |
| Material | Lead zirconate titanate |
| Electrodes | Gold coated |
| Length [inch] | 1.25 |
| Diameter [inch] | 0.25 |
| Wall thickness [inch] | 0.02 |
| $d_{31}$ [m/V] | $-173 \cdot 10^{-12}$ |
| $d_{33}$ [m/V] | $380 \cdot 10^{-12}$ |
| Max. HV [V] | 300 |
| Curie temperature [°] | 350 |
| Resonant frequency [kHz] | 53 |

# Appendix 3.

## Equations of the analytical solution for the cantilever normal spring constant determination

According to analytical calculations presented by Neumeister *et al. (Neumeister et al. 1994)* the shape of the cantilever can be approximated as a triangular plate and two identical prismatic beams (Figure 3.1.app). In this manner, the bending of the whole cantilever upon the normal $F_N$ can be splitted into two movements: a bending of a triangular plate and a deflection of a single prismatic beam. Thus, the total deflection of the cantilever $\Delta_N$ can be written as

$$\Delta_N = \Delta_I + \Delta_{II} + g \cdot \Theta_{II} . \qquad (3.1.app)$$

where $\Delta_I$ is the deflection of clamped triangular plate, $\Delta_{II}$ is the deflection of two beams and $\Theta_{II}$ is their rotation, g $\left( g = \frac{w}{\sin(\alpha)} - d \right)$ is the function depended on the cantilever geometry, i.e. the width of the beam and the opening angle).

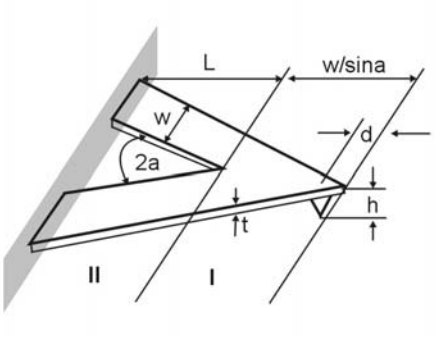


Figure 3.1.app. The triangular AFM cantilever with marked triangular plate (I) and two prismatic beams (II).

The corresponding equations of the deflections and rotation are as follows:

$$\Delta_I = \frac{3 \cdot F}{E \cdot t^3 \cdot \tan(\alpha)} \cdot \left\{ \left( \frac{w}{\sin(\alpha)} - 2 \cdot d \right)^2 - d^2 \cdot \left( 2 \cdot \log\left[ \frac{w}{d \cdot \sin(\alpha)} \right] + 1 \right) \right\} \qquad (3.2.app)$$

$$\Delta_{II} = \frac{F \cdot L^2}{E \cdot w \cdot t^3 \cdot \cos^2(\alpha)} \cdot \left\{ \frac{2 \cdot L}{\cos(\alpha)} + 3 \cdot \left( w \cdot \cot(\alpha) - d \cdot \cos(\alpha) - r \cdot \sin(\alpha) \right) \right\} \qquad (3.3.app)$$

$$\Theta_{II} = \frac{3 \cdot F \cdot L \cdot (1+\nu)}{E \cdot w \cdot t^3 \cdot \cos(\alpha)} \cdot \left\{ \frac{w}{\sin(\alpha)} - d + r \cdot \cot(\alpha) \right\} \qquad (3.4.app)$$

where $t$ is the cantilever thickness, $E$ is the Young's modulus value of the material and, $r$ is the length given by:

$$r = \frac{L \cdot \tan(\alpha) + (w - d \cdot \sin(\alpha)) \cdot (1 - \nu) \cdot \cos(\alpha)}{2 - (1 - \nu) \cdot \cos^2(\alpha)} \cdot \tag{3.5.app}$$

On the other hand, the Equation (Ap. 4.1) can be rewritten as

$$\Delta_N = \frac{F_N}{k_z}. \tag{3.6.app}$$

where $k_z$ is the normal stiffness of the cantilever, and it can be calculated as follows:

$$k_z = \frac{F_N}{\Delta_I + \Delta_{II} + \left( \frac{w}{\sin(\alpha)} - d \right) \cdot \Theta_{II}}, \tag{3.7.app}$$

assuming that the analytical forms of $\Delta_I$ , $\Delta_{II}$ , and $\Theta_{II}$ are known. The main problem of the cantilever stiffness calculation is a lack of the exact knowledge of the cantilever thickness and the Young's modulus value of the material.

**Reference:**

Neumaister J.M., W.A.Ducker – "Lateral, normal, and longitudal spring constants of atomic force microscopy cantilevers", *Rev. Sci. Instrum.*, 65 (1994) 2527–2531

# Appendix 4.

## Distribution of the resonant frequencies

From each recorded spectra, the distribution of the resonance frequency can be created. Figure 4.1.app presents the relatively narrow (approximately 2.2 kHz width) distributions of the resonant frequency, obtained for two types of cantilevers (type C and D), coming from the same silicon wafer (i.e. undergoing the same production conditions). The maxima, corresponding to cantilevers with the nominal spring constants $k_N$ of 0.01 N/m and 0.03 N/m, were centered at 6.16 kHz and 13.82 kHz while the nominal resonant frequencies $\omega_N$ given by the manufacturer were 7 kHz and 15 kHz.

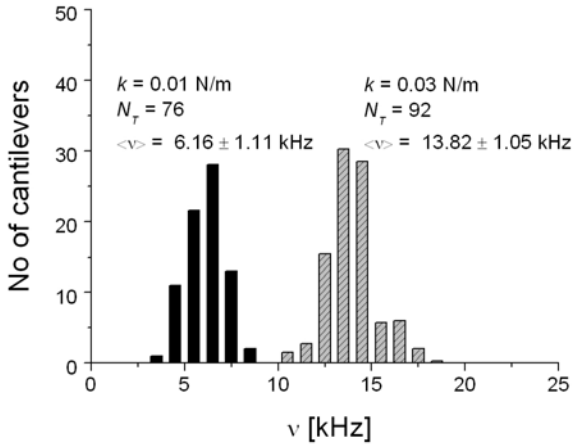


Figure 4.1.app The distribution of the resonant frequencies measured for two types of cantilevers with nominal spring constants of 0.01 N/m and 0.03 N/m coming from the same wafer and used later on for the AFM measurements. $N_T$ is the number of measured cantilevers.

The obtained frequency values were smaller than the nominal ones by about 10% for both cantilevers. In consequence, the determined from the Equation (4.11) cantilever spring constants were 0.008 and 0.026 N/m as compared respectively to 0.01 and 0.03 N/m given by the manufacturer.

# Appendix 5.

## The influence of the contact time on the unbinding force

The other parameter influencing significantly the measured adhesion force value is the contact time of the cantilever tip and the cell surface. The change of the contact time can be applied either directly by instrumentally setting the desired contact time or indirectly by changing the value of the normal loading force $F_N$. Figure 5.1.app presents the dependence of the adhesion force $F_{adhesion}$ as a function of the applied normal force.

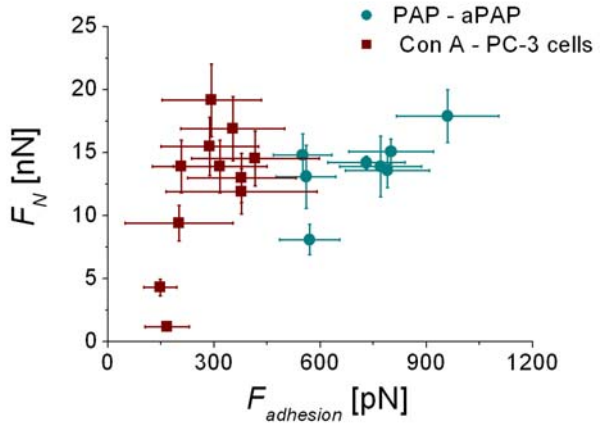


Figure 5.1.app Adhesion force versus loading force obtained for: i) typical antigen−antibody interaction on example of PAP-aPAP (wine squares) and ii) lectin (ConA) −carbohydrate recognition on prostate cells PC-3 (cyan dots).

For the typical antigen−antibody interaction measured on example of PAP[27] and aPAP molecules, the extracted adhesion force ranged from 550 pN to 960 pN. In the other type of recognition where the lectin ConA interacts with mannose-type ligands present on a surface of cancer prostate cells (PC-3), the measured adhesion force showed less variability i.e. changes from 150 pN to 420 pN. The increase of the $F_{adhesion}$ with the normal force can be explained by the larger contact time, facilitating the formation of molecular bonds. However, the force value is also dependent on the density of receptors within the contact between the probing AFM tip and the surface. In particular, the number of receptors becomes larger during probing the cell membrane where the normal, loading force increases the contact area.

[27] PAP − prostatic acid phosphatase; aPAP − monoclonal anti-human prostatic acid phosphatase.

# Appendix 6.

## Young's modulus determination

Cell stiffness was determined in the frame of Sneddon's mechanics *(Sneddon 1964)* describing the elastic behavior of the elastic half–space pushing by a hard axisymmetric indenter of different shapes, such as sphere, cylinder, paraboloid and cone. The cell surface, at first approach, can be modeled by an elastic half–space and the AFM tip can be approximated either by a cone with the open angle $\alpha$ or by paraboloid with the radius of curvature $R$ at the apex. Both models are not limited by a finite tip end radius (unlike the classical Hertz model describing the interaction of a sphere with flat surface) and may be extended for large indentation depths (1–2 μm). In addition, a cell was approximated as an elastic and isotropic material. There are two commonly used models applied for the calculation of the Young's modulus from the AFM measurements. For a paraboloidal one and for conical tip, the relation of the loading force $F$ as a function of indentation $\Delta z$ is given by equations (App.3.1) and (App.3.2), respectively:

$$F(\Delta z) = \frac{4 \cdot \sqrt{R} \cdot E_{cell}}{3 \cdot (1 - \eta_{cell}^2)} \cdot \Delta z^{1.5} \qquad (6.1.app)$$

$$F(\Delta z) = \frac{2 \cdot E_{cell}}{\pi \cdot (1 - \eta_{cell}^2) \cdot \tan \alpha} \cdot \Delta z^2 \qquad (6.2.app)$$

An average value of $E_{cell}$ was then estimated from the Gaussian fit to the distribution of the Young's moduli, assuming the cell Poisson ratio, $\eta_{cell}$, to be 0.5. Errors originate from uncertainties in the tip shape, the spring constant, the contact area, sample heterogeneity, and approximations in the theoretical model used for analysis. One should mention that using AFM it is not possible to determine the absolute Young's modulus value. However, very often for biological samples, the absolute value of the modulus is not needed *(Sokolov 2007)*.

**References:**

Sneddon I.N. − "The relation between load and penetration in the axisymmetric Boussinesq problem for a punch of arbitrary profile", *Int. J. Engng. Sci.,* 3 (1965) 47−57.
Sokolov I. – "Atomic force microscopy in cancer cell research" in *Cancer Nanotechnology,* H.S.Nalwa, T.Webster (eds.), American Scientific Publishers, 2007, New York, ISBN: 1-58883-071-3, *pages*: 1–17.

# Appendix 7.

## Hydrodynamic drag force

The hydrodynamic drag force, $F_{drag,}$ is usually present in AFM measurements since the cantilever experiences a force arising due to viscous friction with the surrounding liquid *(Butt et al. 2005),* like any object moved through a solution.


Figure 7.1.app. The hydrodynamic drag forces acting on AFM cantilever during a) approach and b) retreat.

Hydrodynamic drag acts always in the opposite direction to the cantilever movement. Thus, the force measured by AFM ($F = kx$) is a sum of the true force acting on molecule ($F_{true}$) and the hydrodynamic force ($F_{drag}$)

$$\vec{F} = \vec{F}_{true} + \vec{F}_{drag} \tag{7.1.app}$$

Its value is smaller when cantilever approaches the surface

$$k \cdot x = F_{true} - F_{drag} \tag{7.1a.app}$$

and larger when cantilever is withdrawn from the surface

$$k \cdot x = F_{true} + F_{drag} \tag{7.1b.app}$$

As recently was shown by Alcaraz *el al. (Alcaraz et al. 2002)*, the drag force acting on the cantilever can be described by the following equation (for low Reynolds number $Re < 1$)

$$F_{drag} = \frac{6 \cdot \pi \cdot \eta \cdot a_{eff}^2}{h + h_{eff}} \cdot v_{tip} \tag{7.2.app}$$

where $\eta$ is the viscosity of the liquid, $h$ is the tip-surface separation, $a_{eff}$ is the effective tip radius, $h_{eff}$ is the effective tip height, and $v_{tip}$ denotes the velocity of the AFM cantilever. Currently, there is no satisfactory theoretical model describing the dependence of the drag force on the cantilever geometry. Despite that, it has been shown that the $h_{eff}$ value is close to the nominal value of the tip height (~ 3 μm), and the effective tip radius $a_{eff}$ is of about 22 μm *(Alcaraz et al. 2002)*.

The Reynolds number can be determined on the basis of fluid dynamic theory *(Landau et al. 1987)* modeling the AFM tip as a sphere with the radius $a_{eff}$ using the following formula

$$\mathrm{Re} = \frac{a \cdot v_{tip} \cdot \rho}{\eta} \qquad (7.3.app)$$

where $a$ denotes the particle size moving in viscous medium. For a typical measurement in water, at room temperature, assuming viscosity $\eta$ = 1 mNs/m$^2$, density $\rho$ = 1 g/cm$^3$, cantilever velocity $v$ = 1 μm/s, and the effective tip radius $a_{eff}$ = 1 μm, the Reynolds number is of the order of $10^{-3}$. The hydrodynamic force increases with the velocity of the approaching and retracting tip. The slope rises strongly with the effective tip radius.

In all recent AFM measurements of the interaction forces, the tip velocity varied from few nm/s to about 10 μm/s *(Janoviak et al. 2005)*. At first approach, all biological buffers can be treated as water since usually they are aqueous solutions. Thus, assuming the viscosity of surrounding liquid to be close to the water viscosity, the estimated maximum value of the hydrodynamic force contributing to the total force acting on single molecule is 0.06 pN and 6.28 pN for the tip velocity of 1 μm/s and 10 μm/s, respectively. The hydrodynamic force has to be considered in force measurements at large velocities as than it approaches the magnitude of the measured interaction force. Additionally, the hydrodynamic force is not constant over the tip-sample distance, leading to the enhancement of the effect at small tip-surface separations.

Experimentally, $F_{drag}$ can be estimated from the separation of the approach and retract curves in their non-contact regions (i.e. base line, Figure 7.2.app.). Such estimation is similar to the procedure of AFM determination of the friction force *(Koleske et al. 1995)*.

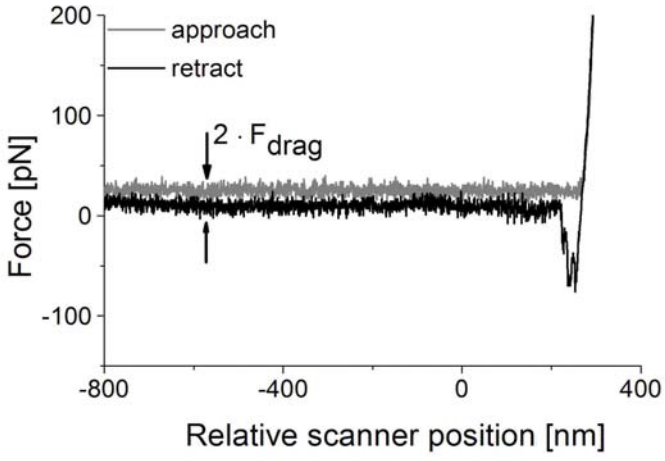


Figure 7.2.app. The idea of the AFM measurement of hydrodynamic force, $F_{drag}$.

Below, there are exemplary distributions of hydrodynamic forces recorded during moving the cantilever in PBS buffer at two velocities: 2.4 μm/s (a) and at 7.7 μm/s (b).

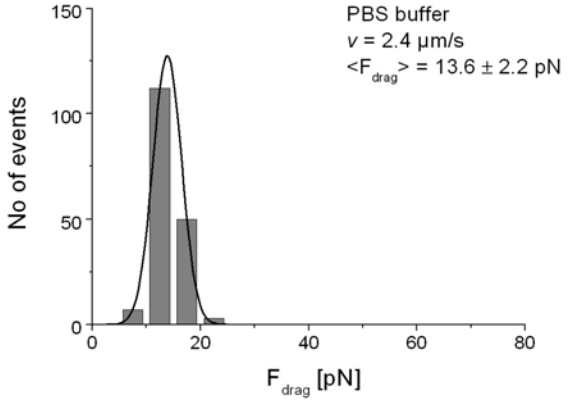


a)

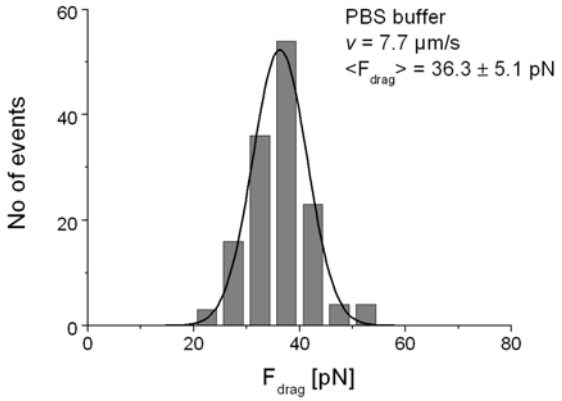


b)

Figure 7.3.app. Distributions of the hydrodynamic force measured in PBS buffer, at the cantilever velocity of 2.4 μm/s (b) and 7.7 μm/s (c).

The corresponding hydrodynamic drag forces are 13.6 pN to 36.3 pN. Thus, assuming that the force measured by AFM is 100 pN, the true force acting on molecule is 81.4 pN and 63.7 pN, respectively.

# Appendix 8.

## Monosaccharide structure – glucose as an example

Monosaccharides are polyhydroxy aldehydes H-[CHOH]$_n$-CHO or polyhydroxy ketones H-[CHOH]$_n$-CO-[CHOH]$_m$-H with three or more carbon atoms. The positions of the carbon atoms (red or green) are determined in a counter-clockwise manner, starting from the place of oxygen atom.

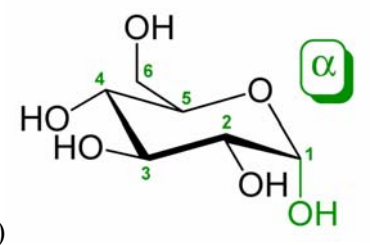


a)

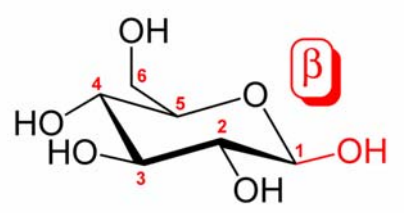


b)

Figure 8.1.app α and β anomers of glucose (Images were adopted from *Nelson et al. 2003*).

The figure above presents the anomers of glucose defined by the orientation of OH group bound to the first carbon atom.

**Reference:**

Nelson D.L., M.M.Cox − "*Lehringer principles of biochemistry*", Worth Publishers, New York third edition, (2003).